AD-A109 813 GEORGIA INST OF TECH ATLANTA ENGINEERING EXPERIMENT --ETC F/G 6/18
INVESTIGATION OF RADIOFREQUENCY RADIATION EFFECTS ON EXCITABLE --ETC(U)
JUL 81 R L SEAMAN, E C BURDETTE, R L DEHAAN F49620-79-C-0055

UNCLASSIFIED AFOSR-TR-82-0020 NL

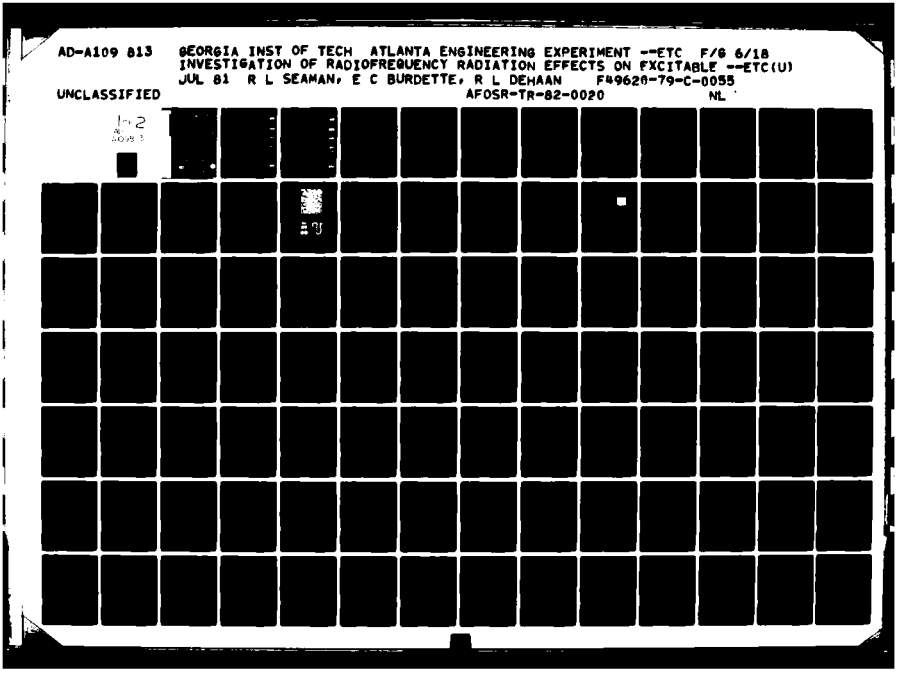

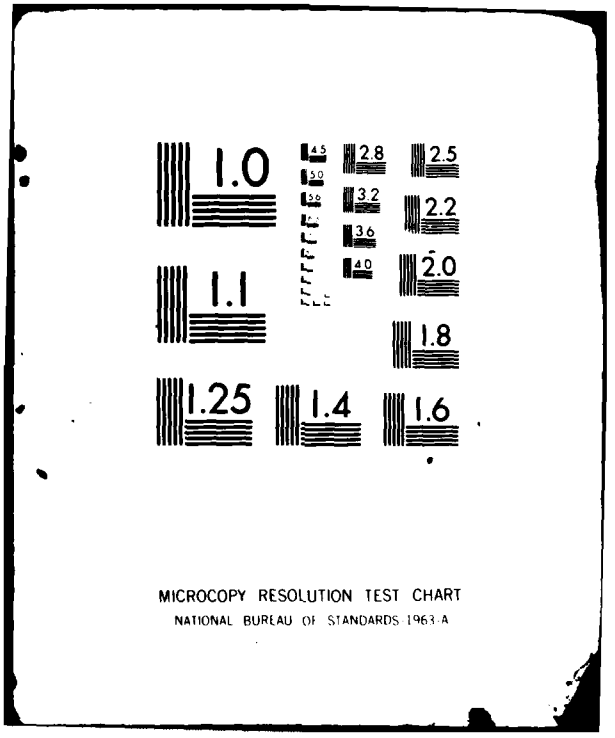
1.0
1.1
1.25
1.4
1.6
1.8
2.0
2.2
2.5
2.8
3.2
3.6
4.0
4.5
5.0
5.6
MICROCOPY RESOLUTION TEST CHART
NATIONAL BUREAU OF STANDARDS 1963-A

AFOSR-TR- 82 -0020

FINAL TECHNICAL REPORT
PROJECT A–2335

LEVEL II

INVESTIGATION OF RADIOFREQUENCY RADIATION EFFECTS ON EXCITABLE TISSUES

By

R. L. Seaman and E. C. Burdette
Biomedical Research Branch
Electronics and Computer Systems Laboratory
Georgia Institute of Technology

and

R. L. DeHaan
Anatomy Department
Emory University School of Medicine

Prepared for

U. S. AIR FORCE
OFFICE OF SCIENTIFIC RESEARCH
LIFE SCIENCES DIRECTORATE
BOLLING AIR FORCE BASE, DC 20332

CONTRACT NO. F49620–79–C–0055

July 1981

GEORGIA INSTITUTE OF TECHNOLOGY
A Unit of the University System of Georgia
Engineering Experiment Station
Atlanta, Georgia 30332

GT EES

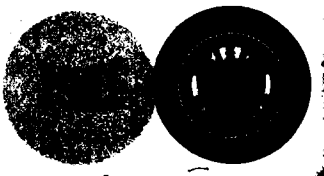

Unclassified

SECURITY CLASSIFICATION OF THIS PAGE (When Data Entered)

REPORT DOCUMENTATION PAGE	READ INSTRUCTIONS BEFORE COMPLETING FORM
1. REPORT NUMBER **AFOSR-TR- 82 -0020** 2. GOVT ACCESSION NO. AD-A109 813	3. RECIPIENT'S CATALOG NUMBER
4. TITLE (and Subtitle) INVESTIGATION OF RADIOFREQUENCY RADIATION EFFECTS ON EXCITABLE TISSUES	5. TYPE OF REPORT & PERIOD COVERED Final Technical Report
	6. PERFORMING ORG. REPORT NUMBER
7. AUTHOR(s) R. L. Seaman, E. C. Burdette, and R. L. DeHaan* Anatomy Department, Emory University School of Medicine	8. CONTRACT OR GRANT NUMBER(s) F 49620-79-C-0055
9. PERFORMING ORGANIZATION NAME AND ADDRESS Engineering Experiment Station Georgia Institute of Technology Atlanta, Georgia 30332	10. PROGRAM ELEMENT, PROJECT, TASK AREA & WORK UNIT NUMBERS 61102F 2312-A5
11. CONTROLLING OFFICE NAME AND ADDRESS Air Force Office of Scientific Research/NL Director of Life Sciences/NL Building 410, Bolling AFB, D.C. 20332	12. REPORT DATE 31 July 1981
	13. NUMBER OF PAGES 92 + v
14. MONITORING AGENCY NAME & ADDRESS(if different from Controlling Office)	15. SECURITY CLASS. (of this report) Unclassified
	15a. DECLASSIFICATION/DOWNGRADING SCHEDULE

16. DISTRIBUTION STATEMENT (of this Report)

Approved for Public Release, Distribution Unlimited

17. DISTRIBUTION STATEMENT (of the abstract entered in Block 20, if different from Report)

18. SUPPLEMENTARY NOTES

19. KEY WORDS (Continue on reverse side if necessary and identify by block number)

Open-Ended Coaxial Exposure Device	Excitable Tissues
Radiofrequency Radiation	Cardiac-Cell Aggregates
Specific Absorption Rate	Interbeat Interval (beat rate)
Electromagnetic Fields	Coefficient of Variation
	Action Potential

20. ABSTRACT (Continue on reverse side if necessary and identify by block number)

Spheroidal aggregates of cultured chick cardiac cells were used to study effects of 2450-MHz radiofrequency radiation (RFR) on excitable membranes. Rhythmically beating aggregates under normal culture conditions were exposed to known amounts of RFR energy in a specially developed open-ended coaxial device. Exposure level was given in terms of Specific Absorption Rate (SAR) in mW/g.

-continued-

DD FORM 1 JAN 73 1473 EDITION OF 1 NOV 65 IS OBSOLETE

Unclassified 153 (50)

SECURITY CLASSIFICATION OF THIS PAGE (When Data Entered)

Short-term recordings with intracellular electrodes suggested that increased variability in beat rate and in action potential maximum upstroke velocity occurred in the range of 10-40 mW/g for continuous wave (CW) RFR and RFR modulated as 10.9-microsecond pulses at 10,000 pps (PW). Long-term recordings with extracellular electrodes and video imaging were used to gather interbeat interval (IBI) data for computing mean IBI and coefficient of variation (CV). Three-minute exposures to CW and PW RFR and to RFR square-wave modulated at 1.6 or 16 Hz were made for SARs between 1.2 and 85.5 mW/g.

Decreases in mean IBI during exposure for SARs greater than 30 mW/g closely matched those expected from induced temperature rises. However, IBI changes at smaller SARs, including an increase at 1.2 mW/g, were not fully explained by temperature changes. Small changes in CV occurred during exposure and were similar to those during sham exposures. In many cases, changes in mean IBI and CV were larger after exposure than during exposure and occurred most often for PW RFR. Beat rates with high initial CV were more sensitive to RFR.

FINAL TECHNICAL REPORT

Project A-2335

INVESTIGATION OF RADIOFREQUENCY RADIATION EFFECTS ON EXCITABLE TISSUES

By

R. L. Seaman, E. C. Burdette, and R. L. DeHaan*

July 1981

Prepared for

U.S. AIR FORCE
Office of Scientific Research
Life Sciences Directorate
Bolling Air Force Base, DC 20332

Contract No. F49620-79-C-0055

Prepared by

BIOMEDICAL RESEARCH DIVISION
Electronics and Computer Systems Laboratory
Engineering Experiment Station
Georgia Institute of Technology
Atlanta, Georgia 30332

* Anatomy Department, Emory University School of Medicine, Atlanta, GA 30322

FOREWORD

Research during this two-year program was performed by personnel in the Biomedical Research Division of the Electronics and Computer Systems Laboratory of the Engineering Experiment Station at the Georgia Institute of Technology and by personnel in the Anatomy Department of the Emory University School of Medicine. This program was sponsored by the U.S. Air Force Office of Scientific Research, Bolling Air Force Base, and the School of Aerospace Medicine, Brooks Air Force Base, under Contract No. F49620-79-C-0055. Dr. R. L. Seaman served as Principl Investigator during the latter part of the second year and the Final Technical Reporting period. This Final Technical Report summarizes work done on this program, designated as Georgia Tech Project A-2335, during the period from 1 March 1979 through 30 April 1981.

This multidisciplinary research program was made possible by the efforts of several people. Mr. E. C. Burdette served as Principal Investigator during the inception of the program and was responsible for the updated dosimetry in the second year. Ms. B. J. Duke and Mr. D. C. Redd, of the Emory Anatomy Department, carried out the many technical details involved with culturing cardiac-cell aggregates and with measuring their electrical properties. Mr. P. G. Friederich and Mr. D. J. Freedman performed many of the first-level statistical analyses. Dr. A. R. Moser developed the computer programs for analyzing and plotting data at Georgia Tech.

Respectfully submitted,

Ronald L. Seaman

Ronald L. Seaman
Principal Investigator

Approved:

J.C. Toler

J. C. Toler, Manager
Biomedical Research Division

TABLE OF CONTENTS

LIST OF FIGURES

LIST OF FIGURES

-continued-

LIST OF FIGURES

-concluded-

LIST OF TABLES

I. INTRODUCTION

A. Background

Over the past several decades, the use of radiofrequency radiation (RFR) for military, industrial, and consumer applications has increased dramatically. Because of its ability to penetrate and heat tissue, there has been a corresponding increase in concern that this type of electromagnetic radiation might adversely affect biological systems. While animal research has conclusively shown various adverse effects when RFR exposure levels are high enough to induce significant heat loads, there are conflicting results for lower levels.

Interest in the effects of radiofrequency radiation on biological systems has existed for quite some time. In many cases, interest has focused on the effects of RFR on excitable tissues, namely, nerve and muscle. The normal function of these tissues involves changing electric fields and ionic currents which can be altered by applied static and slowly changing electromagnetic fields. It is conceivable that higher-frequency fields, such as those associated with RFR, could also interact with the naturally occurring fields of these tissues. In this section, a brief review of the literature on RFR cardiac effects and on other topics relevant to the subject of this report is presented.

Some of the earliest research on RFR cardiovascular effects was reported in the Soviet literature and is summarized by Presman [1, pp. 116-124] and Baranski and Czerski [2, pp. 117-122]. Rabbits were exposed to pulsed- and continuous-wave (CW), 2400- or 3000-MHz radiation at incident power densities of 3-5 and 7-12 mW/cm^2. Small increases and decreases in heart rate were observed and depended on the body region exposed. Decreases in heart rate were attributed to stimulation of the peripheral nervous system since they were absent when the exposed skin was anesthetized. Increases in heart rate were attributed to effects on the central nervous system and were dominant when only the head was exposed. It was also concluded that pulsed radiation had a stronger effect than did CW radiation.

Replications of these studies have been carried out using 2400-MHz CW and pulsed radiation [3,4]. With CW energy applied only to a rabbit's head, no significant change in heart rate was observed with 10 mW/cm^2 incident power density and only the highest level used, 100 mW/cm^2, was effective in increasing heart rate. With CW or pulsed RF energy applied at 20 mW/cm^2 to the entire dorsal surface of the rabbit, no difference in response was seen. Respiration rate was found to be more sensitive than heart rate in these studies. These results led to the conclusion that previously reported changes in heart rate were most likely due to chance variations. A more recent study also supports this conclusion [5].

Various criticisms have been directed at the above Soviet studies [2]. Major among these are the use of exposure conditions with different field characteristics (far-field versus near-field exposure) in the different studies and the necessity of using enough animals to detect small changes reliably. There were also substantial differences in exposure levels. Thus, it can be seen from the various studies that the effects of low level RFR on heart rate in an intact animal are far from resolved.

Isolated heart preparations have been used in attempts to delineate direct effects on cardiac tissue. In denervated frog hearts, no change in heart rate was seen in response to an incident field of 0.06 mW/cm^2, while exposure of intact frogs produced effects similar to those which had been observed in rabbits [1, p. 122]. In another study, 1425-MHz radiation pulsed at low repetition rates was found to be effective in causing arrhythmias in isolated frog hearts but only for certain delays from the occurrence of the P wave of the electrocardiogram [6]. Pulse duration was 10 microseconds and pulses were delivered coincident with the P wave, 100 milliseconds after the P wave, or 200 milliseconds after the P wave. Arrhythmias were observed in 50 percent of the irradiated cases with the longer delay, a much higher incidence than for other cases. However, replications of these experiments have failed to confirm this effect [7,8].

Some interesting results have been obtained from isolated hearts using CW radiation at 960 MHz applied with a capacitor irradiator [9-12]. For turtle hearts, Specific Absorption Rate (SAR) in the range of 2 to 10 mW/g caused a decrease in heart rate while larger SARs and generalized heating caused an increase in heart rate [9,10]. Results from drug studies suggested that the decreases seen at small SARs were due to neurotransmitter release from nerve remnants in the heart [10]. Similar decreases in heart rate have been found in isolated rat hearts for SARs of 1.3 to 2.1 mW/g [11,12] and drug studies again indicated an interaction with nerve remnants [12]. These apparent interactions of low-level RFR with remnant nerve components suggested that other than purely thermal mechanisms were taking place.

Several other isolated preparations of excitable tissue have been utilized in attempts to identify mechanisms for RFR interaction with excitable membranes. Much of this work was triggered by early Russian investigations using frog sciatic nerves which showed not only apparent increases in excitability and conduction velocity with RFR but differences in effects produced by CW and pulsed 2400-MHz RFR [13]. This research and related work has been reviewed recently [1, pp. 157-159; 14]. Researchers conducting replicates of these experiments with 2450-MHz RFR at SARs of 0.3-1500 mW/g CW and 0.3-220 mW/g pulsed RFR attributed all effects to heating of the nerve [15]. Other nerve and muscle preparations with RFR typically applied for several minutes revealed no microwave effect beyond that of heating [15,16]. However, for RFR applications longer than 20 to 30 minutes, an accelerated rundown of frog sciatic nerves was observed [14]. This effect, which was measured as decreased amplitude of the stimulated compound action potential, took place over 1- to 2-hour exposures. The accelerated decrease in vitality seemed to be a RFR interaction with a Na-K pump since ouabain eliminated the microwave effect [17]. The threshold for this effect was between 5 and 10 mW/g and, judging from the illustrated data, the effect can occur in the absence of changes in conduction velocity.

Pacemaker neurons from an invertebrate have been studied to obtain information on RFR effects at the cellular level [18,19]. These neurons

were exposed to 1500- and 2450-MHz RFR in a stripline exposure device and their transmembrane potentials were recorded during exposure. Both decreases and increases in firing rate were observed, with some changes occurring for SARs as low as 2 mW/g. Not all RFR-induced slow changes in firing rate were reproduced by warming the preparation. In addition, rapid changes were most often seen for pulsed RFR and were not seen with heating. These findings pointed to RFR processes other than thermal ones and to possible different mechanisms operative for pulsed RFR. A study using the birefringence of crab nerve has indicated larger and more persistent changes caused by pulsed RFR than by CW RFR or equivalent heating [20].

There have been attempts to explain RFR interaction with excitable tissues with mathematical models of possible mechanisms. Directly-induced transmembrane potential has been estimated to be on the order of a few hundred microvolts in the central nervous system of animals exposed to an incident field power density of 10 mW/cm^2 [21]. Rectification of induced microwave currents to produce effective direct currents has been proposed [18] and can be predicted on the basis of nonlinear conductance [22] or capacitance [23] in the membrane. Experimental evidence for nerve membrane RFR rectification [24] and plant-cell membrane rectification at lower frequencies (1-5 MHz) [25] has recently appeared. From a microscopic-level analysis, it has been concluded that rectification cannot be effective at frequencies above an estimated 32 MHz because of transit time effects, and that effects on individual membrane particles are probably more significant than rectification at higher frequencies [26]. This is plausible since not all of the effects seen in neural pacemakers can be explained in terms of equivalent direct currents [19]. Models of RFR effects on membranes include one based on the Hodgkin-Huxley equations [27] and one based on quantum mechanics [28]. These models and theoretical studies assume an RFR interaction with the membrane; very few of them have been tested experimentally.

From this brief review, it can be seen that the effects of RFR on excitable tissues have not been completely resolved, with conflicting results often reported. In addition, the mechanisms by which RFR can interact with these tissues have not been defined. It was against this background that the cardiac-cell aggregate system was used to define RFR effects more completely and to investigate various mechanisms. This aggregate system, as described in this report, offered several advantages for RFR studies.

B. Research Objectives

The overall objective of this program was to investigate the effects of pulsed- and continuous-wave radiofrequency radiation on the electrical properties of beating cardiac-cell aggregates, both singularly and when joined together in chains. The specific research objectives can be summarized as the following:

1. development of an exposure system to provide well-characterized dosimetry for cellular-level RFR exposure,
2. investigation of possible alterations in spontaneous beat rate and action potential characteristics (resting potential, threshold potential, maximum upstroke velocity) during RFR exposure of aggregates under conditions of different external potassium concentrations,
3. investigation of possible alterations in specific slow- and fast-channel ion currents during RFR exposure,
4. investigation of possible modification of pharmacological agent interaction with ion channels during RFR exposure, and
5. investigation of possible RFR interaction with neurotransmitter actions on aggregate electrical activity.

C. Report Organization

There were several significant goals achieved during the 26 months of technical performance on this research program. Since accurate dosimetry was important for defining effective and noneffective RFR levels on the cardiac-cell aggregates, a major objective was to develop an exposure system appropriate for the aggregates. Development and characterization of an open-ended coaxial exposure device is described in Section III

with plots of received RF fields by immersed antennas and of SAR computed from temperature measurements. The cardiac-cell aggregate preparation, which is described in Section II, proved to be very useful in studying RFR effects on excitable membranes. Methods of recording from the aggregates, the experimental protocol, and the collection and analysis of data are also described in Section II. Results obtained from these experiments are presented and discussed in Section IV for various RFR exposure conditions with plots of statistics on aggregate beat rate, the principal parameter studied. Conclusions based on the results of these studies and recommendations for future studies are given in Section V.

II. EXPERIMENTAL PROCEDURES

A. Cardiac-Cell Aggregate Preparation

The multicellular nature of heart tissue, and other tissues as well, normally places severe limitations on the ability to investigate its electrical and molecular properties. The fact that cardiac muscle is composed of individual cells connected by junctions of low but varying resistance into fibers of complex geometry [29,30] guarantees that voltage gradients must exist within such fibers, and currents crossing the membrane of one cell may differ from those flowing in a distant cell. In 1972, the spheroidal heart cell aggregate (Figure 1) was introduced as a tissue culture model for studies of the electrical properties of the heart cell membrane [31,32]. The advantages that these aggregates offer over more traditional cardiac preparations include the following:

1. All cells within an aggregate are closely coupled by low-resistance junctions while the non-junctional myocyte membrane exhibits large resistive, capacitive and inductive elements [33]. For spheroids of 200 μm diameter or smaller, signals in the frequency range 0-20 Hz are experienced essentially simultaneously throughout the entire membrane [34,35]. Thus, each aggregate approximates an isopotential system for both spontaneous and imposed signals.

2. Because of these properties, the aggregate action potential approximates a true non-propagated membrane potential, whose electric field builds and collapses with each beat. For this situation,the time derivative of transmembrane potential is equal to the transmembrane current divided by the membrane capacitance. For this reason, the maximal slope of the action potential upstroke (MUV) is a good measure of total inward current for a single aggregate.

3. Aggregates can be prepared in any size within a 30-300 μm diameter range from a few cells to several thousand cells, containing 10^{-7} to 10^{-2} cm^2 of membrane. Because of their nearly spherical shape and the known amount of intercellular space, the total cell surface contained within an aggregate can readily be calculated from the aggregate diameter [36,37], taken as $2(ab)^{1/2}$, where a and b are the major and minor hemiaxes

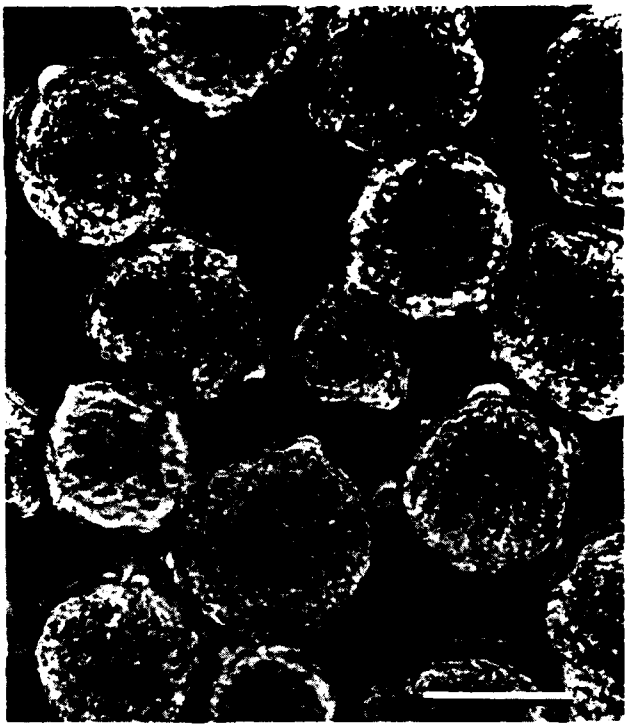

Figure 1. Field of spheroidal heart cell aggregates after 48 hrs of gyration culture. Scale - 100 µm.

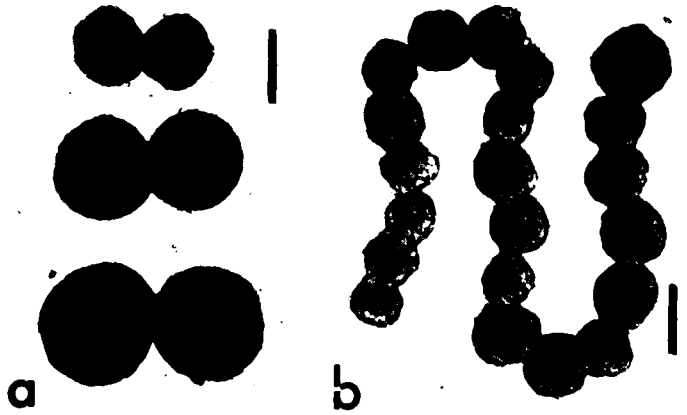

Figure 2. Linear configurations of spheroidal aggregates.
a. Aggregates arranged in equal-sized pairs, photographed 20 minutes after initial adhesion. Only the smallest pair had achieved beat synchronization; after an additional 20 minutes, all do. Scale: 100 µm.
b. A chain of 21 aggregates, photographed about 90 minutes after construction; all of the aggregates in the chain were beating in synchrony. Scale: 200 µm.

seen from a top view of the preparation. Total aggregate volume (V_a) is obtained from $V_a = 4/3\ \pi ab^2$. Since 20% of V_a equals extracellular space, the number of cells per aggregate (N) can be calculated from $0.8\ V_a/V_c$, where the mean cell volume ($V_c = 600\ \mu m^3$) was derived from a mean cell diameter d of 10.8 μm (Atherton and DeHaan, unpublished), and the total cell surface is calculated as $N\pi d^2$. Using an observed value for DNA per cell of 2.8 picogram measured in single ventricle cell suspensions and in chicken erythrocytes, we have also previously estimated N by measuring aggregate DNA content. Total DNA per aggregate was determined by the method of Giles and Myers from pooled groups of counted and sized aggregates. The mean cell volume calculated from these DNA assays was 651 μm^3, and the values of N determined from the ratio total DNA/cell DNA agreed within $\pm$ 1% with those calculated from measurements of aggregate diameter. The total membrane area of an aggregate 150 μm in diameter is $7.8 \times 10^{-3} cm^2$.

4. Aggregates are "sticky"; they can be formed into pairs, chains, or clusters (Figure 2) in which electrical coupling junctions are quickly established at points of contact. Such multi-aggregate systems soon take on a coordinated, synchronized beat [38,39]. Diffusion of ions and other molecules into and out of the intercellular tissue spaces is rapid. Longitudinal ionic currents are created by the action potential propagating along a chain.

5. Aggregates can be prepared from hearts from any desired embryonic age, from stages prior to the time the organ begins to beat to hatching or shortly thereafter. Such spheroids reflect accurately the physiological and pharmacological properties of the intact donor tissue.

6. Aggregates can be maintained in healthy condition for many days in culture, while maintaining spontaneous and rhythmic beating.

7. Because they are naturally "space clamped", that is, virtually isopotential over a reasonable range of frequencies, aggregates can be subjected to voltage clamp analysis of their current-voltage relationship [36]. This capability has recently been utilized to show directly the appearance of sodium channel current I_{Na} in aggregates from 3-day hearts maintained for an additional 3-5 days in culture [40].

For the investigations described in this report, measurements were made on spheroidal aggregates of chick heart cells maintained in tissue culture. The cells were derived from embryos of white Leghorn chickens by procedures standard in Dr. DeHaan's laboratory. After incubation for 7 days at 37.5°C, embryos were harvested in amniotic fluid and decapitated. Their hearts were dissected free, trimmed of extraneous tissue, and the ventricles were dissociated with trypsin by techniques which have been previously reported [32,34,36]. Aggregates were prepared by placing an inoculum of 5×10^5 or 8×10^5 cells in 3 ml of 818A culture medium on a gyratory shaker. Cells were allowed to aggregate during gyration at 62 rpm and 37.5°C in an atmosphere containing 5% CO_2, 10% oxygen, and 85% nitrogen. In all but one experiment in the first year of this program, aggregates were used after 48 hours of gyration. In the second year, 72-hour aggregates were used for the majority of experiments in order to obtain more regular beat rates.

At the end of a 48-hour gyration period, each aggregation flask typically contained up to 200 spheroidal clusters which ranged in diameter from 60 to 250 μm and contained $10^2 - 10^4$ cells each (Figure 1). The several hundred individual cells in each aggregate were beating spontaneously and rhythmically in a coordinated fashion. For experiments, aggregates were poured into a plastic dish containing either 818A or a balanced salt solution and the volume brought to 4 ml. The plastic dish was placed under a microscope on a heating plate modified for RF exposure (Section III). Temperature, pH, gaseous atmosphere, and evaporation were controlled and mechanical vibration minimized.

The rhythmic beat of the heart is its most striking characteristic, but the rhythm is not as regular as it first seems. Consecutive interbeat intervals (IBIs) in the spontaneous heartbeats of healthy adults are not identical; rather there is a small, apparently random variation of about 2% around an ideal mean interval. Cardiac-cell aggregates beating spontaneously in culture also exhibit a fluctuation of about 2% around a mean IBI, but for small cell clusters (fewer than 100 cells), the spontaneous fluctuation in IBI increases inversely with the number of cells comprising a cluster [41]. For example, a cluster comprised of 75 coupled cells

showed a spontaneous fluctuation in IBI of 3.9%, whereas consecutive IBIs in a 2-cell group varied by 23.5% from the mean. It was argued that the spontaneous fluctuation in IBI should be directly related to the amplitude of membrane voltage noise and that a perturbation that alters voltage noise should also affect the fluctuation in IBI. It has recently been shown that a major component of membrane voltage noise stems from the random opening and closing of voltage-sensitive specific ion channels [33] so that a perturbation of ion channels should also cause a change in IBI fluctuation.

During the course of this program, the beat rate was not always as regular as desired for some of the studies. Irregular beating took the form of either on-off beating activity or flurries of rapid beating. In on-off beating, aggregates beat in a regular manner for a minute or so, stopped beating for a comparable duration, and then resumed beating at a regular rate only to stop again later. This on-off cycle was itself stable for hours and all aggregates from the same culture flask exhibited a similar pattern. Flurries consisted of 10-15 second periods of very rapid beating before and after which the beat rate was regular. When flurries were present, they occurred from a minute to several minutes apart with no apparent pattern. Although these beating abnormalities were not studied in detail, it seemed that they were more prevalent in the fall than in the spring, indicating a possible seasonal basis. No results were obtained from aggregates showing on-off beating. The impact of flurries is discussed in Sections IV and V.

During a 6-week period in the latter part of the second year of this program, no experiments were run because of contaminated aggregate cultures. The source of contamination was successfully traced to a bottle of fetal bovine serum, a component of the culture medium. Round cocci and chains of bacteria, after morphological identification by wet mount and isolation on blood agar plates, were determined to be alpha streptococcus. To eliminate the contamination, sodium penicillin G and streptomycin sulfate were substituted for gentamicin, which is not specific for alpha streptococcus. The contamination resulted in fewer data for RFR experiments during the spring when IBI was normally more regular.

B. Recording Methods

To record spontaneous beats of aggregates or aggregate chains undisturbed by electrode penetration or other invasive observational techniques, beating activity was monitored in some experiments with the aid of a closed-circuit video system. Shown schematically in Figure 3, this system was modified from one described previously [41,42]. A closed circuit television (TV) camera (Panasonic WV-400P), positioned at the photo-ocular of a microscope, projected the image of an aggregate onto a TV screen. A photodetector placed over the edge of the image sensed the change in light level caused by movement during a beat. The photodetector's amplified output was observed on an oscilloscope and recorded on magnetic tape for later analysis.

In previous studies, aggregates were transilluminated to give a sharp-contrast TV image. The exposure device (described in Section III) did not allow this method to be implemented in RFR studies so alternate methods to illuminate the aggregate were devised. Illumination from the top provided an aggregate image with too little contrast for the edge to be detected reliably. Various intense light sources were tried to be sure that the light level was adequate. Next, aggregates were placed on a small glass platform in the culture dish and small reflectors were placed under the shelf to illuminate aggregates. In a few experiments using the shelf, aggregate images were sharp enough to be detected. Results from one of these experiments were reported in Annual Technical Report No. 1. However, in most cases, the photodetector output was too small and noisy to be useful.

Two types of illumination with a large plastic optic fiber were attempted. The illumination level was not adequate when a fiber directed light beneath the platform described above. It was felt that more light could be delivered by orienting the fiber vertically instead of horizontally. This strategy led to a modified exposure device in which the fiber was incorporated into the cable's dielectric; however, the illumination level was still inadequate. Both dissecting and compound microscopes were used in these imaging trials to span a wide range of magnifications. It may still be possible to use an optic fiber approach with the right

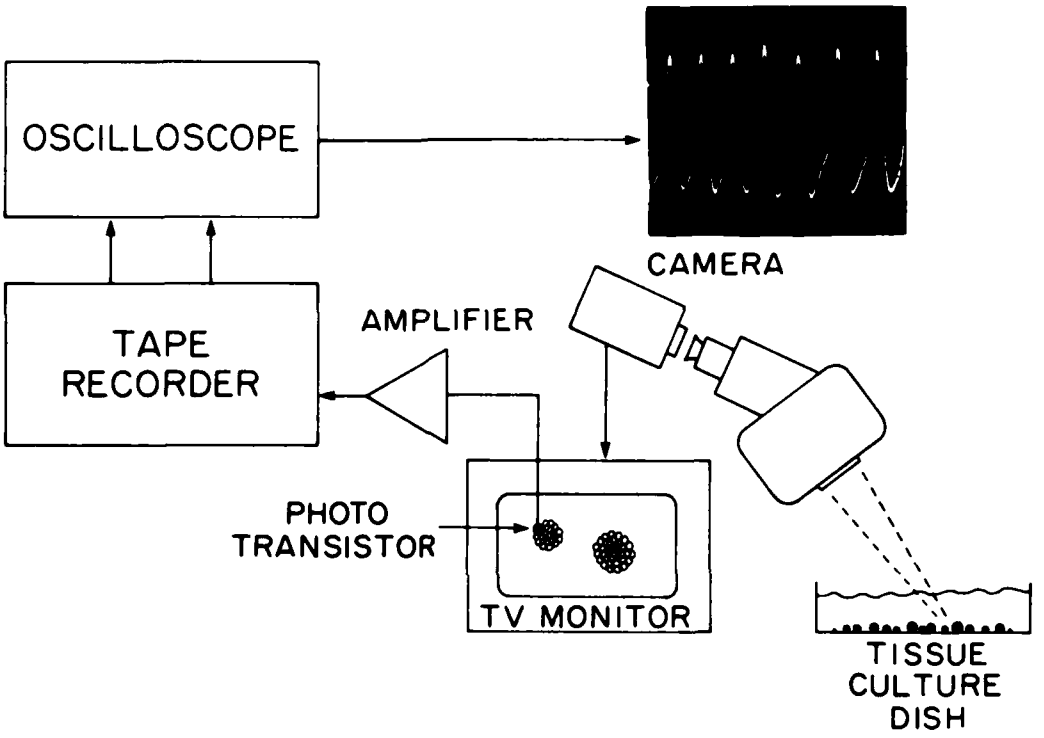

Figure 3. Block diagram of the video recording apparatus used to obtain trains of interbeat intervals. Insert: a typical record of the moving edge of an aggregate, showing the output of the photo-transistor applied to the image on the monitor screen.

combination of intense light source, microscope magnification, and photodetector.

A successful method of imaging aggregates with the TV system was found during the second year of this program. A microscope with high magnification and capable of epi-illumination was used both to illuminate and to view an aggregate on the bottom of a dish through the microscope objective. This system was compatible with the RFR exposure device described in Section III with no modifications necessary. Aggregate images with good contrast filled about a fourth of the TV screen so that a photodetector signal was easily obtained. In fact, individual heart cells could be sharply imaged, opening the possibility of conducting later RFR studies on beat rates of single cells. The basic configuration of this system was also that shown in Figure 3. It was found that a plastic culture dish, and not a Petri dish, had to be used to prevent an aggregate's moving along the bottom of the dish. This movement, apparently a result of aggregate contractile activity, would cause the aggregate's edge to drift from under the photodector. After the development of valid technical details, one successful video RFR experiment was performed during the microscope's loan period and is discussed in Section IV.

For recording electrical activity with microelectrodes in the first year of this program, aggregates were allowed to settle to the bottom of a 35-mm Falcon® plastic tissue culture dish. Aggregates became firmly attached to the dish bottom in about 1 hour and continued beating rhythmically for many hours. A microelectrode pulled from capillary glass tubing and filled with 3M KCl was used to impale an aggregate. Transmembrane potential was amplified by preamplifiers having a very high input impedance and the amplified signal was displayed on a storage oscilloscope and recorded on magnetic tape for later analysis. This equipment is shown in the block diagram of Figure 4 which includes a one-shot used in later studies. In these studies reported in Annual Technical Report No. 1, the action potential parameters analyzed included maximum diastolic potential, maximum positive potential [43], and maximum upstroke velocity which is the largest rate of voltage change during the rapid change to maximum positive potential. In addition, interbeat interval

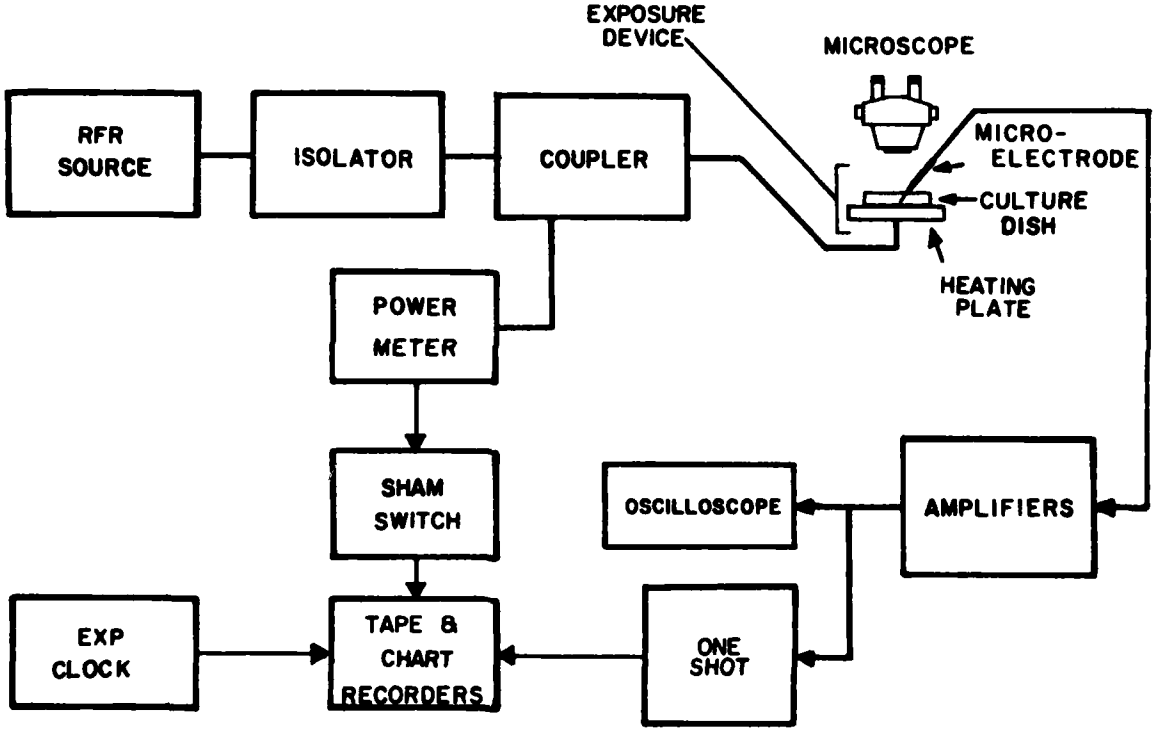

Figure 4. Block diagram of experimental setup. The RFR source consisted of a low-level signal generator, a TWT amplifier, and a PIN modulator when required. The power meter and sham switch provided the RFR which was recorded. The one-shot device was used only with extracellular electrodes.

(IBI), the time between action potentials, was measured. Long-term recording was difficult to achieve with these intracellular microelectrodes so that only small numbers of action potential measurements could be made on a single aggregate.

During the second year of this program, extracellular electrodes were used to record the electrical activity of an aggregate for extended periods, sometimes for several hours. This recording technique allowed larger quantities of IBI data to be gathered than with other techniques. These electrodes were made from glass pipettes, as were the intracellular electrodes, but were much larger. Tip outer diameters ranged from 100 to 200 μm and typical inner diameters were about 15 μm. They were pulled by hand from disposable 20-μl Corning sampling pipettes over an open flame. Tips were inspected under a microscope to insure that a properly shaped blunt tip had been pulled. Electrodes were then filled with either a balanced salt solution compatible with the 818A bathing medium or, later, 818A medium.

For recording with extracellular electrodes, aggregates were allowed to settle to the bottom of a Falcon® plastic Petri dish. Since aggregates did not attach to this type dish, they could be easily moved around on the bottom. To establish extracellular recording, an aggregate was gently pulled to the electrode tip by applying negative pressure to the electrode's fluid. Physical contact was verified by direct observation through the microscope. Care had to be taken not to apply excessive pressure which would damage cell membranes at the region of electrode contact. A good physical seal between aggregate and electrode resulted in a signal of 1-4 mV.

Voltage at the electrode tip was picked up by a silver/silver chloride pellet in the electrode holder fluid and amplified in two stages. The amplified signal was displayed on an oscilloscope but was too fast (200-300 μs) to be recorded on available magnetic tape. To provide a recordable signal indicative of beat occurrence, the electrode signal was made to trigger a one-shot device which provided a 5-volt, 1-200 millisecond pulse for each beat signal. The recorded version of this longer pulse provided a reliable timing signal which could be analyzed later. The

experimental setup was again that shown in Figure 4. A typical amplified electrode signal and a triggered pulse are illustrated in Figure 5.

After a stable electrical signal was obtained, each aggregate was moved to the same location in all RFR experiments by means of the micromanipulator supporting the electrode. All aggregates studied with the extracellular electrode were positioned 1 mm above the Petri dish bottom and directly over an imaginary circle midway between coax conductors. At this elevated location in the bathing medium, SAR gradients were smaller than at the bottom with the electric field oriented in an almost horizontal radial direction.

C. Data Collection and Analysis

During the first year, most data were obtained from intracellular recordings of aggregate electrical activity although one successful video experiment was also performed. For the intracellular experiments, electrical parameters were computed from measurements made on photographs of oscilloscope displays of tape-recorded action potentials. The RFR exposure durations ranged from 21 seconds to 5.3 minutes and most exposures were continuous wave (CW) and pulsed (PW) 2450-MHz RFR. Pulsed RFR consisted of 10.9-microsecond pulses at a repetition rate of 10,000 pulses per second. From first-year experiments described in Annual Technical Report No. 1, it was concluded that RFR exposures with durations on the order of a few minutes were appropriate in aggregate experiments.

Experiments during the last 14 months (second year) of this program included one with video techniques and exposure durations of 8 minutes. For all other experiments, an exposure duration of 3 minutes was used. Capabilities for 16-Hz square-wave modulation and slower 0.8-1.7 Hz gated on-off modulation were added in the second year. Several fixed SAR levels including zero SAR, or sham, were used for aggregate exposures. Exposure levels and shams were randomly ordered in some experiments by using random numbers generated by a hand calculator. The RFR exposure levels and modulations are further described in Section III and, as appropriate, in Section IV.

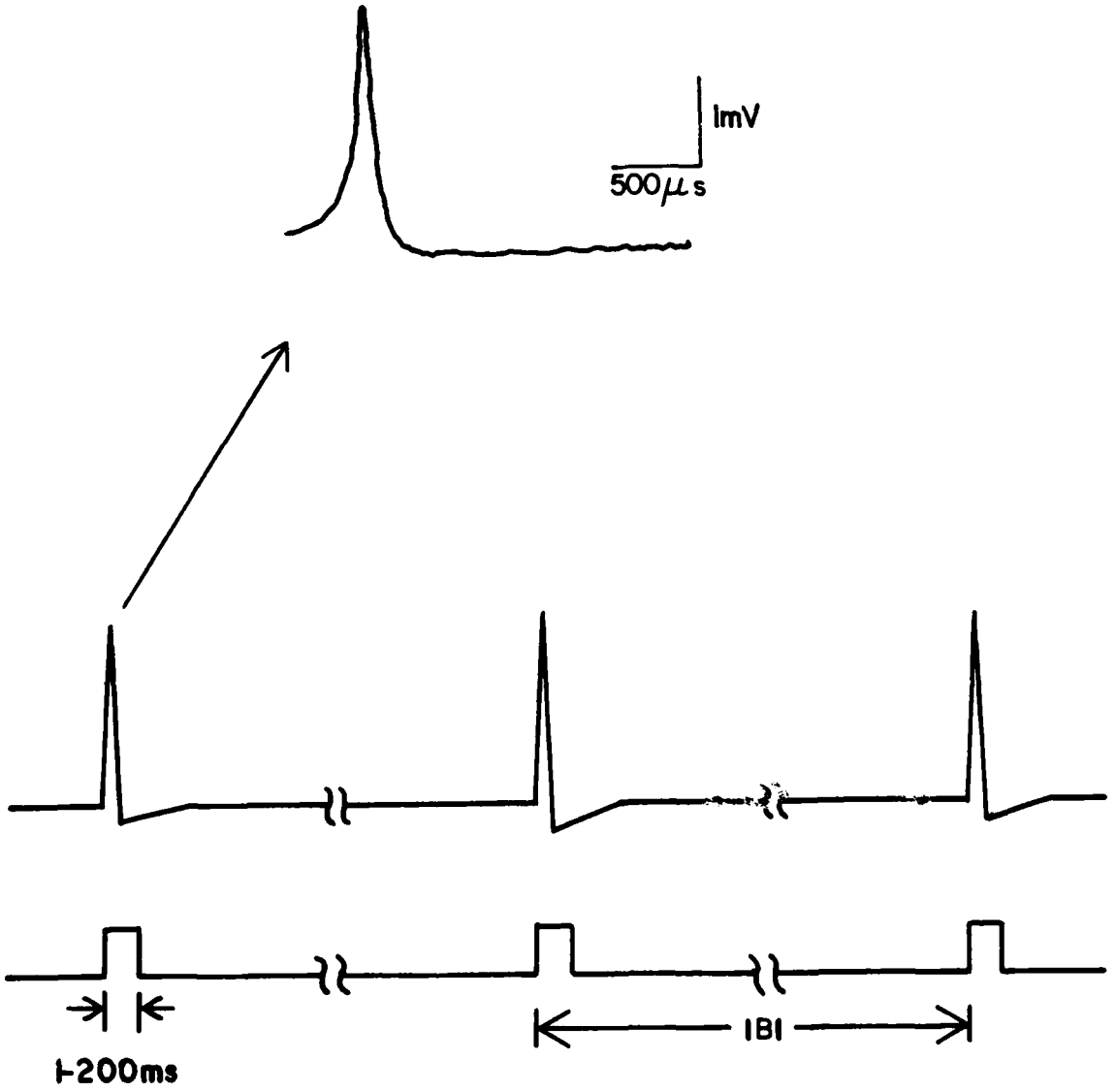

Figure 5. Typical signal from extracellular electrode. Top: Tracing of oscilloscope display of a single extracellular action potential. Bottom: Schematic representation of extracellular action potential and triggered one-shot pulse to show timing relationships.

Timing of RFR exposures during an experiment was simplified in the second year with the use of an experiment clock. Timing with a stopwatch in earlier experiments had caused some inconsistencies in exposure and between-exposure periods. The experiment clock's digital circuit was a free running multivibrator with a period of 190 seconds (approximately 3 minutes). The frequency of this output was divided by 2 to derive an exposure signal which indicated exposure on and off periods. Both clock and exposure signals drove light-emitting diodes (LEDs) which were visible to experimenters. Radiofrequency radiation or sham exposure was applied during a 190-second lighted period of the exposure-signal LED. The 190-second exposures were separated by 190-second periods of no exposure. The clock signal was recorded on magnetic tape along with a signal indicative of a beat occurrence (either photodetector or one-shot output) and a RFR signal. The RFR signal came from the forward power meter, which provided a 0-1 volt signal proportional to forward RFR power to the exposure device described in Section III, and from the sham switch, which was depressed during sham exposures to give a -1 volt signal. The RFR signal was coincident with the exposure signal except for delays in turning on and off RFR and sham exposures. A sketch of clock and RFR signals is shown in Figure 6 which also defines the terminology adopted to describe data analysis periods. Exposure and no-exposure periods consisted of two parts indicated by the experiment clock. The half-period interval just before an exposure was designated PRE; the interval just after an exposure, POST. The POST interval was followed by a POSTPOST interval which was usually the PRE interval for the next exposure. The exposure period itself was divided into the intervals BEG (for beginning) and END. Experimental results are described in terms of these five intervals in Section IV.

Interbeat intervals (IBIs) from video and extracellular-electrode RFR experiments were analyzed in the same way using either the recorded photodetector output or the recorded one-shot output. This analysis procedure as it was applied to first-year video data was briefly described in Annual Technical Report No. 1. It was not necessary to amplify and filter the replayed signal from the second-year video experiment using

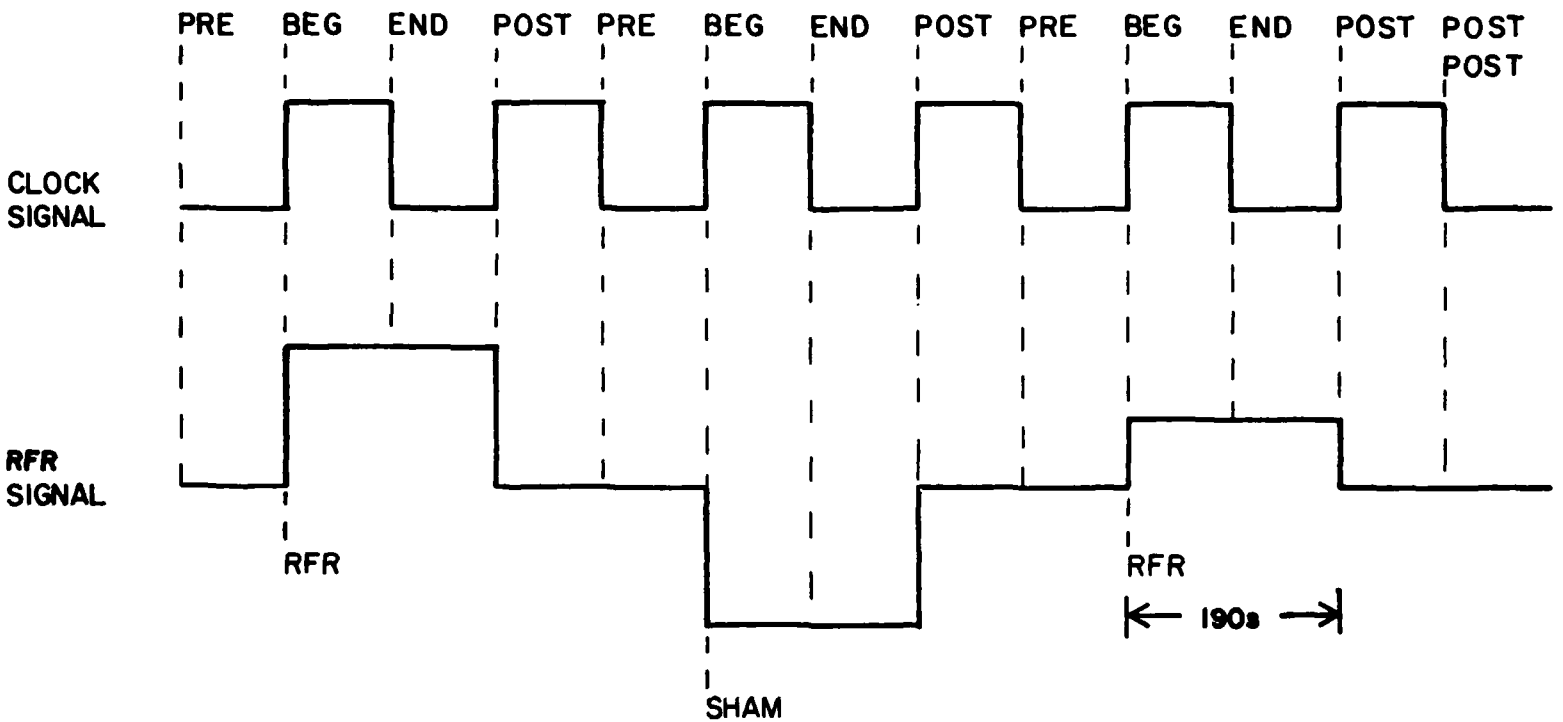

Figure 6. Sketch of the experiment clock and RFR signals showing exposure intervals. These signals were recorded on magnetic tape and stripchart to facilitate data analysis.

the epi-illumination microscope as had to be done with other video data. Thus, because recordings obtained in second-year experiments were fed directly to the computer, there was a much smaller chance of error being introduced at this point in the analysis. The recorded signal was replayed into the Schmitt-trigger level detectors of a DEC PDP-11/40 computer system at Emory University. An existing program was used to sort IBIs into 5-millisecond bins to form a histogram, as had been done previously [41]. For later comparison, a histogram was produced for each interval of each exposure within an experiment and recorded photographically from a CRT display. The variety of IBI distributions is illustrated by the three sample histograms of Figure 7. For each histogram produced, the same computer program was used to create a disk data file of bin contents. At a later time, a newly written computer program accessed this data file and computed several statistical parameters for each histogram. For several experiments, mean IBI (with standard deviation) and coefficient of variation (CV) were later plotted by hand. Also, for these same experiments, mean IBI and CV values were averaged for each exposure condition within an experiment to reduce the influence of occasional spontaneous IBI variations. To remove the effect of variations from exposure to exposure and experiment to experiment, mean IBI and CV values for a particular exposure level and modulation type were normalized to PRE-interval values by dividing all five values (PRE through POSTPOST) by the respective PRE value for each exposure. Normalized IBI and CV were also plotted by hand for these same experiments.

Because of the large amount of computation and plotting necessary to present IBI results, programs for processing these data were written for the Georgia Tech CDC CYBER 70 Model 74-28 computer. Data from the PDP computer printouts were entered through remote terminals. The CYBER system performed computations to normalize and average the data, listed both entered and processed data, and plotted the data by exposure and experiment. These processed data are presented and discussed in Section IV.

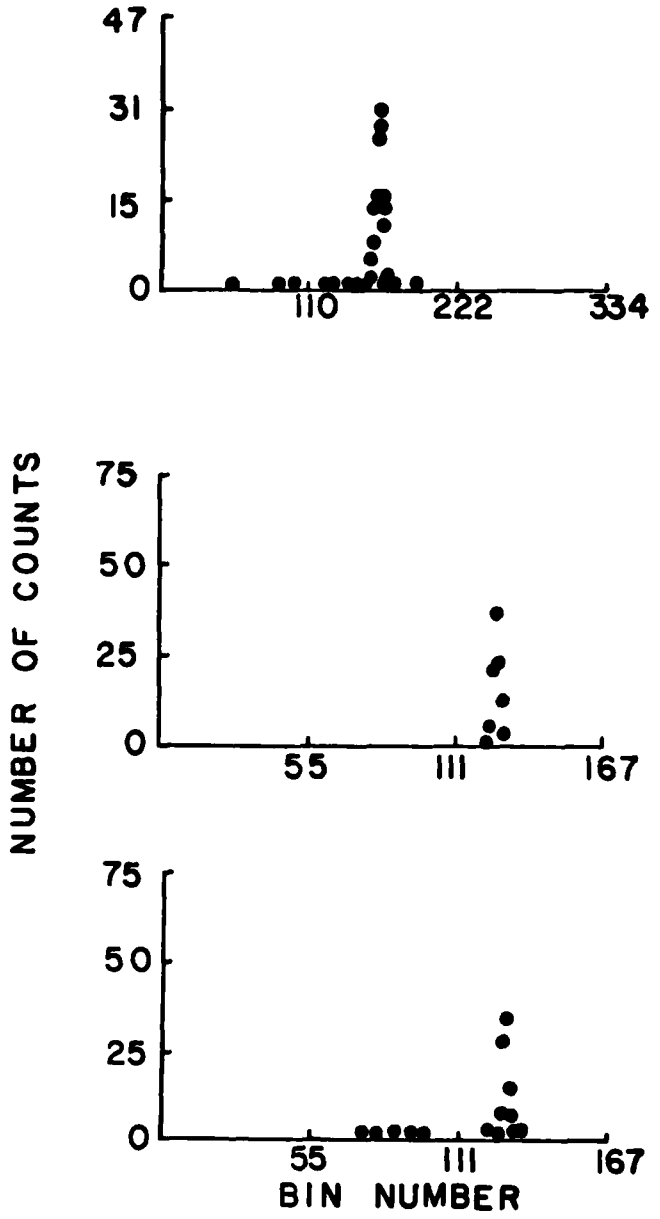

Figure 7. Examples of interbeat interval (IBI) histograms. Each bin was 5 milliseconds wide. IBIs were sorted into bins according to their durations, e.g., bin number 100 contained one count for each IBI of 500 milliseconds.

Several experimental tasks were made easier by the 4-channel strip chart recorder purchased in the second year. It was used to record extracellular electrode output and the triggered one-shot pulse described above on two channels. Experiment clock and RFR signals were recorded on the other two channels. This ongoing record was useful during an experiment as a history of events which could have been missed by observing only the oscilloscope screen and as a guide to trends in the electrode signal which determined experimental manipulations. Information concerning an experiment was also written on the chart to provide a fairly complete record of events for each experiment. This record was especially useful in the Emory computer phase of the data analysis when signals were replayed from magnetic tape and had to be classified according to quality and exposure condition. The chart recorder thus facilitated data analysis and insured its quality.

III. RADIOFREQUENCY RADIATION EXPOSURE SYSTEM

An RFR exposure system was developed to deliver RFR to the cardiac-cell aggregates used in this program. Development of an open-ended coaxial exposure device was accomplished in the first year of the program while its characterization was done during the first and second years. In this section, there is a brief review of the candidate exposure devices, a revised characterization of the open-ended coaxial exposure device, a description of the system used to deliver RFR, and a list of measured dielectric properties of aggregate media. Careful consideration was given to the exposure device and its characterization in order to assure that accurately known doses (SARs) of RFR were delivered to aggregates.

A. Review of Candidate Exposure Devices

It was desired to have an exposure device which would deliver RFR to aggregates under conditions as near as possible to regular electrophysiological recording conditions. For recording from aggregates in Dr. DeHaan's laboratory, the aggregates were normally in bathing medium in a culture dish resting on a circular heating plate. During the first year of this program, five candidate RFR exposure devices were considered to identify a system which was compatible with existing recording practices. Evaluation of these devices was described in Annual Technical Report No. 1 and is briefly reviewed here.

A horn illuminator for free-field exposure and an enclosed waveguide were ruled out early. As well as delivering RFR to the preparation, the horn illuminator would expose microelectrodes and amplifiers to RFR. This exposure was undesirable because of electronic artifacts which would be recorded. Also, high power levels would be required to deliver significant RFR to the preparation. For the preparation enclosed in a rectangular waveguide, significant problems with electrode access and illumination were foreseen and this scheme was not pursued.

The problems seen with the horn-illuminator and enclosed-waveguide methods for RFR exposure led to detailed consideration of a waveguide-slot radiator. In this method, the culture dish was placed over a slot

cut in a sidewall of rectangular waveguide. With RFR applied from the bottom and microelectrodes entering the preparation from above, it was expected that there would be good isolation of the electrodes from the RF fields. However, in order to achieve significant SAR in the bathing medium, the slot had to be made larger than anticipated and radiation fields were established beyond the culture dish. These fields would couple to microelectrodes and amplifiers placed near the culture dish. Also, there was an undesirable alteration of RF fields in the bathing medium when objects in the radiation field beyond the culture dish were moved. Results for a slot in coaxial cable were similar to those for waveguide slots. Various slots and culture-dish configurations were evaluated in terms of SAR in the bathing medium and were described in detail in Annual Technical Report No. 1.

B. Open-Ended Coaxial Exposure Device

After the experiences with the above four exposure devices, three of which involved radiating RF fields, it was decided to investigate a technique in which a RF capacitive field would couple to the bathing medium and the aggregates it contained. In this approach, a coaxial cable opened into an extended ground plane on which the culture dish rested. This ground plane when constructed of brass could incorporate the brass heating plate already used. As described in Annual Technical Report No. 1, it was found that no measurable radiated field existed beyond the culture dish and that more RF energy was coupled to the bathing medium than with the radiating slots for the same net input power. Figure 8 is an isometric projection of the open-ended coaxial device which was fabricated for use in experiments with cardiac-cell aggregates. A section of 1/4-inch semi-rigid cable opened into the circular brass heating plate. The cable's cut end was flush with the upper surface of the heating plate. Another circular brass plate with a hub was attached to the bottom of the regular heating plate to insure structural strength and electrical continuity of the ground plane. The cable's type-N connector which mated with another coaxial cable is not shown in Figure 8. During the second year, a second exposure device was built and differed from the first by the addition of an optic fiber to the cable's

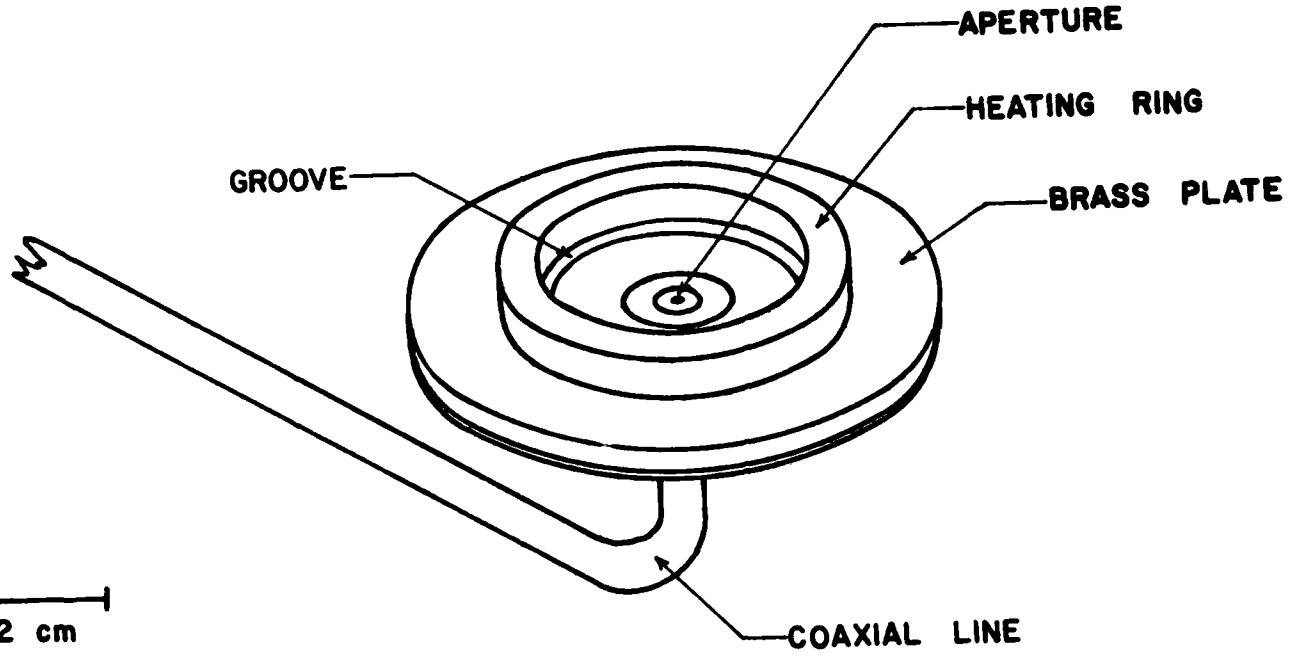

Figure 8. Isometric projection of open-ended coaxial exposure device. The bottom rim of a 35-mm culture dish fitted into the groove for mechanical stability and direct contact of dish and aperture.

dielectric in an attempt to improve visualization of aggregates with video techniques.

The distribution of RF fields in the culture dish in the open-ended coaxial exposure device has been further characterized in the second year by measurements of electric fields and temperature changes. Electric fields were probed with two small antennas fashioned from standard 0.047-inch semi-rigid coaxial cable. One antenna was a vertical monopole 2.7 mm long; the other, a horizontal dipole 2.9 mm long, shorter than the dipole used in the first year. Temperatures were measured with very small thermistors with nonmetallic leads to minimize field interactions [44]. The rate of temperature rise at the onset of RFR at 2450 MHz was used to compute a SAR for each location of the thermistor. Plots of antenna received powers and of the computed SAR derived in the first year were given in Annual Technical Report No. 1. However, near the end of the first year, it was decided to recheck computed SAR values and antenna measurements for two reasons. First, because of the large gradient in field intensity at the bottom of the dish, it was decided to position aggregates 1 mm or more above the bottom and there was insufficient information on fields at these elevated positions. Second, at the review of AFOSR research programs held in San Antonio during January 1980, the need to recheck computed SAR values was identified.

Information for two types of aggregate elevation was required. One type of elevation was required for placing an optical reflector under the aggregate to obtain a video image. A small glass platform (or "shelf") was chosen for this application. The other type of elevation was the aggregate being held in position by an extracellular electrode 1 mm above the bottom of the dish. The dosimetry in the second year was done to specify SAR accurately for these two cases.

Horizontal antenna scans (cuts) were made just above a glass platform in a culture dish containing 4 ml of balanced salt solution. Three parallel scans were made with the diameter of the open-ended coaxial cable perpendicular to these scans taken as the zero position, or center, for each scan. For the vertical monopole, received power was maximum over the center of the coax as shown in Figure 9 and was about 0.26 mW

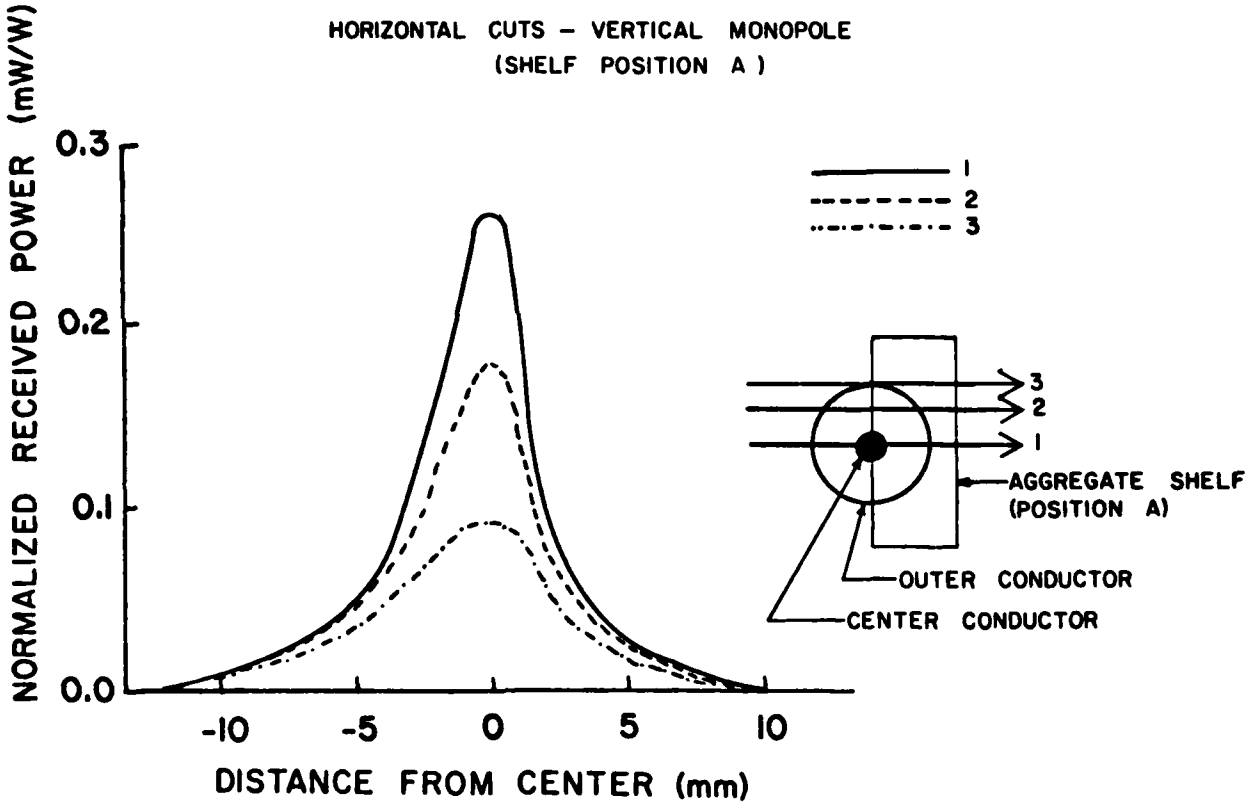

Figure 9. Normalized received power with horizontal scans of monopole over glass platform (shelf). Vertical monopole tip 1.16 mm (shelf height) above the bottom of the dish.

per watt of net input power to the exposure device. The central location of maximum received power agreed with results obtained in the first year without a shelf present. For the horizontal dipole, received power was maximum at about 3.5 mm from the center for a radial scan as shown in Figure 10 and was about 0.38 mW per net watt. Received power for other scans with the dipole showed maxima at about 3 mm from "center" and were comparable to those seen in scans at the same distance from bottom made in the first year.

For extracellular electrode recording, aggregates were suspended 1mm above the bottom of the dish over an imaginary circle halfway between the open-ended coaxial cable's conductors. To study the fields at this location, vertical scans were made with the horizontal dipole and the thermistor. As shown in Figure 11, the received power from the dipole falls off with distance above the bottom of the dish. At 1 mm, the change with distance is about 2.5 times less than at the bottom. This set of measurements confirmed the smaller field gradient at elevated positions which provided more uniform exposure of an aggregate and reduced changes in SAR which might be introduced by positioning errors. Figure 12 shows the SAR determined for 4 positions along this same vertical scan line. At 1 mm, the SAR was 83.5 mW/g per watt of net input power. Since the aggregate could be positioned within 0.1 mm of this location with the extracellular electrodes, positioning error would result in a maximum deviation of about 5% from this value.

Values of SAR were also determined at the bottom of the dish as a function of radial distance from the open-ended coaxial cable's center. As shown in Figure 13, SAR at the bottom decreased from a maximum of 233 mW/g per watt of net input power at the center to 35 mW/g at 3.2 mm from the center. These values were less than the values which had been derived in the first year. For the locations of aggregates on the dish bottom studied in the first year, the SAR was found to be one-fifth of that originally computed and SAR for first-year experimental results should

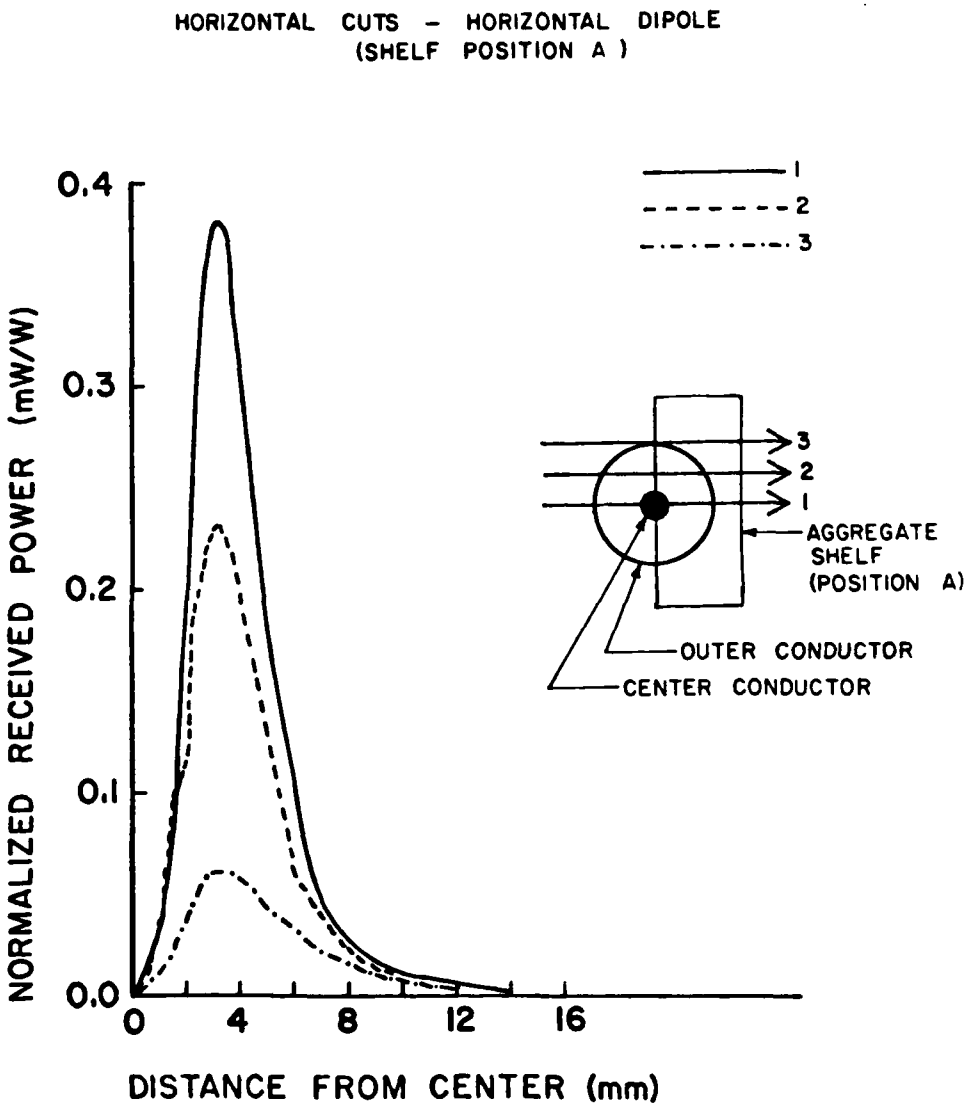

Figure 10. Normalized received power with horizontal scans of dipole over glass platform (shelf). Horizontal dipole 1.16 mm (shelf height) above the bottom of the dish.

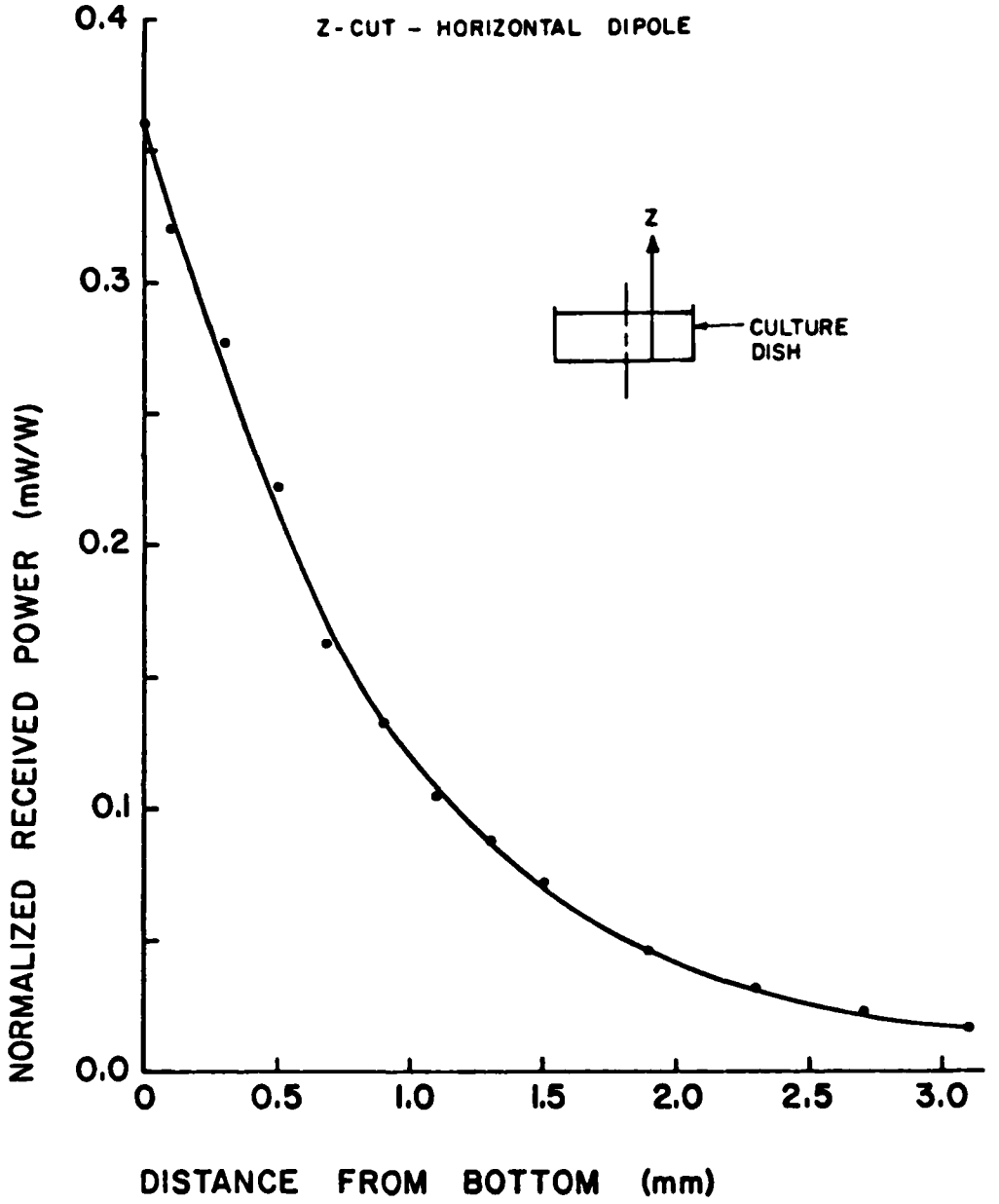

Figure 11. Normalized received power with vertical scan of dipole. . Dipole positioned midway between the center and outer coaxial conductors, radial distance of 1.6 mm.

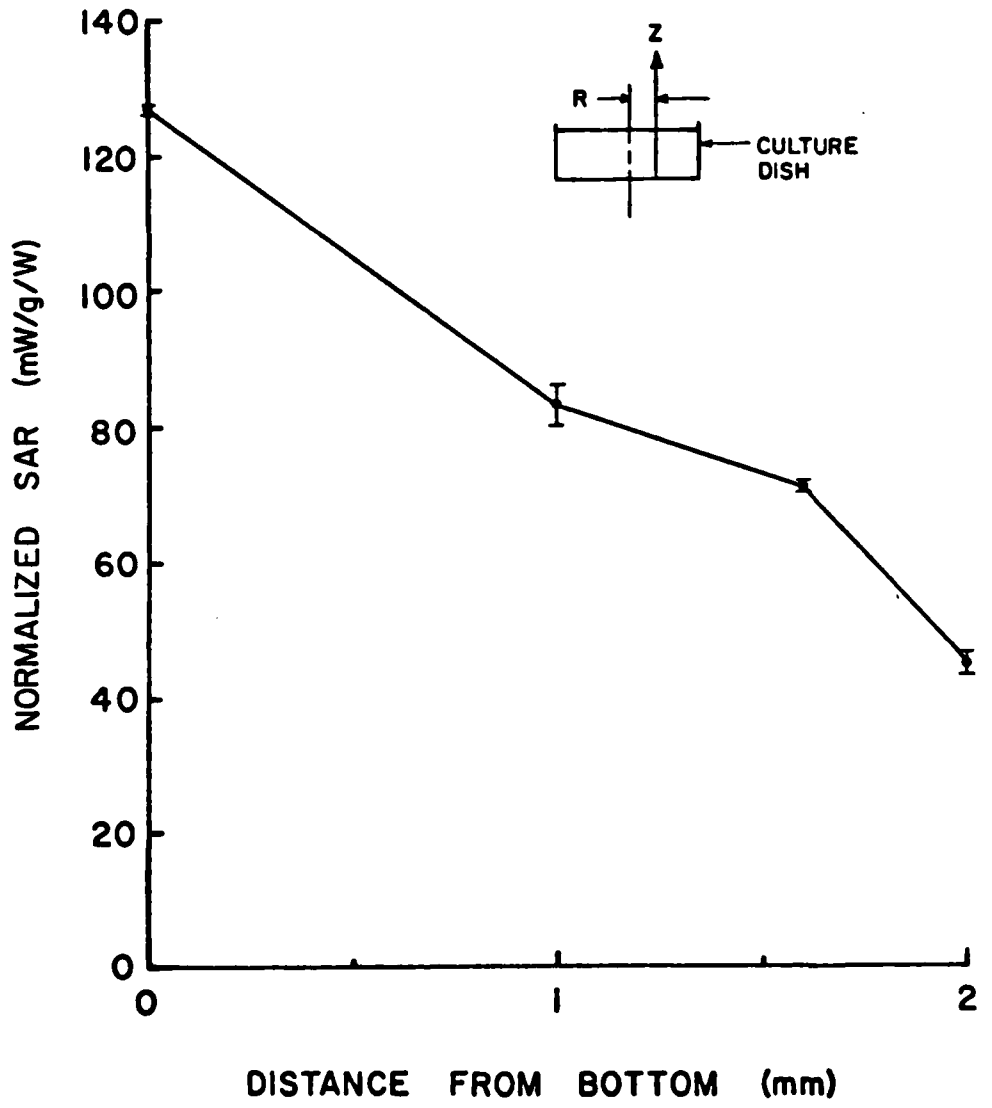

Figure 12. SAR as a function of distance from bottom of the culture dish. Radial distance 1.6 mm, midway between coaxial conductors. Normalized to watt of net input power to exposure device.

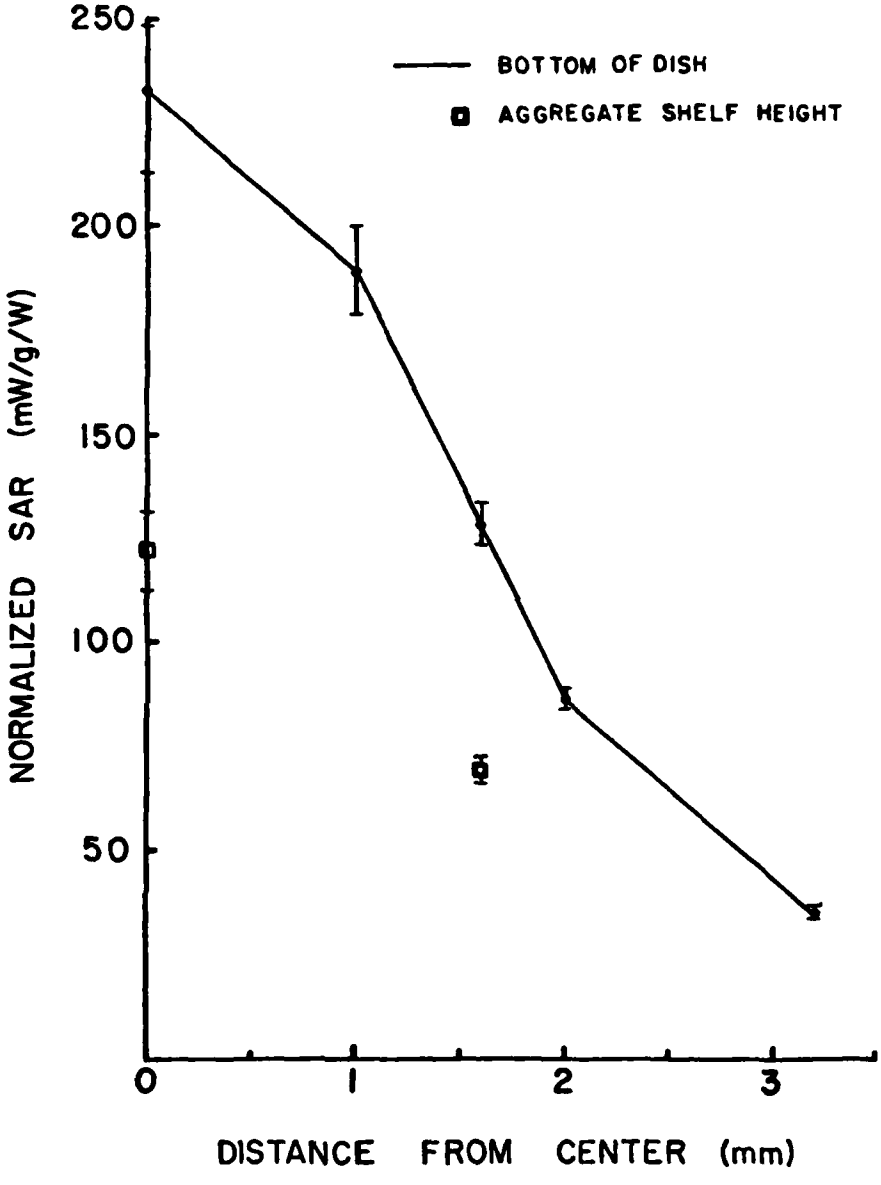

Figure 13. SAR as a function of radial distance at bottom of and at 1.16 mm (shelf height) above bottom of culture dish. Normalized to watt of net input power to exposure device.

be revised accordingly. Thus, in Annual Technical Report No. 1, SAR ranged from 2 to 200 mW/g in Figures 14 and 15 and SAR was 0.4 and 40 mW/g in Figure 16. The more recent SAR data for locations at the height of the shelf used for the video experiment in the first year agreed with SAR derived earlier so that the SAR values in Figures 18 and 19 were found to be accurate.

C. Exposure System Equipment and Modulation Capability

The open-ended coaxial exposure device described above was connected to appropriate RFR sources and measuring instruments to provide a system capable of exposing cardiac-cell aggregates to a variety of SARs and modulations. The system design is general enough to allow exposure of other cellular preparations to RFR at these SARs and modulations and, with minor equipment substitutions, to RF frequencies other than the 2450 MHz used.

A block diagram of the exposure system is part of Figure 4. The RFR signal source provided CW and pulsed PW RF power at a maximum of 1 mW. This power was amplified by a Hughes Model 1177H S-band TWT Amplifier equipped with an isolator to protect its output from reflected power. For later experiments, an HP Model 8731B PIN Modulator was placed between the source and this amplifier to obtain the square wave modulations described below. The TWT Amplifier output was connected by coaxial cable to the exposure device through a Narda 20 dB Bidirectional Coupler which sampled powers transmitted to and reflected from the exposure device. The difference of these powers was the net input power to the exposure device which was used to calculate SAR values. Reflected power was measured at least once for each experiment to assure consistent operation of the exposure device.

All RFR exposures in aggregate experiments were at an RFR frequency of 2450 MHz. Continuous wave RFR was provided by the source and TWT Amplifier and was designated by the letter "C" in the results. In addition to CW RFR, three principal modulations were imposed on the RFR to which aggregates were exposed. Pulsed modulation consisting of 10.9-microsecond pulses at 10,000 pps was available from the source. This PW modulation, with duty cycle of 0.109, was designated by the

letter "P" in the results. With the PIN Modulator driven by a properly offset square wave from a Wavetek Signal Generator, the CW output of the source was square-wave modulated at 16 Hz and was designated by the letter "M" in the results. Slower square-wave modulation (or gating), usually at 1.6 Hz, with the PIN Modulator was designated by the letter "G" in the results. In the first year, 60-millisecond pulses at 1.5 pps were called gated CW.

D. Medium Dielectric Properties

Measurements of the dielectric properties of the media used with the cardiac-cell aggregates were performed using a probe technique previously developed at Georgia Tech [45]. The dielectric properties were expressed as dielectric constant, conductivity, and loss tangent. They were measured for 818A culture medium and a balanced salt solution at a frequency of 2450 MHz for temperatures between 24 and 40°C. Dielectric properties of the two media were similar over this temperature range, except for higher dielectric constant for the culture medium at higher temperatures, as seen in Tables I and II.

These dielectric properties were important to obtain for possible future determination of RF field distribution in the culture dish using analytical methods. Such an analysis will provide a valuable basis for verification of the experimental measurements reported here. The similarity assured that the antenna field measurements in balanced salt solution were representative of fields in 818A medium used most often in aggregate experiments. Also, the physical interaction of electromagnetic fields with cardiac-cell aggregates in bathing medium depended on the dielectric properties of the aggregates and of the medium. Theoretical consideration of the interactions will require knowledge of the dielectric properties of both.

TABLE I

DIELECTRIC PROPERTIES OF AGGREGATE CULTURE MEDIUM 818A

Temperature (°C)	Dielectric Constant	Conductivity (mmho/cm)	Loss Tangent
24	75.3	30.43	.296
26	74.7	30.27	.297
28	73.9	30.06	.298
30	72.4	29.69	.301
32	70.5	29.22	.304
34	67.7	27.99	.303
36	64.6	27.29	.310
38	61.3	26.04	.312
40	58.8	25.01	.312

TABLE II

DIELECTRIC PROPERTIES OF BALANCED SALT SOLUTION

Temperature (°C)	Dielectric Constant	Conductivity (mmho/cm)	Loss Tangent
24	73.8	30.24	.301
26	72.3	29.85	.303
28	68.9	29.02	.309
30	65.9	28.30	.315
32	62.8	27.26	.319
34	58.5	25.89	.325
36	53.9	24.02	.327
38	49.1	22.23	.332
40	45.2	20.77	.337

IV. EXPERIMENTAL RESULTS

A. Radiofrequency Radiation Effects on Aggregate Interbeat Interval

The open-ended coaxial exposure device described in Section III was used to expose cardiac-cell aggregates to a variety of RFR SAR levels and modulations. During the first year, several experiments were performed with intracellular electrodes to record aggregate transmembrane potential. The results of those experiments have been described in detail in Annual Technical Report No. 1. Briefly, changes were observed in action potential maximum upstroke velocity (MUV) and interbeat interval (IBI) while no changes were observed in other parameters. Exposures were mainly to CW and PW RFR with a few gated-CW exposures. Exposure durations ranged from 21 seconds to 5.3 minutes. When the manually extracted data from several experiments were pooled, MUV and IBI showed apparent increases in variability during RFR exposure. These increases occurred in the SAR range of 10-40 mW/g using revised SAR values. An experiment with six 30-second exposures to CW RFR at 0.4 and 40 mW/g (using revised SAR values) and with 13 sham exposures was conducted to investigate changes in MUV and IBI. Small changes in mean values consistent with the previous pooled data were found but were not statistically significant because of the large overlap of data values.

It was decided at this time to pursue the investigation of possible RFR effects on the variability of beat rate. It was clear that if there was an RFR effect on aggregates at the SAR levels being investigated, it was a small, or subtle, one on the parameters observed. To reveal small effects, large numbers of IBIs were desired for averaging and statistical testing. Thus, in the first year, an extended experiment using video recording techniques was carred out with 5-minute exposures to several SAR levels of CW RFR. As described in Annual Technical Report No. 1, Figures 18-20, decreases in IBI occurred for about 4 mW/g and larger SAR. Changes in variability, expressed as the coefficient of variation, were not consistent for exposures at the same SAR for 0.3 to 31.1 mW/g.

The relationship between aggregate beat rate (BR) and interbeat interval should be noted at this point. Results in Annual Technical

Report No. 1 were given as changes in BR or IBI. Results for the second year described below are for IBI. The shift to IBI was due mainly to the ease of analyzing IBI with existing computer programs. With IBI given in milliseconds, the BR in beats per minute is easily found from

$$BR = 60{,}000/IBI. \quad (1)$$

Conversely, IBI in milliseconds is given by

$$IBI = 60{,}000/BR. \quad (2)$$

Thus, one parameter can easily be changed to the other. For example, an aggregate with an IBI of 500 milliseconds has a BR of 120 beats per minute. Due to the reciprocal nature of this relationship, a small change of, say, less than 5% in one parameter gives a similar but opposite change in the other. For example, a 4% decrease in IBI is equivalent to a 4.2% increase in BR.

At the beginning of the second year, it was decided to pursue the long-term recording of IBI using video techniques to clarify possible RFR effects on IBI variability. However, because of the technical difficulties described in Section II, the success of the first-year video experiment could not be repeated with then-available equipment. One successful video experiment using a borrowed epi-illumination microscope is included below as experiment G. Only a limited number of RFR exposures were carried out during this experiment. Also, SAR was not determined for this system in which the microscope objective was immersed in the bathing medium approximately 2 mm above the aggregate. Because of the limited data and undetermined SAR in this experiment, it's results were considered preliminary. However, it was shown that this system provided a noninvasive method for recording IBI during RFR exposure. Because of the various difficulties encountered with video recording methods, alternate recording methods were pursued.

Successful long-term recording of aggregate electrical activity was obtained in several experiments using extracellular electrode techniques.

Because of the vertical approach of an electrode and the essentially horizontal RF electric field at the aggregate, it was expected that very little RF-induced artifact would be recorded. This was indeed the case since with the high amplifier gains associated with extracellular recording, a small induced potential of 40 μV referred to the electrode tip was seen with aggregate SAR of 84 mW/g. The source of this potential was not investigated but was presumed to originate at the electrode tip.

Table III is a summary of second-year experiments which were encoded alphabetically, A through L. Except for experiment G in which video recording was used, results were obtained using extracellular electrodes. The experiment code in Table III consists of the experiment letter code and the number of the aggregate in that experiment which was exposed. Results were obtained from two aggregates in experiments E and K. Table III presents the number of RFR exposures by level and modulation for each exposed aggregate. The modulation code is explained in Table III as well as in Section III. The RFR level is given as the power meter reading (in μW) of sampled forward power to the exposure device. This reading was 40 dB down from the forward power, i.e., a 200-μW reading represented 2 W of forward power. As described in Section III, the average forward power and the average reflected power were used to calculate aggregate SAR. Sham exposures during which no RFR was applied to aggregates were conducted for each experiment and are designated by "SH" in Table III.

For most experiments, bulk temperature measured with a YSI thermistor outside the RF field was a nominal 37°C and did not deviate more than 0.3°C from the average temperature within an experiment. Aggregate L1 was exposed to RFR at bulk temperatures of 37°C and 28°C. Sham exposures at 36°C were performed in experiments B and E and at 38°C in experiment B.

In experiment D, 0.1% bovine serum albumin (BSA) was added to the bathing medium in an attempt to reduce the incidence of rapid beating. The BSA caused a slowing of BR over the course of the experiment. This slowing corresponded to a progressive lengthening of IBI which precluded results from experiment D from being compared to results from other experiments. Results from experiment D were not used for data reported here.

TABLE III

NUMBER OF EXPOSURES BY RFR AND TEMPERATURE CONDITION

Experiment	T28	T36	T38	SH	10C	10P	60C	60P	60M	60G	70C	70P	200C	200M	200G	400C	600C
A1				5	3												3
B1		2	2	10	3	3					3	3					
C1				5							6	5					
D1 (BSA)				6	3	3					3	3					
E1		3		4	3							3					
E2				3		3											
F1				3							3	4					
H1				6	3	3	3	3									
I4				3			3	3									
J6				6					4	3			3	3	3		
K1				3			3		3	3			1	1	2+1*	1	
K3				3					3	3					1**		
L1				3									3	3	3	3	
L1 ($28^{o}C$)	3												3		3***	3	
G1 (Video)				2			2	2									

Notes: T28, T36, T38 indicate sham exposures at 28, 36, and 38 ^{o}C, respectively.
All other exposures were at 37 ^{o}C, except for those in second line of L1 which were at 28 ^{o}C.

SH = sham exposure, no RFR applied
C = continuous wave, not modulated
P = pulse modulated, 10.9μs pulses at 10 kpps
M = square wave modulated at 16 Hz
G = square wave modulated, or gated, at 1.6 Hz, unless noted otherwise as follows:
* 1 at 1.0 Hz, ** 1.7 Hz, and *** 0.8 Hz

Experimental conditions and procedures were those described in Section II. Aggregates used in these experiments were measured to be 150-200 μm in diameter. Experiments A through F were conducted in the fall and early winter of 1980 using aggregates cultured for 2 days, except for experiment A in which 4-day aggregates were used. Experiments G through L were conducted in the spring of 1981 using aggregates cultured for 3 days. For the analysis of IBI, 100 IBIs were usually used for each experimental interval (PRE through POSTPOST) at 37°C. However, 50 to 90 IBIs were used for experiments E, F, and H. For slower BRs in experiments D with BSA and L at 28°C, 30-to-80 and 60 IBIs were used, respectively.

A uniform format was adopted for plotting the mean IBI and CV data derived from the histogram analysis of IBI. The plots were generated by the Georgia Tech CDC CYBER 70 Model 74-28 computer system using a Versatek plotter. Figures 14-16 show results from experiment A, with each figure containing the results from a different RFR-exposure condition. The experimental conditions for each of these figures and the figures which follow in this Section are denoted in the title in the following sequence:

- experiment identifier, as given in Table III;
- nominal bulk temperature, in degrees Celsius preceded by the letter T;
- RFR level and modulation, using the system of Table III explained above; and
- SAR at the aggregate, calculated in mW/g from forward and reflected powers.

The RFR levels given in these figures are exact readings from the power meter and are sometimes slightly different from the nominal values used in Table III. For example, exposures designated by 60P in Table III were done using 57 and 58 μW readings. The difference between designated values in Table III and actual values were due to an inability to set the RF source output attenuator accurately and repeatably and, in some cases, to a decrease in the power output capability of the TWT Amplifier. The SAR values were calculated from actual power readings.

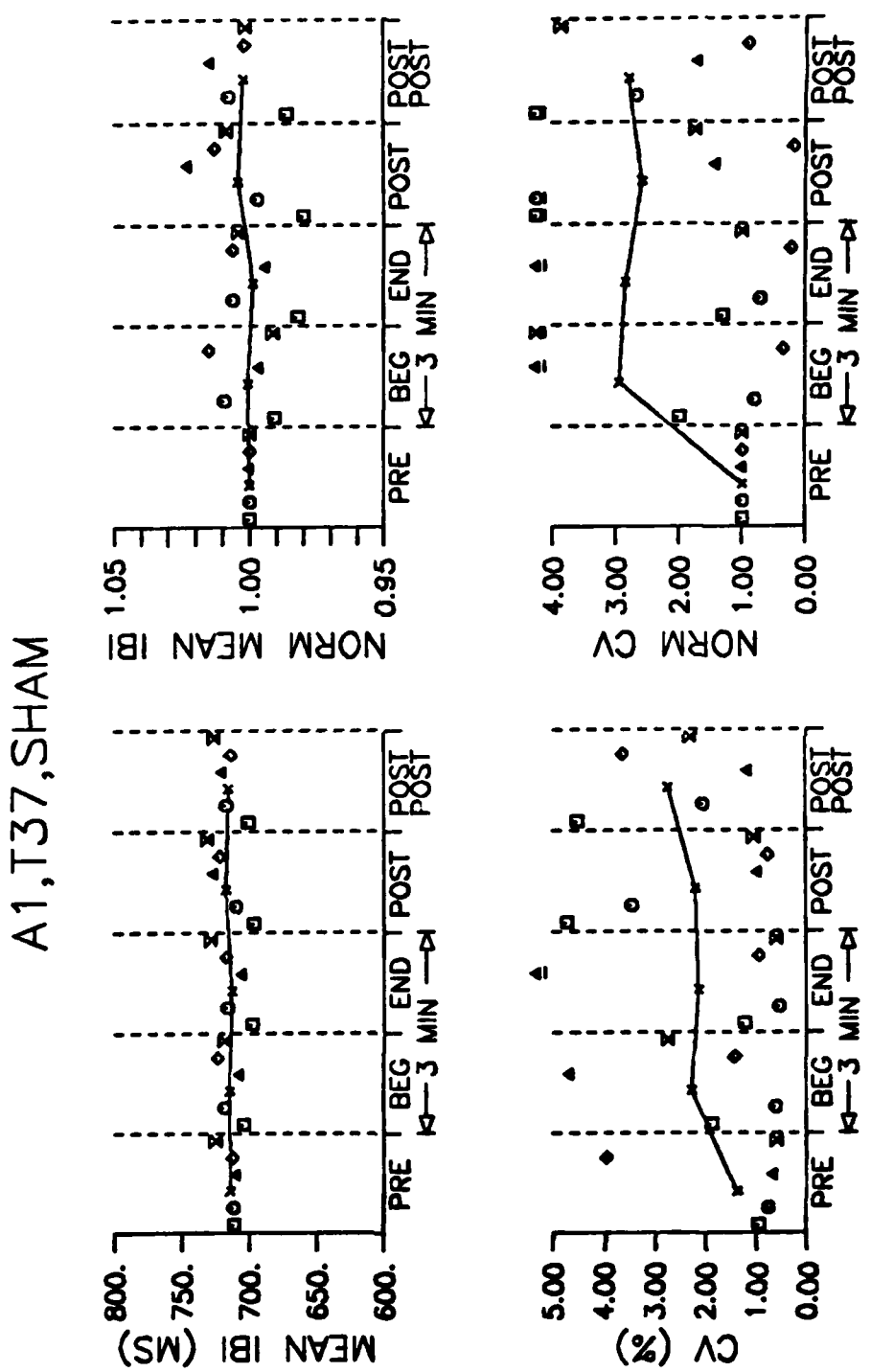

Figure 14. Results from experiment A, sham exposures.

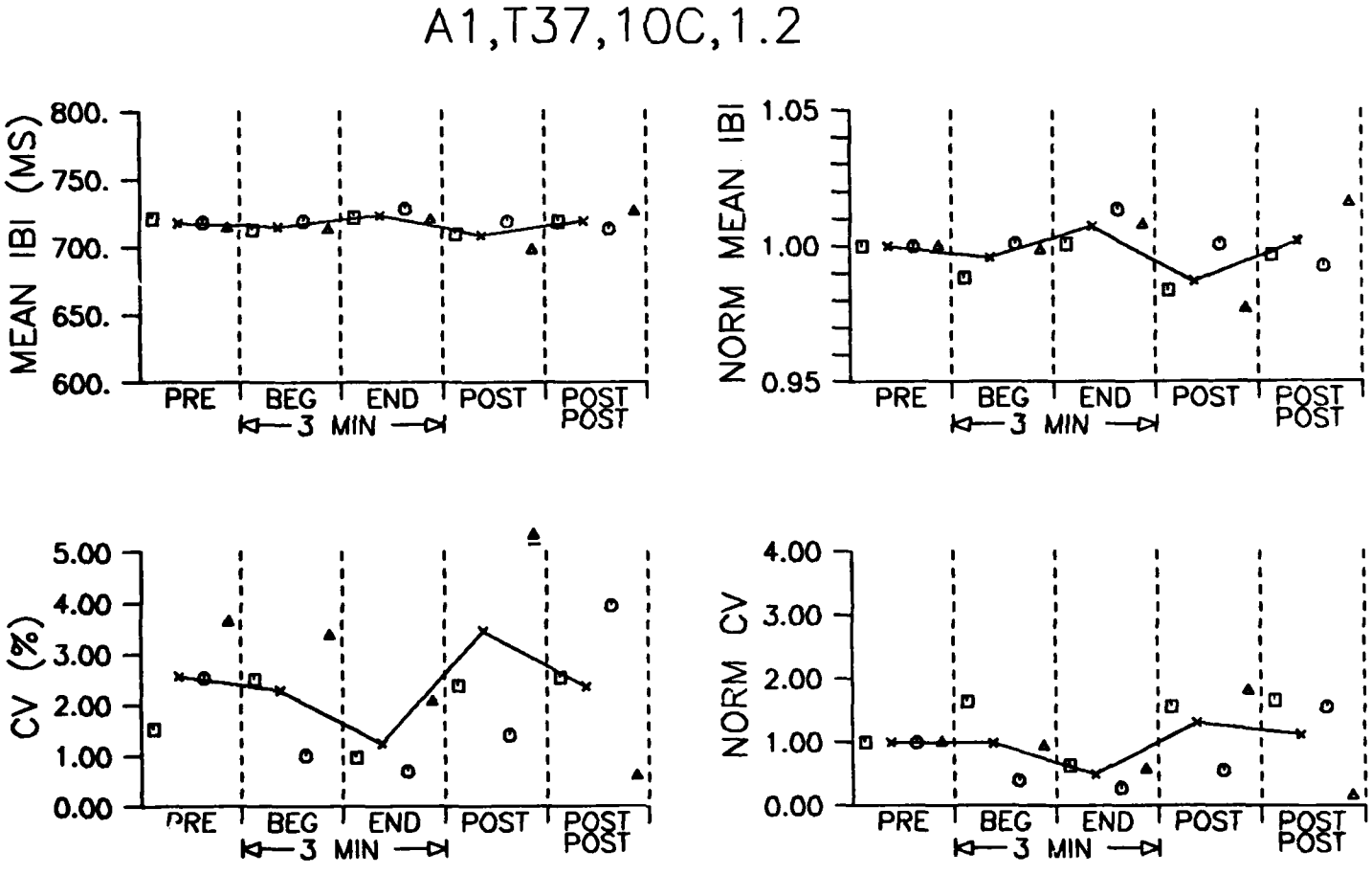

Figure 15. Results from experiment A, exposures to 1.2 mW/g CW.

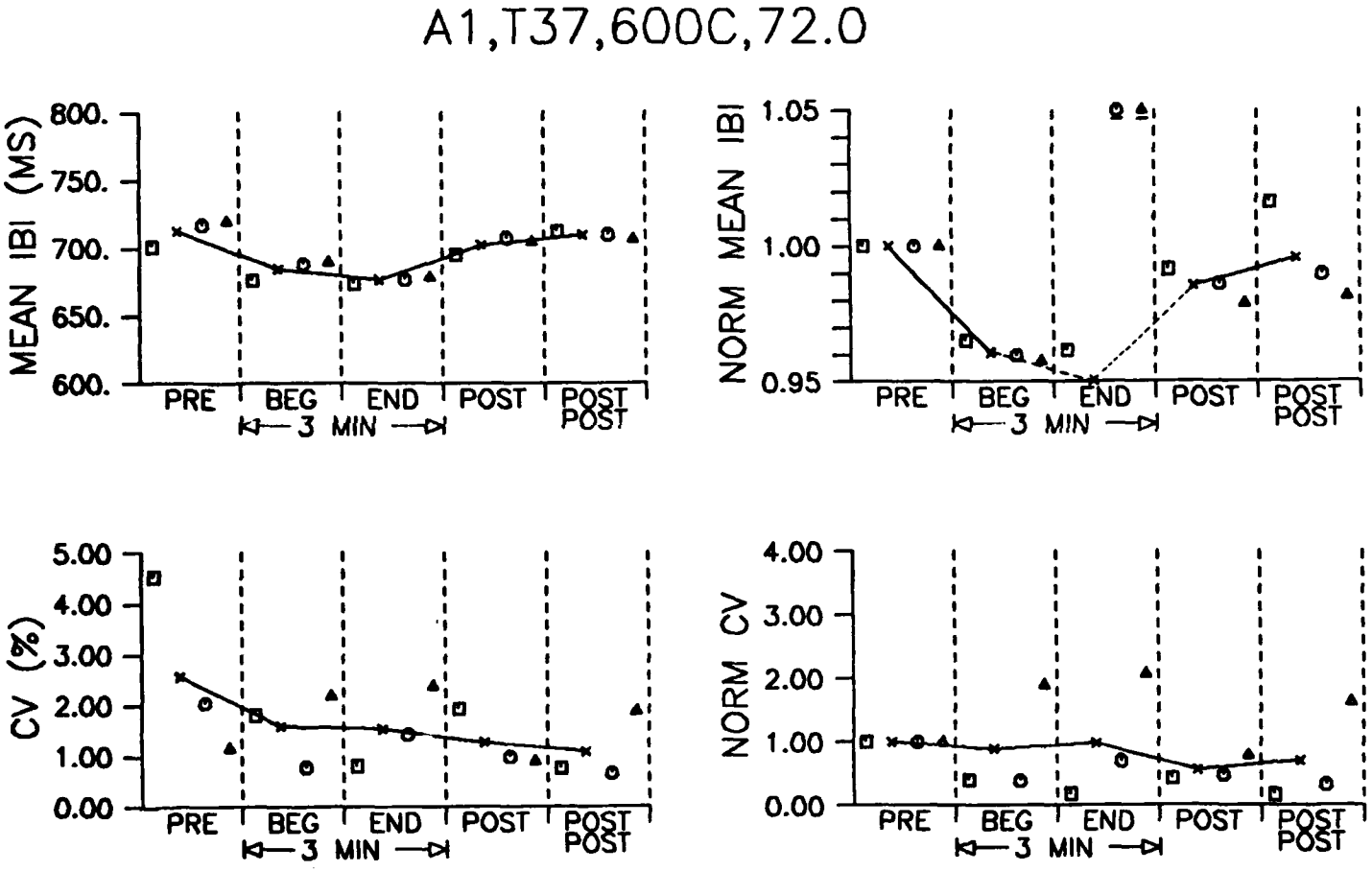

Figure 16. Results from experiment A, exposures to 72.0 mW/g CW.

Four individual plots are given in each figure illustrating IBI results (e.g., Figure 14). The two plots on the left show the mean IBI and CV, top and bottom, respectively, derived from computer analysis of tape recorded data. For each parameter, a value is given for each of the five intervals associated with each exposure. Results from each exposure in an experiment are represented by the same symbol in the plots. A maximum of six symbols were available to represent six different exposures. Average values for each interval are indicated by x's which are connected by lines in each plot. Off-scale values are shown by underscored points above a plot. Exposure temporal sequence is represented left to right in each interval. The two plots on the right show the normalized mean IBI and normalized CV values derived by procedures described in Section II. The same symbol coding for exposures is retained in these plots.

Figures 14-16 show data for 5 sham exposures, 3 exposures to 1.2 mW/g CW RFR, and 3 exposures to 72.0 mW/g CW RFR, respectively, in experiment A. For individual sham exposures (no RFR), mean IBI varied from PRE-exposure values by less than 2% (Figure 14). Averaged across the 5 sham exposures, mean IBI changed less than 0.5% from the PRE-exposure averaged mean IBI. The CV for this aggregate was quite variable, ranging from about 0.6% to greater than 7%, as seen in the CV plot of Figure 14. In the plot of normalized CV, it is seen that, on the average, CV increased to about three times its PRE-exposure value. For exposure to 1.2 mW/g CW RFR (Figure 15), mean IBI, on the average, increased by 0.7% during exposure (END) and decreased by 1.3% just after exposure (POST). The CV was again variable but, on the average, decreased to about one-half of the PRE-exposure average value during END and increased to about 1.3 times during POST. For exposure to a larger SAR of 72.0 mW/g of CW RFR (Figure 16), mean IBI decreased by an average 4% and 5% during BEG and END intervals with 1.5% reduction remaining during POST. The CV was smaller here than in Figures 14 and 15 and showed a reduction to 0.56 and 0.71 of PRE-exposure average CV during POST and POSTPOST.

Figures 17-19 show data for 3 exposures each to sham, 12.2 mW/g CW RFR, and 12.2 mW/g PW RFR, respectively, in experiment I. For sham exposure (Figure 17), averaged mean IBI changed by 0.6% across the five intervals and CV, ranging mostly between 2% and 3%, on the average was within 1 and 1.25 of the PRE-exposure average. For exposure to 12.2 mW/g CW RFR (Figure 18), averaged mean IBI changed by less than 0.5% across all intervals and averaged CV increased to about 1.8 times the PRE-exposure average during END. For exposure to 12.2 mW/g PW RFR (Figure 19), averaged mean IBI decreased by 0.5% during exposure (BEG and END), by about 2% during POST, and by about 1% during POSTPOST. The CV had PRE values between 2% and 3% which were comparable to sham-exposure values. Averaged CV increased by 1.2 times during BEG, 2.4 times during POST, and 1.2 times during POSTPOST. All three individual POST values were greater than PRE-exposure values while one individual value each for BEG and POSTPOST was greater.

Figures 14-19 show the results from experiments A and I. In addition, they show the difficulty of analyzing IBI data on an experiment-to-experiment basis when mean IBI and CV values were variable among exposures to the same RFR or sham conditions. As many as possible exposures to one condition were done for each experiment. However, practical considerations usually allowed about 3 exposures to each of a few conditions during an experiment. In order to reduce the effects of variable mean IBI and CV during an experiment, the results for similar RFR exposures from different experiments were combined. This was done by averaging the averaged mean IBI and averaged CV values from all exposures to the same RFR condition. This second level of averaging combined data from each column in Table III by utilizing the same computer programs which averaged and plotted results for individual experiments.

Inter-experiment averaging was done separately for fall experiments and spring experiments for two principal reasons. First, as described in Section II, IBI was less regular in the fall and was reflected in higher CVs for fall experiments than for spring experiments. Second, between fall and spring experiments the cable connecting the bidirectional coupler to the exposure device was changed and caused a different power

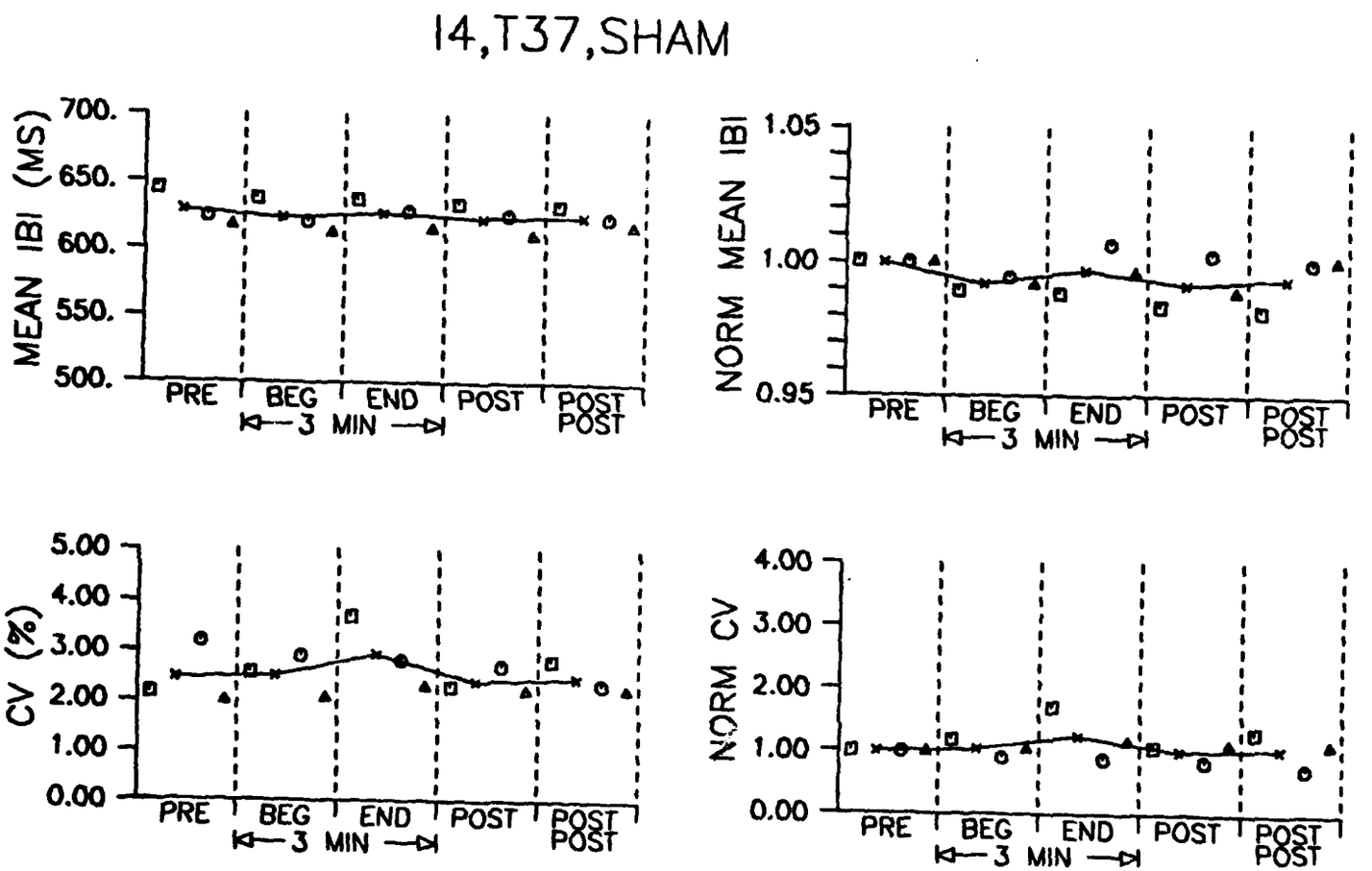

Figure 17. Results from experiment I, sham exposures.

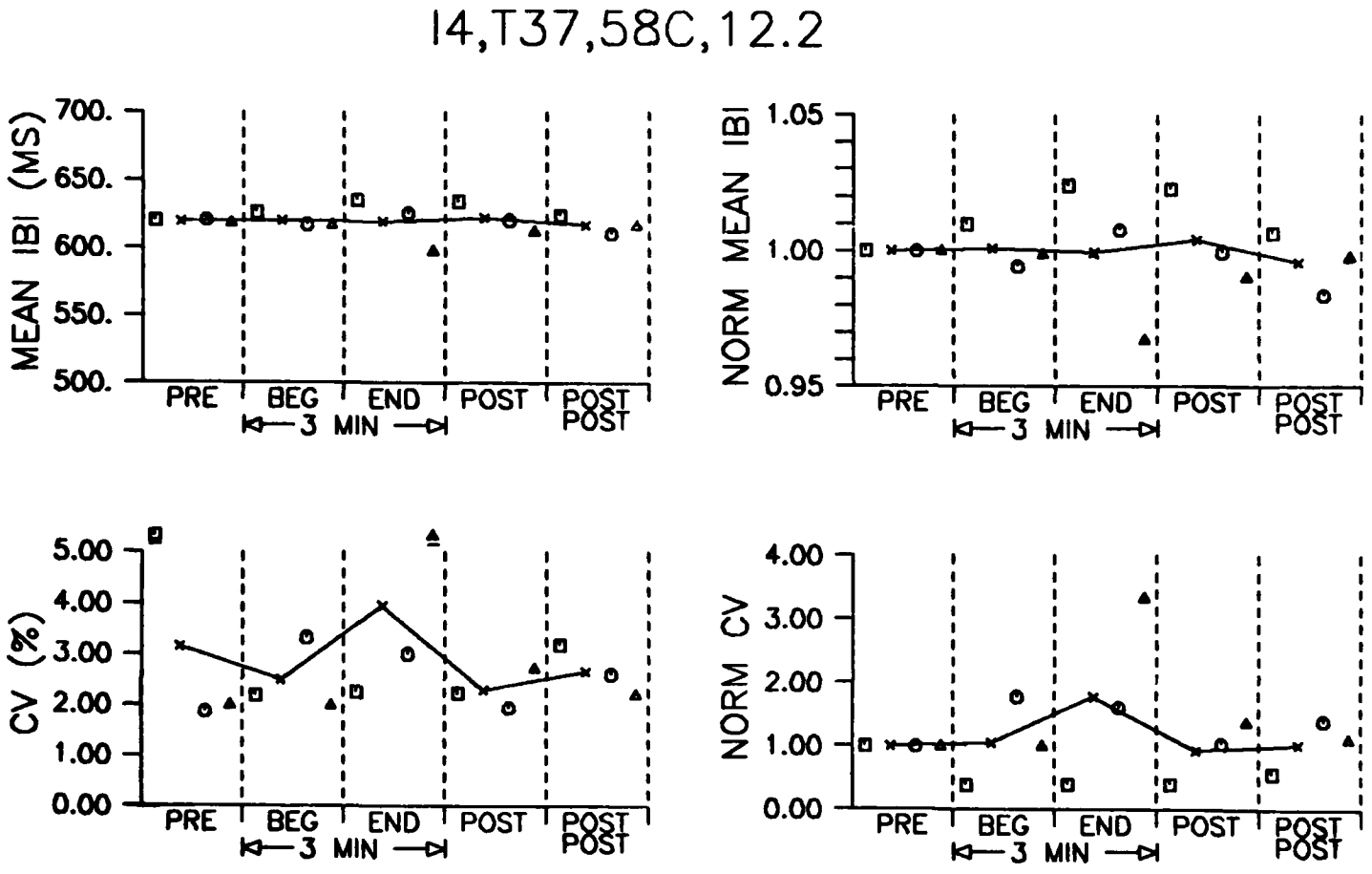

Figure 18. Results from experiment I, exposures to 12.2 mW/g CW.

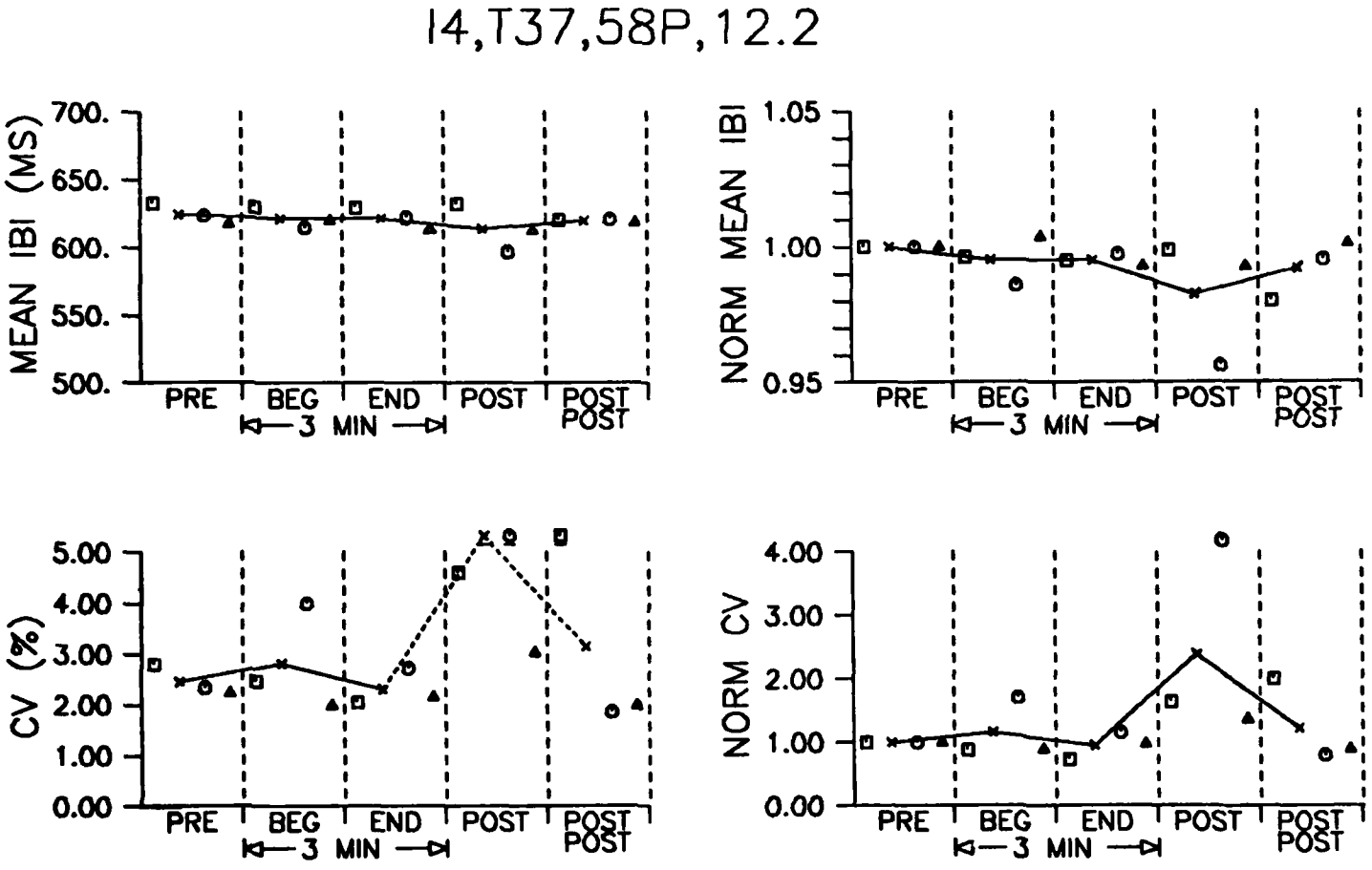

Figure 19. Results from experiment I, exposures to 12.2 mW/g PW.

to be reflected from the exposure device for the same forward power resulting in a different SAR for the same power meter reading. An additional difference between fall and spring experiments was in the antibiotic used in the culture medium, as described in Section II.

Results for similar RFR exposures in fall experiments A, B, C, E, and F at 37°C were averaged and results for similar RFR exposures in spring experiments H through L at 37°C were averaged. Results from experiment D were not included because of the dominant slowing caused by BSA. It should be noted that the results from each experiment were weighted equally regardless of number of exposures within an experiment.

Figures 20 through 24 present results averaged for fall experiments. For each figure, experiments are represented by different symbols. Figure 20 shows the results of sham exposures for the 6 fall experiments with 3 to 10 exposures each. Mean IBI range was different for each experiment: a minimum of 627 to 639 milliseconds (off-scale points) for experiment C and a maximum of 875-910 milliseconds for experiment E2. Averaged across the experiments, normalized mean IBI changed less than 1%. For individual experiments, average CV within an exposure interval of 95 seconds ranged from 1.01% to 8.47%. Averaged across experiments, CV was in the range of 2.2% to 4.9% and the normalized CV ranged between 0.85 and 1.6 times PRE-exposure values.

Figure 21 shows the results of exposures to 1.2 mW/g CW RFR for 3 fall experiments. Averaged across the experiments, normalized mean IBI increased by about 1% during END while normalized CV increased slightly during BEG, decreased to 0.387 during END, and increased after exposure to 1.37 during POSTPOST. Figure 22 shows the results of exposures to the same SAR of 1.2 mW/g for PW RFR in 2 fall experiments. Averaged for the experiments, normalized mean IBI increased during and after exposure by a maximum of 1.6% during POST while normalized CV decreased with a minimum of 0.468 during POST.

Figure 23 shows the results of exposures to 8.4 mW/g CW RFR for 3 fall experiments. Averaged across the experiments, normalized mean IBI decreased by about 2% during END with a smaller decrease during BEG while normalized CV increased to 1.85 and 1.67 during END and POST and

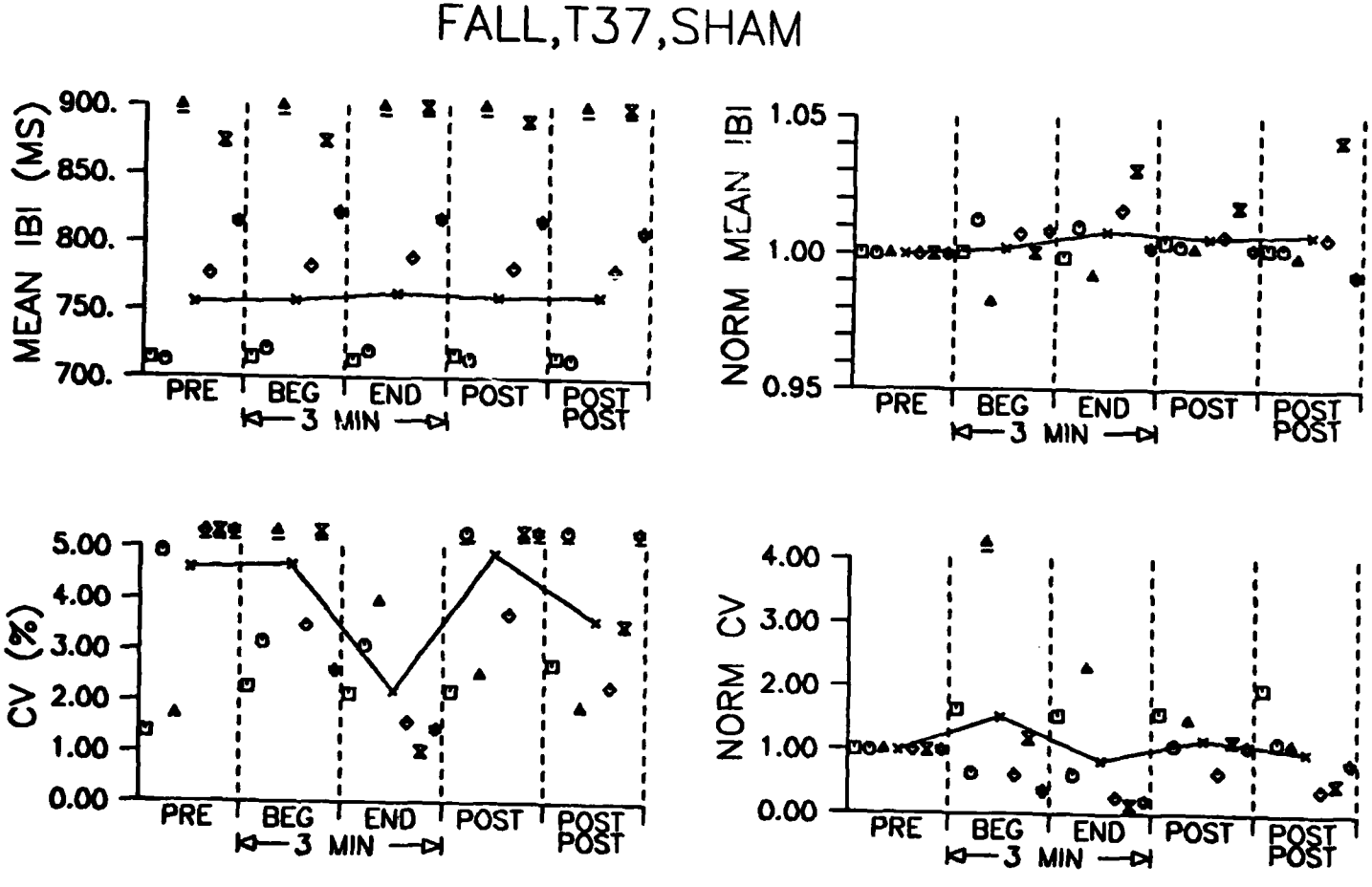

Figure 20. Results from fall experiments, sham exposures.

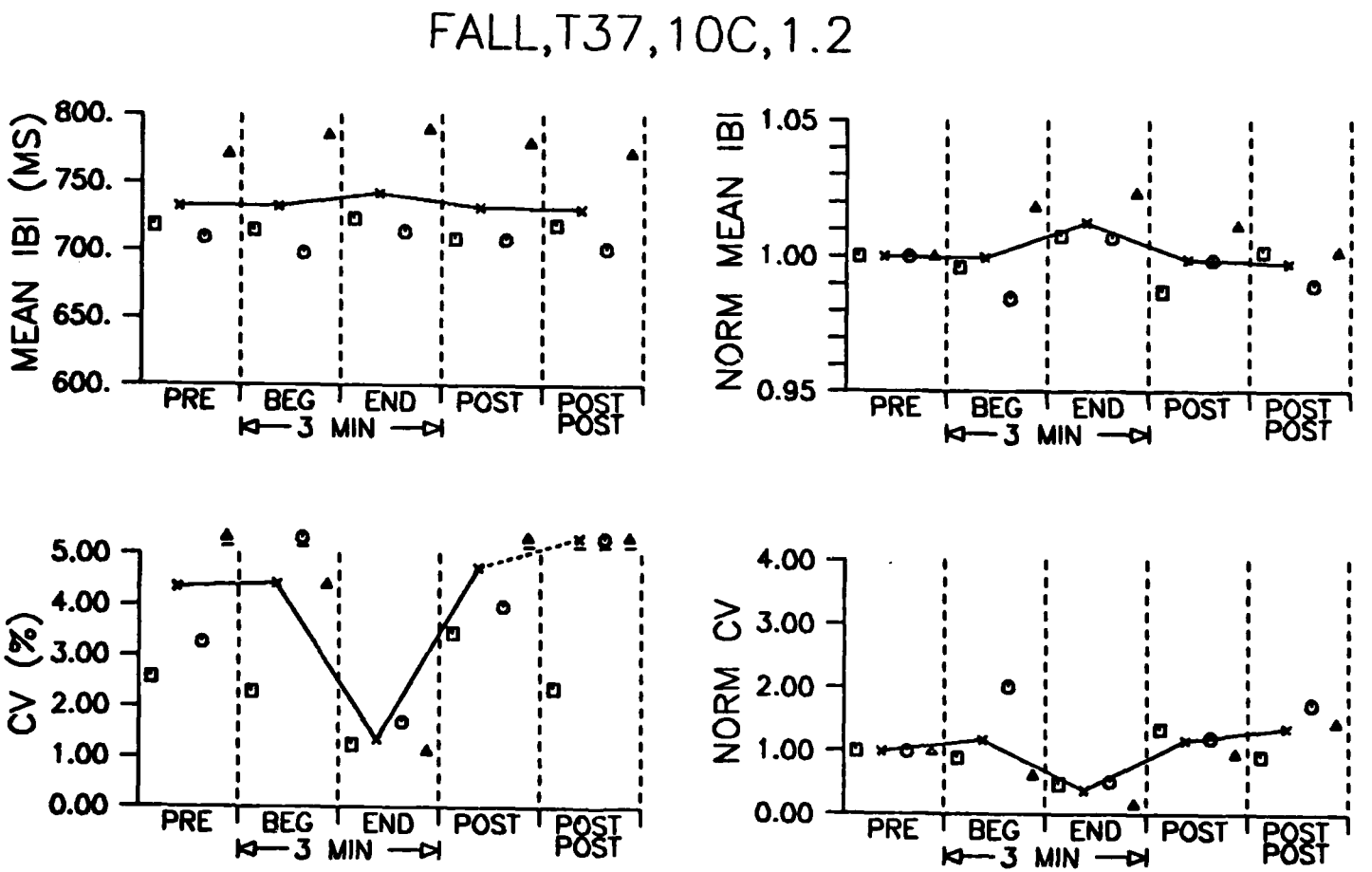

Figure 21. Results from fall experiments, exposures to 1.2 mW/g CW.

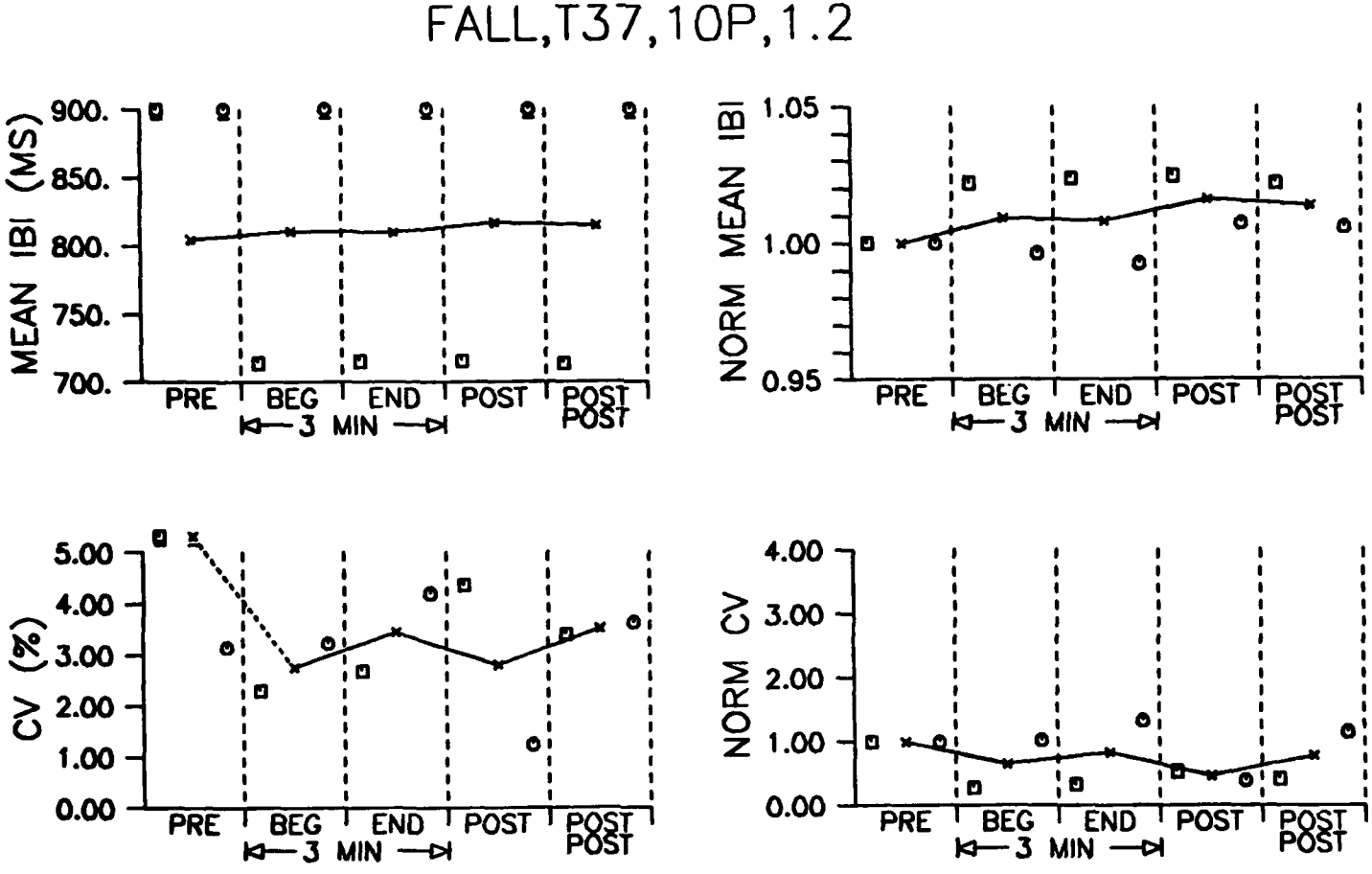

Figure 22. Results from fall experiments, exposures to 1.2 mW/g PW.

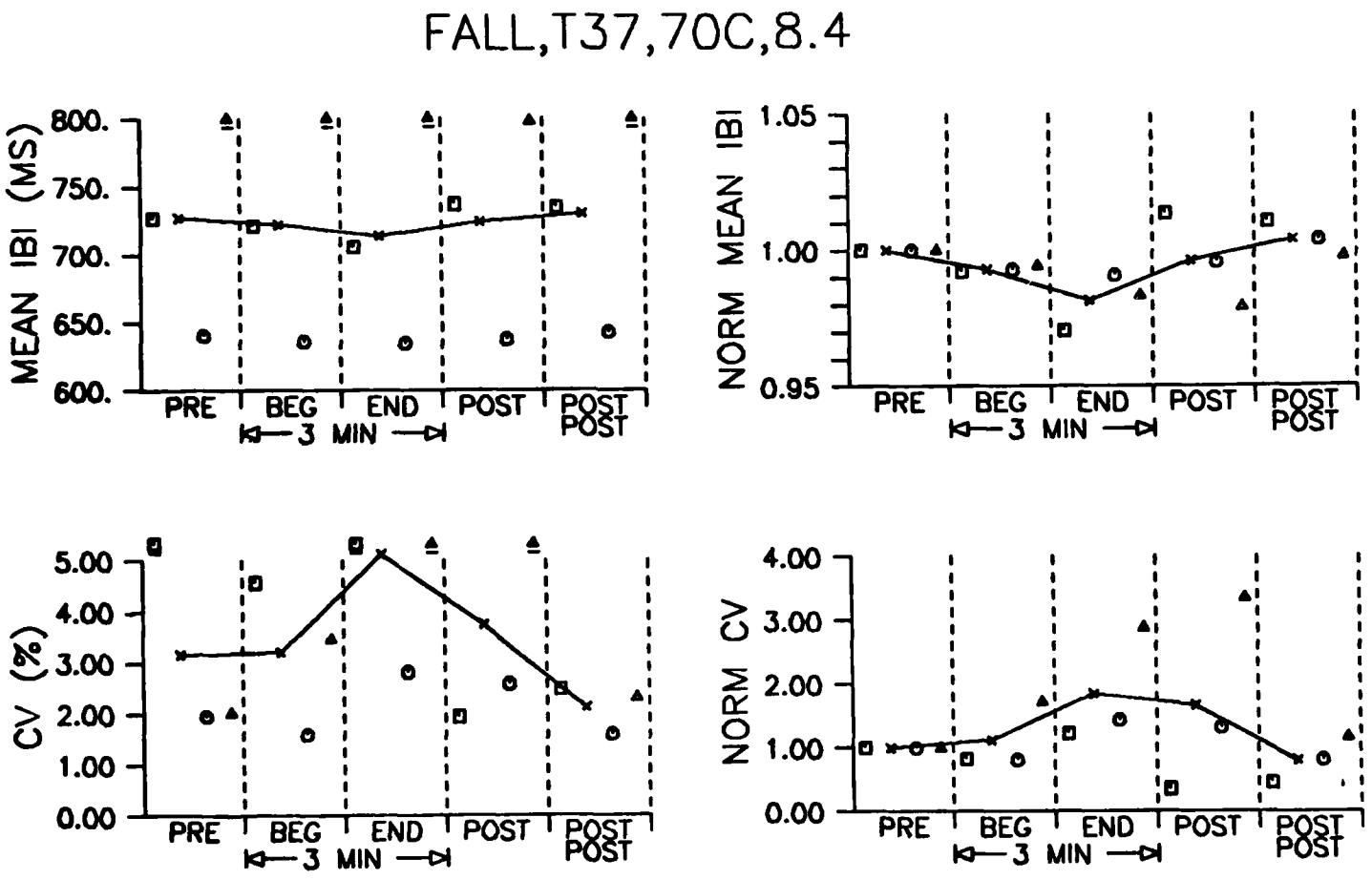

Figure 23. Results from fall experiments, exposures to 8.4 mW/g CW.

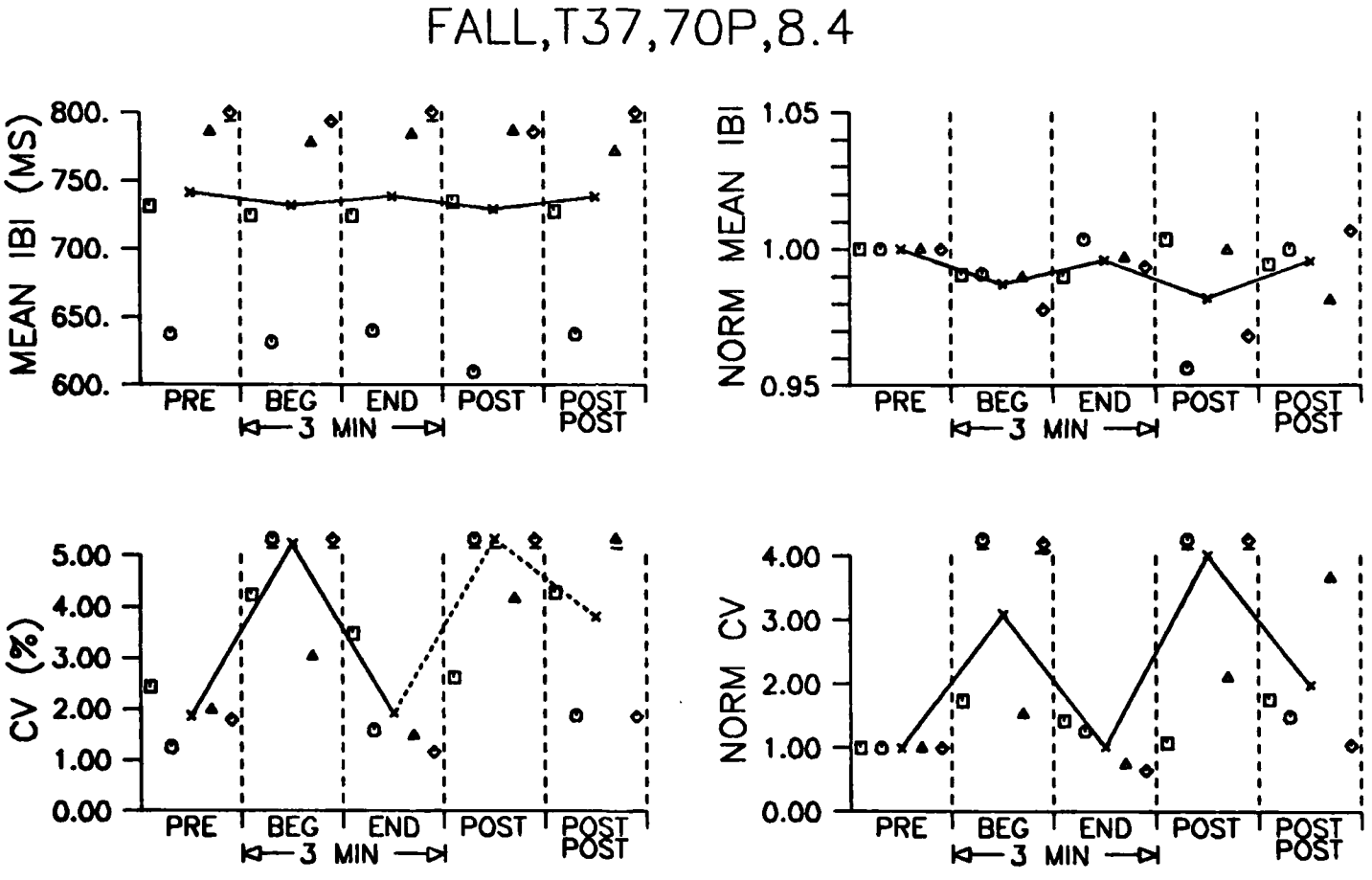

Figure 24. Results from fall experiments, exposures to 8.4 mW/g PW.

then decreased to 0.80 during POSTPOST. Figure 24 shows the results of exposures to the same SAR of 8.4 mW/g for PW RFR for 4 fall experiments. Averaged across the experiments, normalized IBI decreased by 1.3% and 1.8% during BEG and POST with other changes within 0.5% while normalized CV jumped to high values of 3.1 and 4.0 during BEG and POST with lower values during END and POSTPOST. The same M-like pattern in CV appeared in the plot of normalized CV. All four BEG CV values and 3 of 4 POST CV values were considerably larger than PRE-exposure values. The simultaneous decrease in mean IBI and rise in CV was caused by flurries described in Section II.

Figures 25 through 33 present results averaged for spring experiments. For each figure, experiments are represented by different symbols. Figure 25 shows the results of sham exposures for the 6 spring experiments with 3 or 6 exposures each. Mean IBI range was again different for each experiment: a minimum of 605 to 614 milliseconds for experiment K3 and a maximum of 775 to 805 milliseconds (off-scale points) for experiment H. This range was lower than for the fall experiments. Averaged across the experiments, normalized nean IBI again changed less than 1%. For individual experiments, average CV within an exposure interval ranged from 0.472% to 8.957%. Averaged across experiments, CV was in the range of 2.0% to 3.3% which was smaller than for fall experiments. Averaged normalized CV ranged between 1.1 and 1.9 times PRE-exposure values.

Figure 26 shows the results of exposures to 12.1 mW/g CW RFR for 3 spring experiments. Averaged across experiments, normalized IBI fell off during exposure and did not recover. However, this decrease was caused by results from one experiment while in the other two, normalized mean IBI stayed within 1% of PRE-exposure values. Normalized CV was relatively constant except for an increase during POSTPOST caused by a high value from one experiment. Figures 27, 28, and 29 present results of spring exposures to the same SAR of 12.1 mW/g but for 2 experiments of "PW" P,3 experiments of "modulated" M, and 3 experiments of "gated" G modulation, respectively. For these cases, normalized mean IBI deviated more than 0.5% from PRE-exposure values in a few notable instances. Normalized mean IBI fell by 5% during the POST interval of PW (Figure

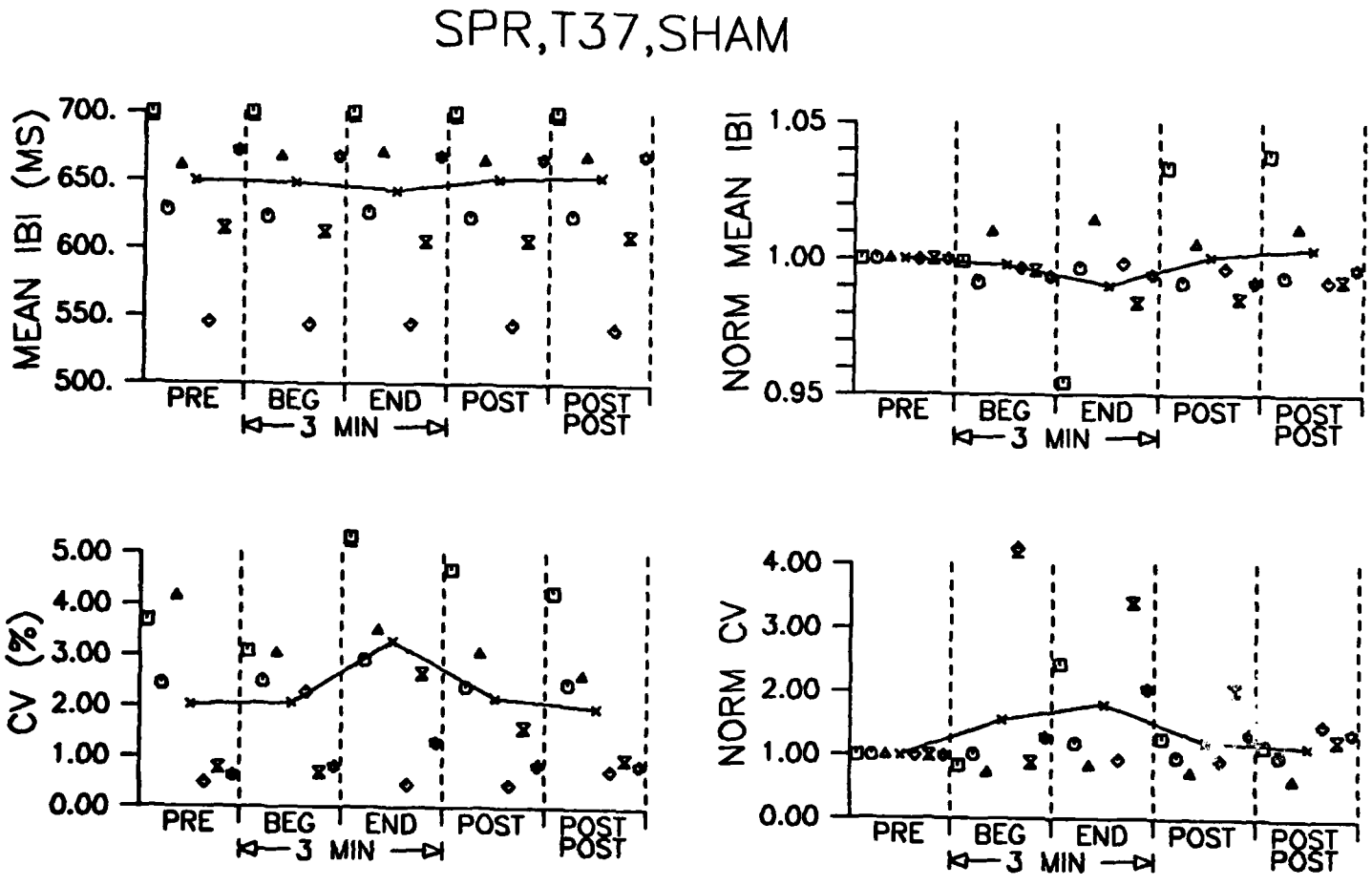

Figure 25. Results from spring experiments, sham exposures.

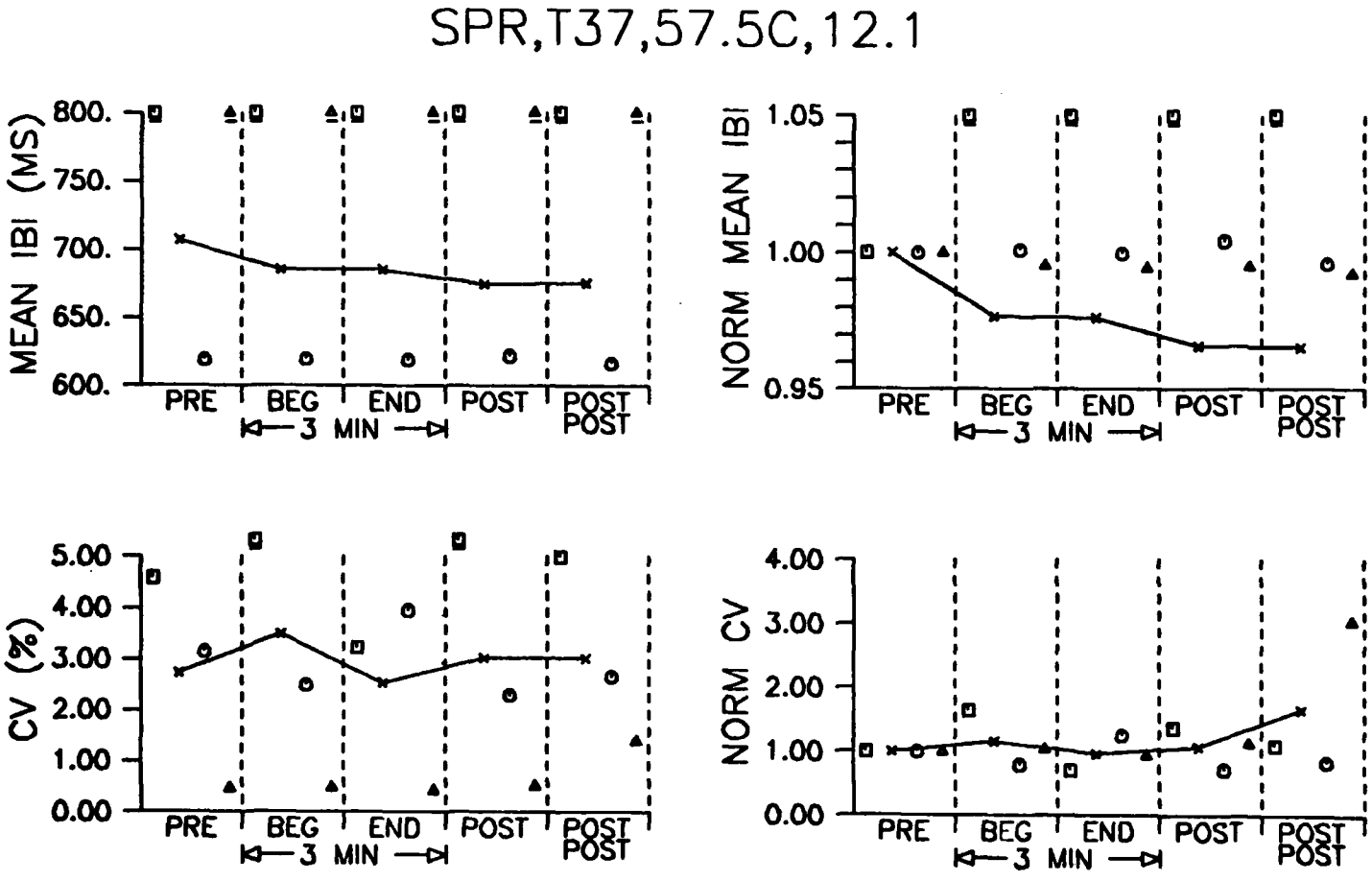

Figure 26. Results from spring experiments, exposures to 12.1 mW/g CW.

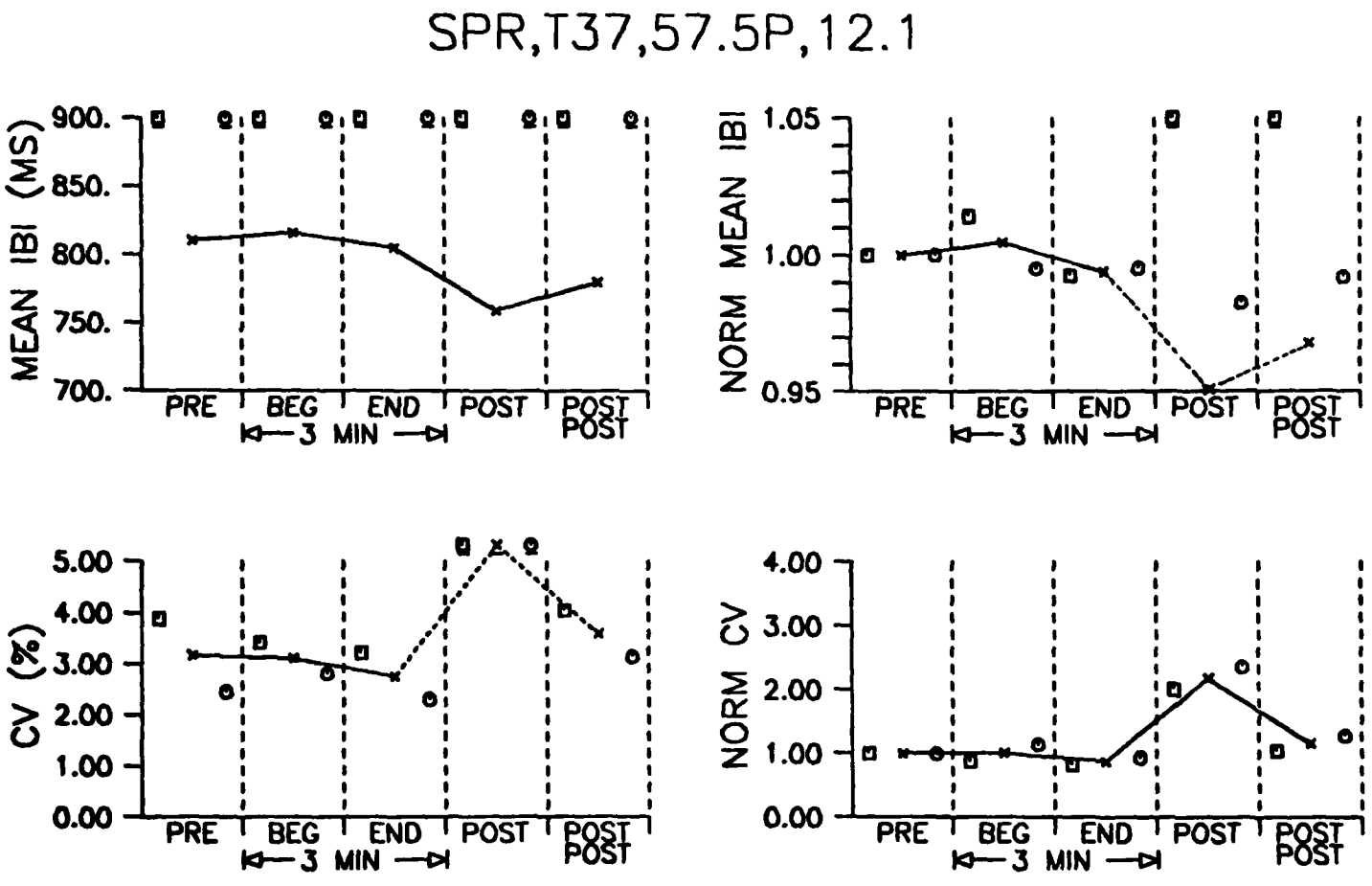

Figure 27. Results from spring experiments, exposures to 12.1 mW/g PW. The actual value of END average normalized mean IBI is 0.945.

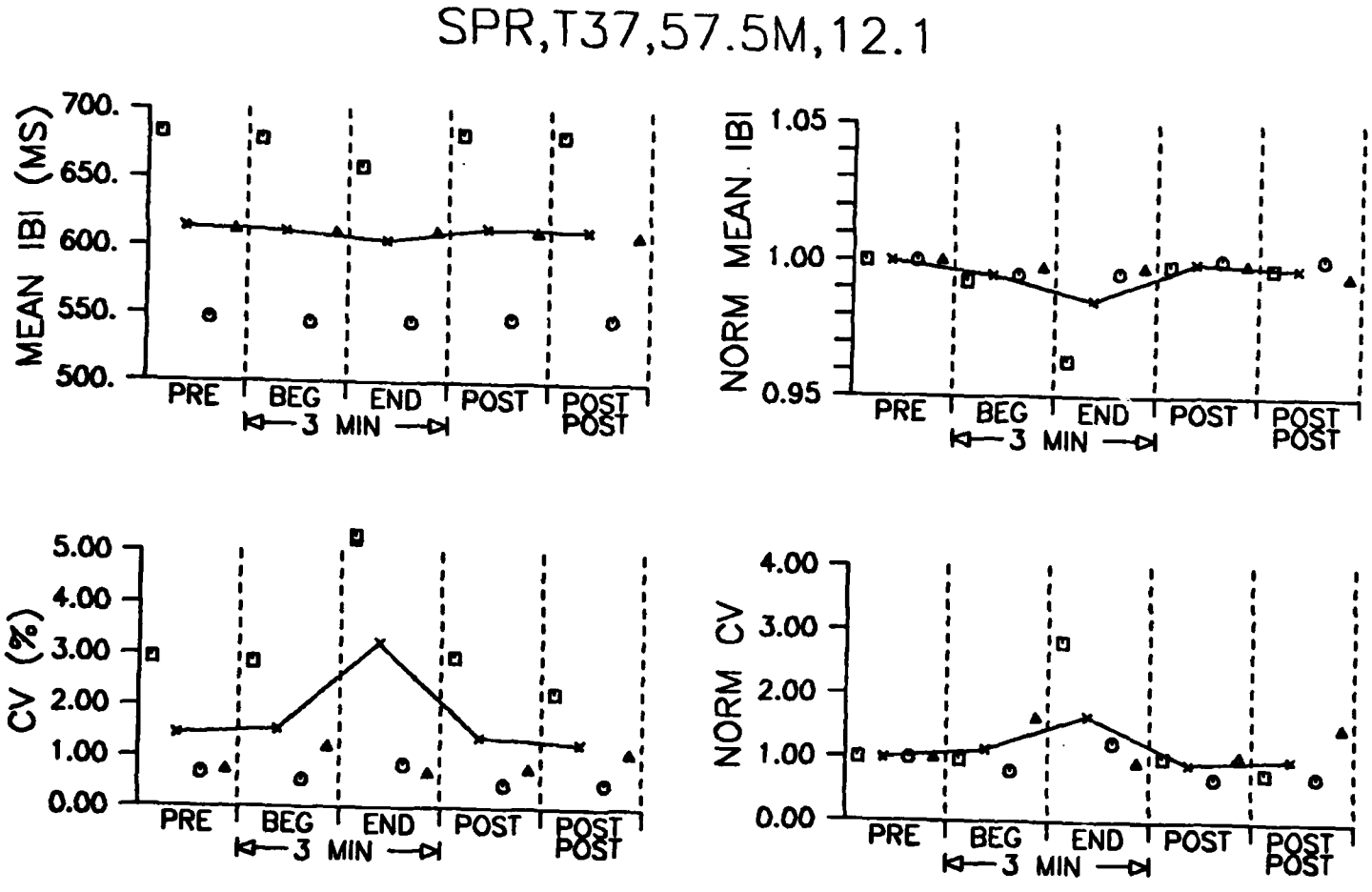

Figure 28. Results from spring experiments, exposures to 12.1 mW/g square-wave modulated at 16 Hz.

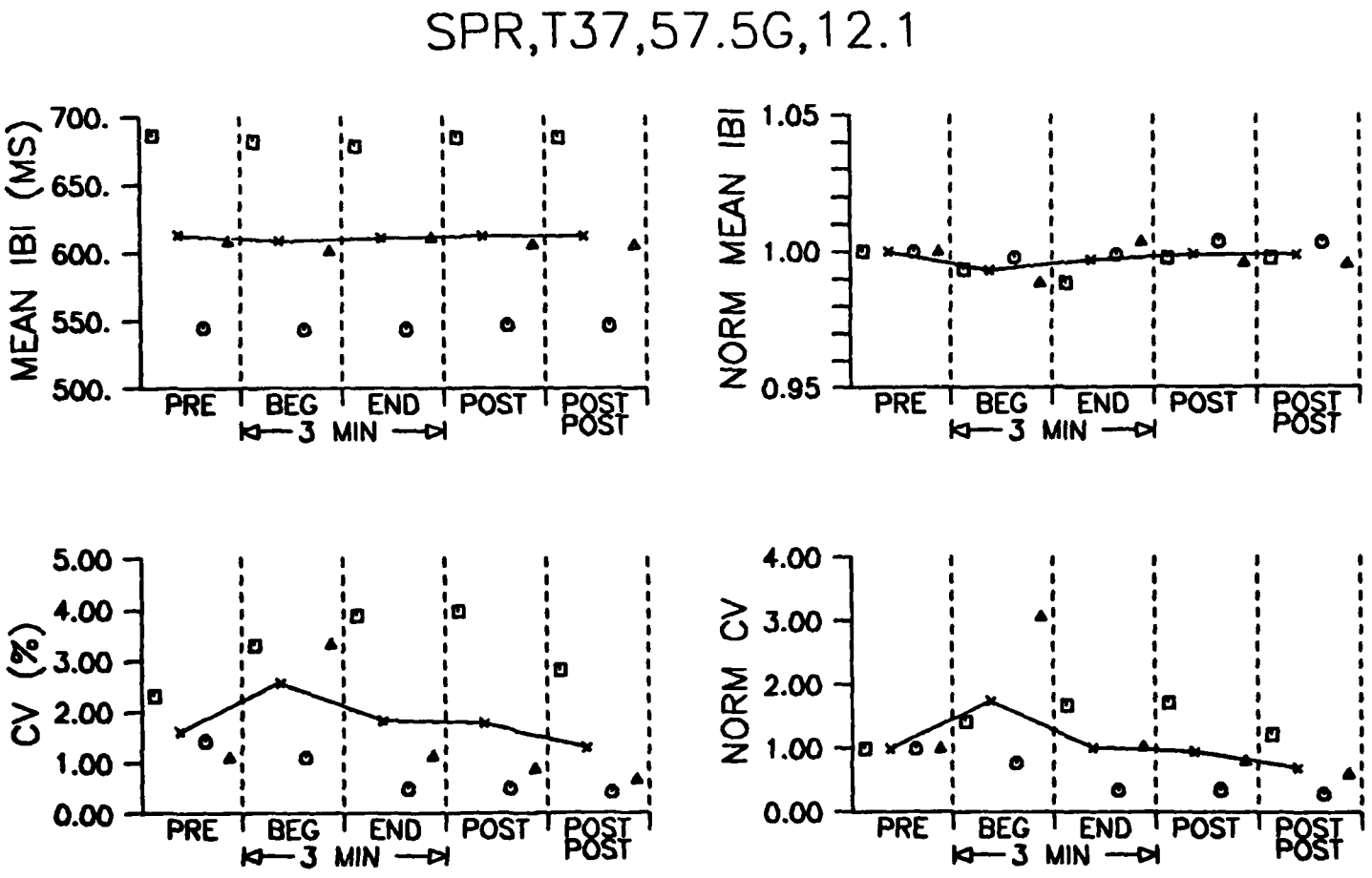

Figure 29. Results from spring experiments, exposures to 12.1 mW/g square-wave modulated at 1.6 Hz.

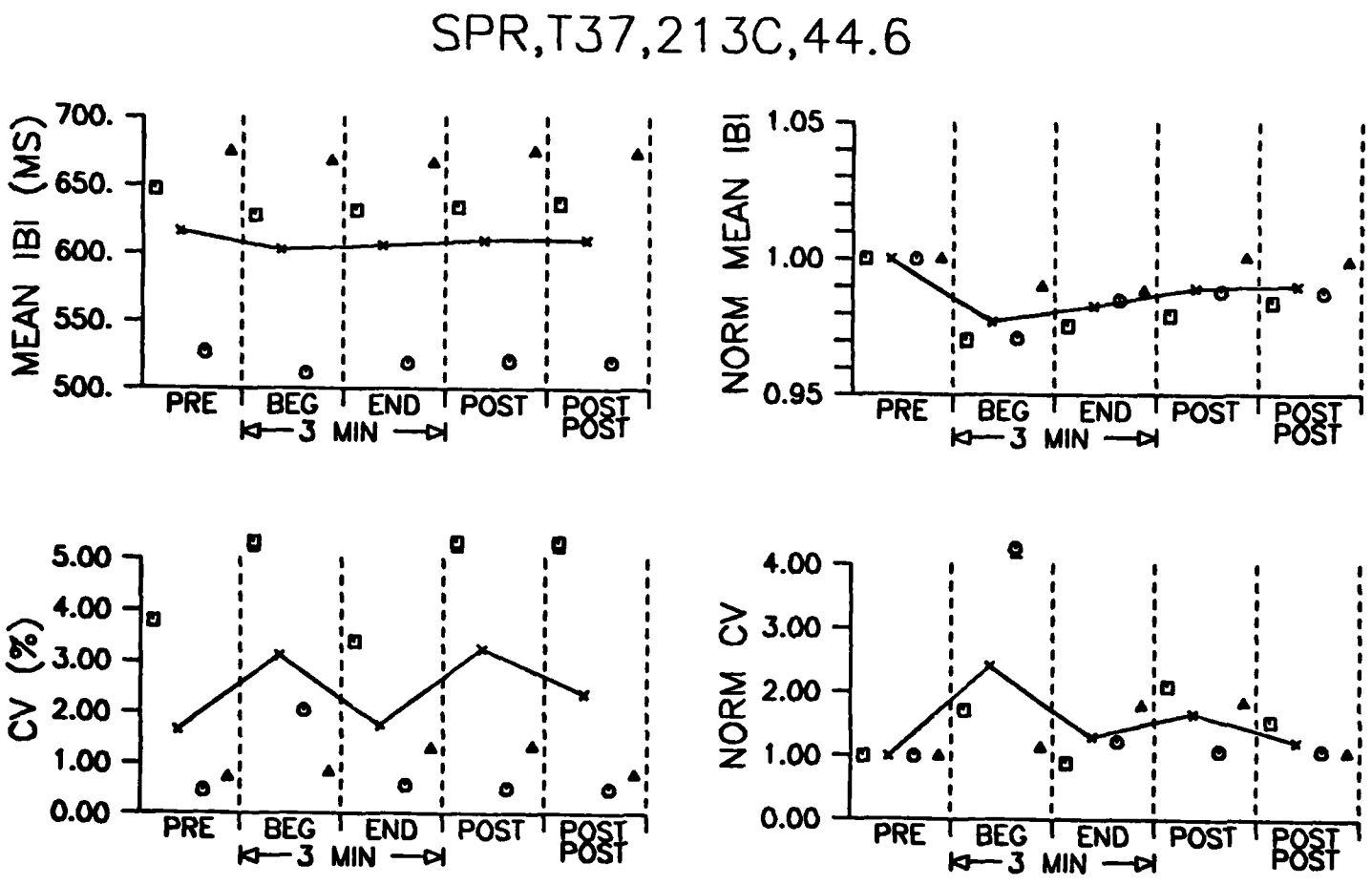

Figure 30. Results from spring experiments, exposures to 44.6 mW/g CW.

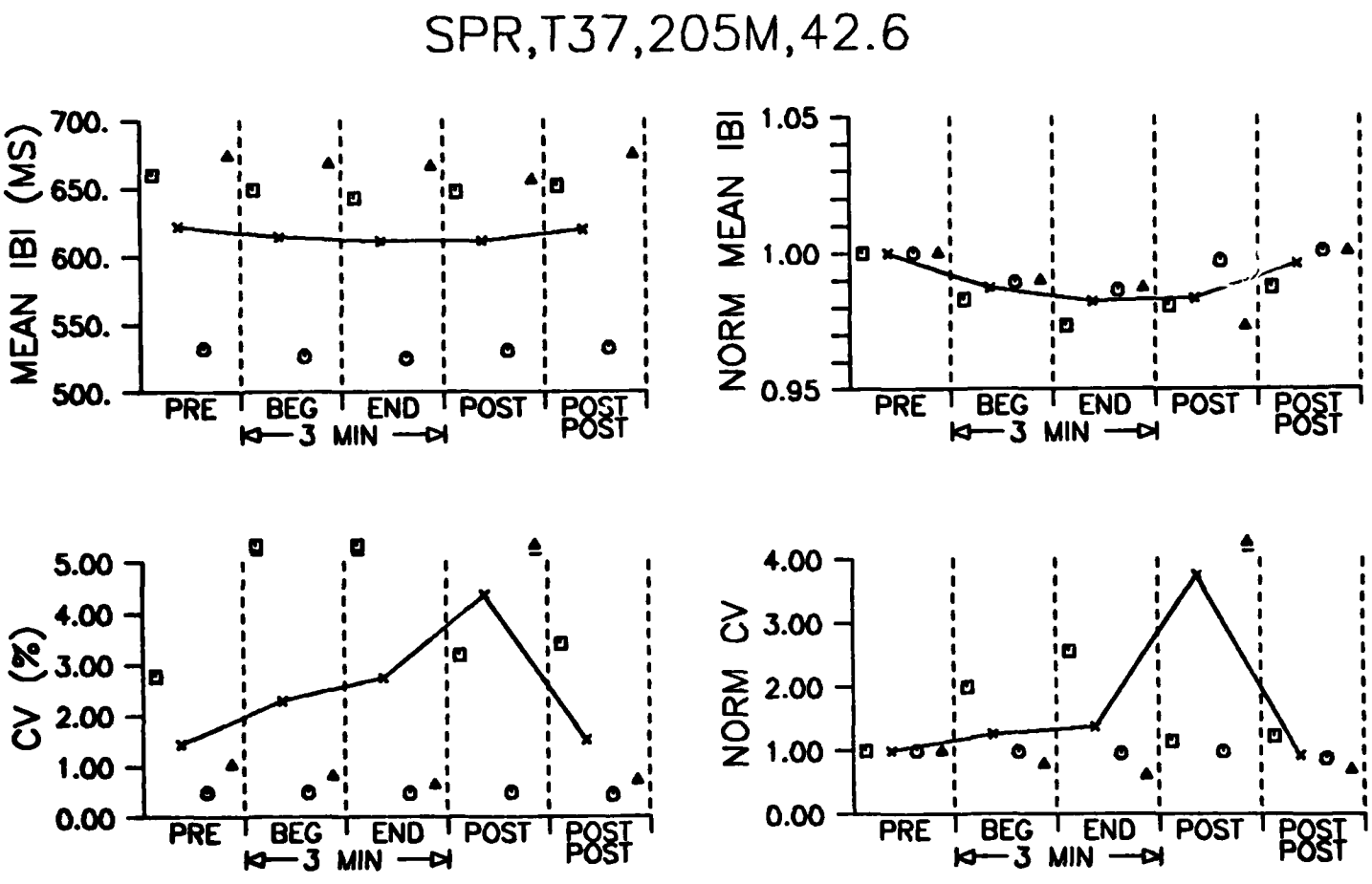

Figure 31. Results from spring experiments, exposures to 42.6 mW/g square-wave modulated at 16 Hz.

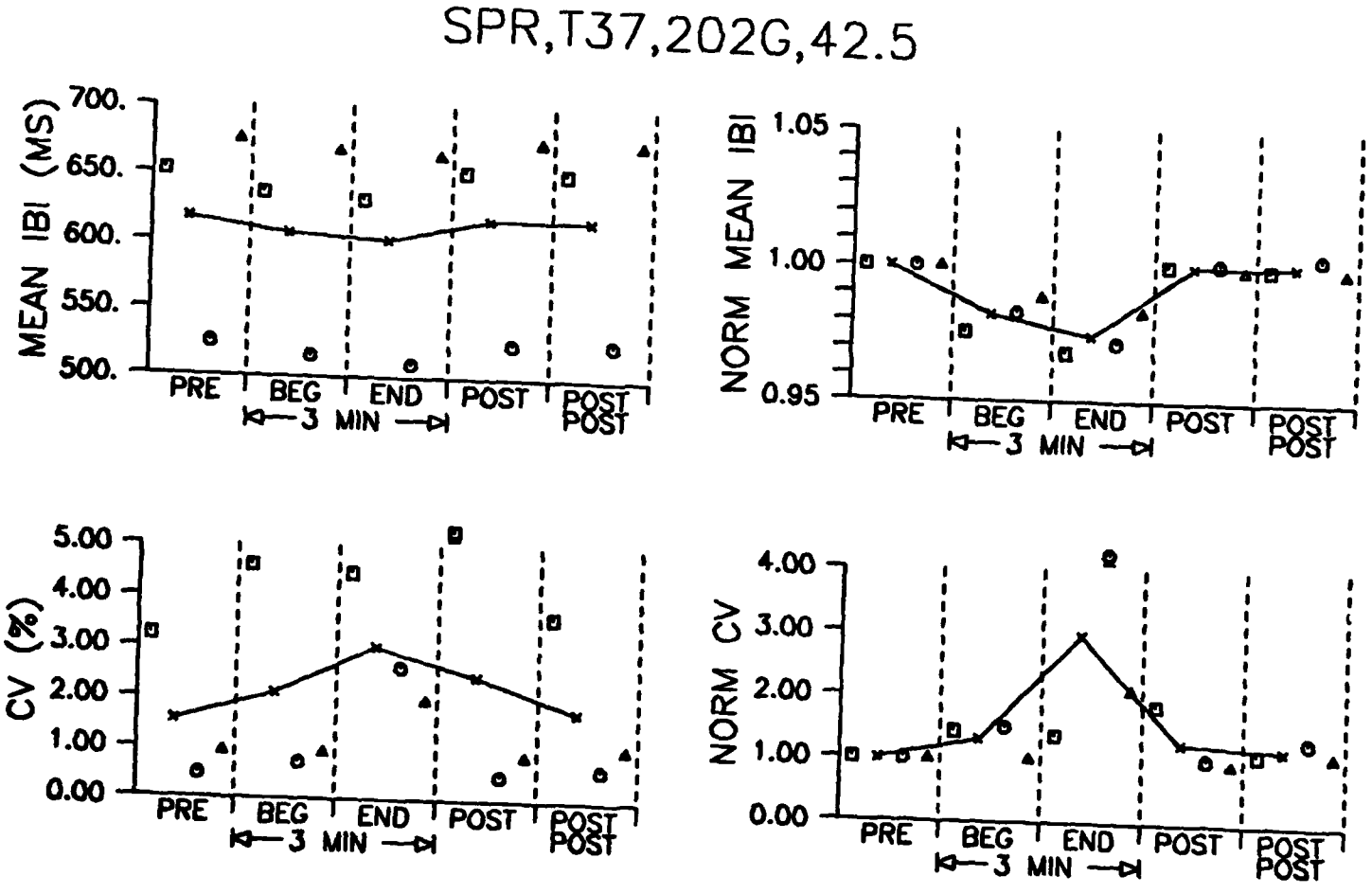

Figure 32. Results from spring experiments, exposures to 42.5 mW/g square-wave modulated at 1.6 or 1.7 Hz.

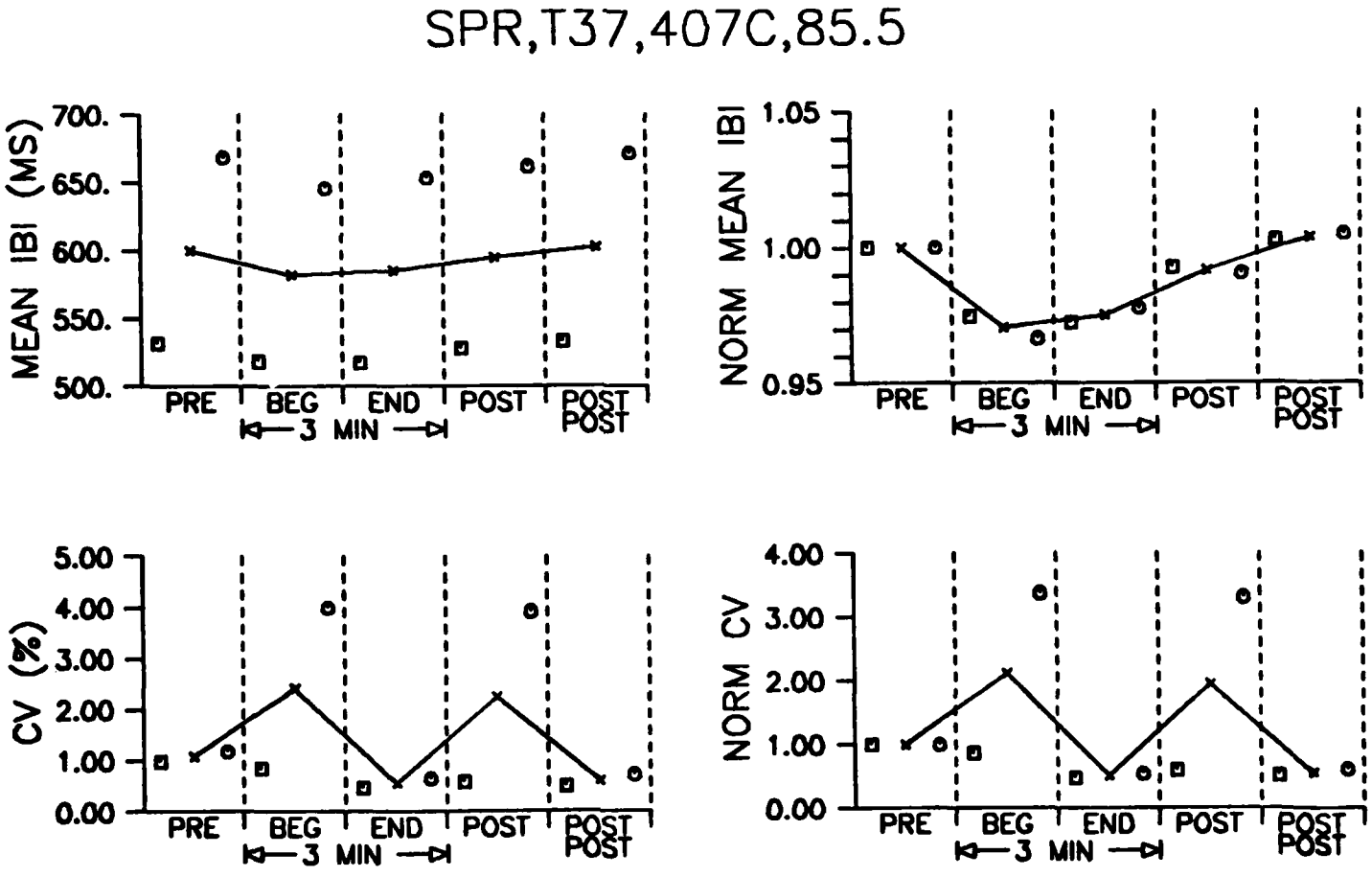

Figure 33. Results from spring experiments, exposures to 85.5 mW/g CW.

27) and was still smaller by 3.2% during POSTPOST; fell by 1.5% during END of "modulated" M (Figure 28); and fell by a more modest 0.7% during BEG of "gated" G (Figure 29). Each of these 3 decreases in normalized mean IBI was accompanied by increases of normalized CV (2.18 for P POST, 1.66 for M END, and 1.75 for G BEG) which was otherwise close to unity. Large changes in normalized mean IBI and normalized CV were seen in both P experiments, in 1 of 3 M experiments, and in 1 of 3 G experiments.

Figures 30, 31, and 32 present results of exposures to RFR for SAR from 42 to 45 mW/g for C (CW), M, and G, respectively, for the same spring experiments. Average normalized mean IBI decreased for exposure to each type modulation at this SAR by the following amounts:

	BEG	END	POST	POSTPOST
C:	2.3%	1.7%	1.1%	1.0%
M:	1.3%	1.8%	1.6%	0.4%
G:	1.8%	2.6%	0.0%	0.0%

The decreases during exposure were fairly consistent from experiment to experiment for each modulation and were similar for C, M, and G, with the G changes being slightly larger. The normalized mean IBI for G returned to PRE-exposure values in POST and POSTPOST while, for C and M, it was still smaller during these intervals. Normalized CV was larger for every interval for this SAR level, except for a M POSTPOST value of 0.935. For each modulation, there was one interval with a much larger average normalized CV: 2.42 for C BEG, 3.76 for M POST, and 2.97 for G END. These high average values were caused by one large individual value for C and M, but all three individual values were larger for G.

Figure 33 presents the results of 2 spring experiments for 85.5 mW/g CW RFR. Normalized mean IBI decreased by 2.9% and 2.5% during exposure (BEG and END), was smaller by 0.9% during POST, and was 0.4% larger during POSTPOST. Averaged normalized CV showed an M-like pattern with larger values of 2.12 and 1.96 for BEG and POST and smaller values of 0.516 and 0.565 during END and POSTPOST. Changes in IBI were similar for the 2 experiments while the higher CV values were largely due to

results from the experiment with 3 exposures at this SAR. The decrease in mean IBI during exposure averaging 2.7% were larger than those during 44.6 mW/g CW in Figure 30 which averaged 2.0%. The M-like pattern in CV was similar to that in Figure 30 and smaller than the one seen in Figure 24 for 8.4 mW/g PW for fall experiments.

In summary, Figures 16 and 20 through 24 present results from fall experiments; Figures 25 through 33, results from spring experiments, all at bulk temperatures of 37°C. In addition, results from all 10C and 10P experiments were averaged to give the plots shown in Figures 34 and 35. This procedure combined results from 1 spring experiment at 2.1 mW/g with results from fall experiments at 1.2 mW/g for each modulation: 3 for CW and 2 for PW. In general, the combined results were comparable to those in Figures 21 and 22 for 1.2 mW/g. For CW (Figure 34), there were small decreases in normalized mean IBI during BEG and POST while normalized CV increased to 1.47 during BEG and decreased to 0.486 during END. For PW (Figure 35), normalized mean IBI was within 0.6% of PRE-exposure values for all intervals while normalized CV decreased during BEG, POST, and POSTPOST. This combination of data from 1.2 and 2.1 mW/g may not have been valid since the effects are generally opposite between SARs. Later analysis across the total SAR range showed a pattern into which these changes appeared to fall, as discussed below.

In experiment L, exposures for sham and CW RFR conditions were done with bulk temperature at 28°C. As noted below, this aggregate's CV (5.10 average) was high at this temperature. The large IBI variability was also evident in mean IBI whose averaged normalized values deviated by as much as 4% from PRE-exposure values for 3 sham exposures. Despite this variability, there were definite reductions in mean IBI during 42.6 mW/g and 89.2 mW/g CW RFR exposures, as shown in Figures 36 and 37, respectively. At the lower SAR, average normalized mean IBI decreased by 3.6% and 2.6% during BEG and END and was 1.5% and 1.8% smaller during POST and POSTPOST. Normalized CV was much higher during exposure -- 9.42 times for BEG and 5.64 times for END -- and then returned to lower values after exposure. At the higher SAR, average normalized mean IBI decreased similarly to 2.3%, 2.6%, 1.6%, and 1.9% below the PRE-exposure

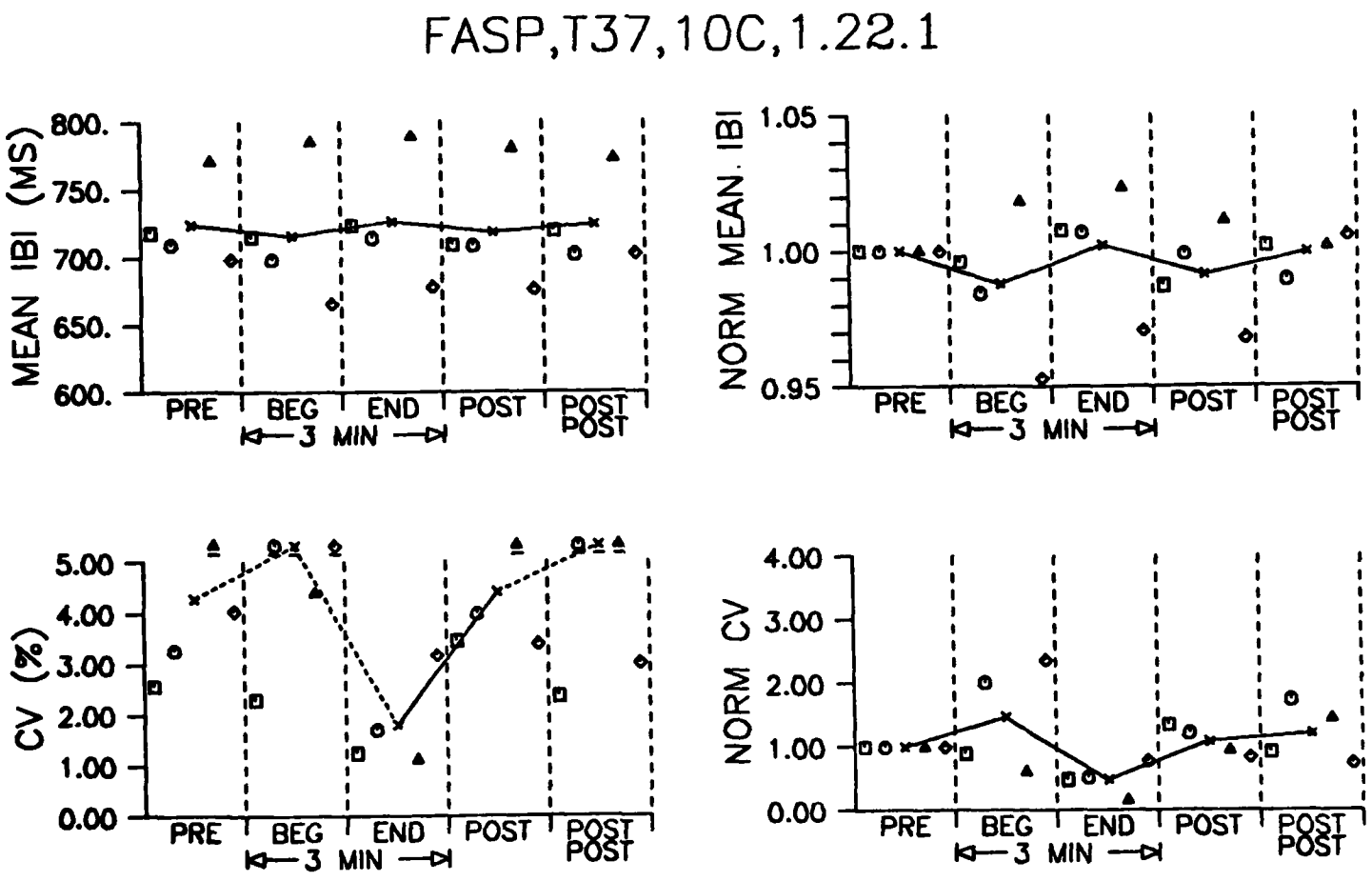

Figure 34. Results from 3 fall experiments and 1 spring experiment, exposures to 1.2 and 2.1 mW/g CW, respectively.

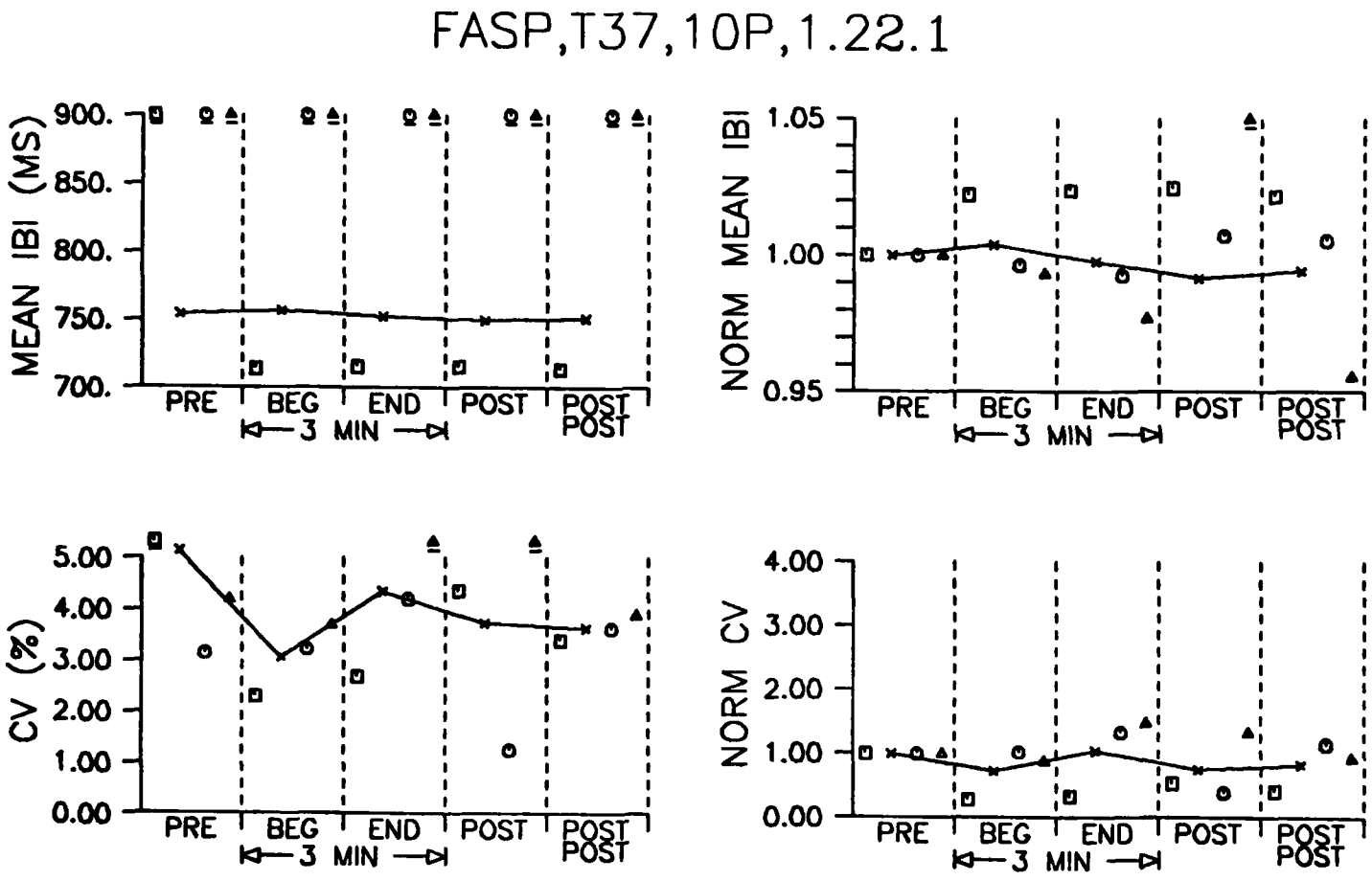

Figure 35. Results from 2 fall experiments and 1 spring experiment, exposures to 1.2 and 2.1 mW/g PW, respectively.

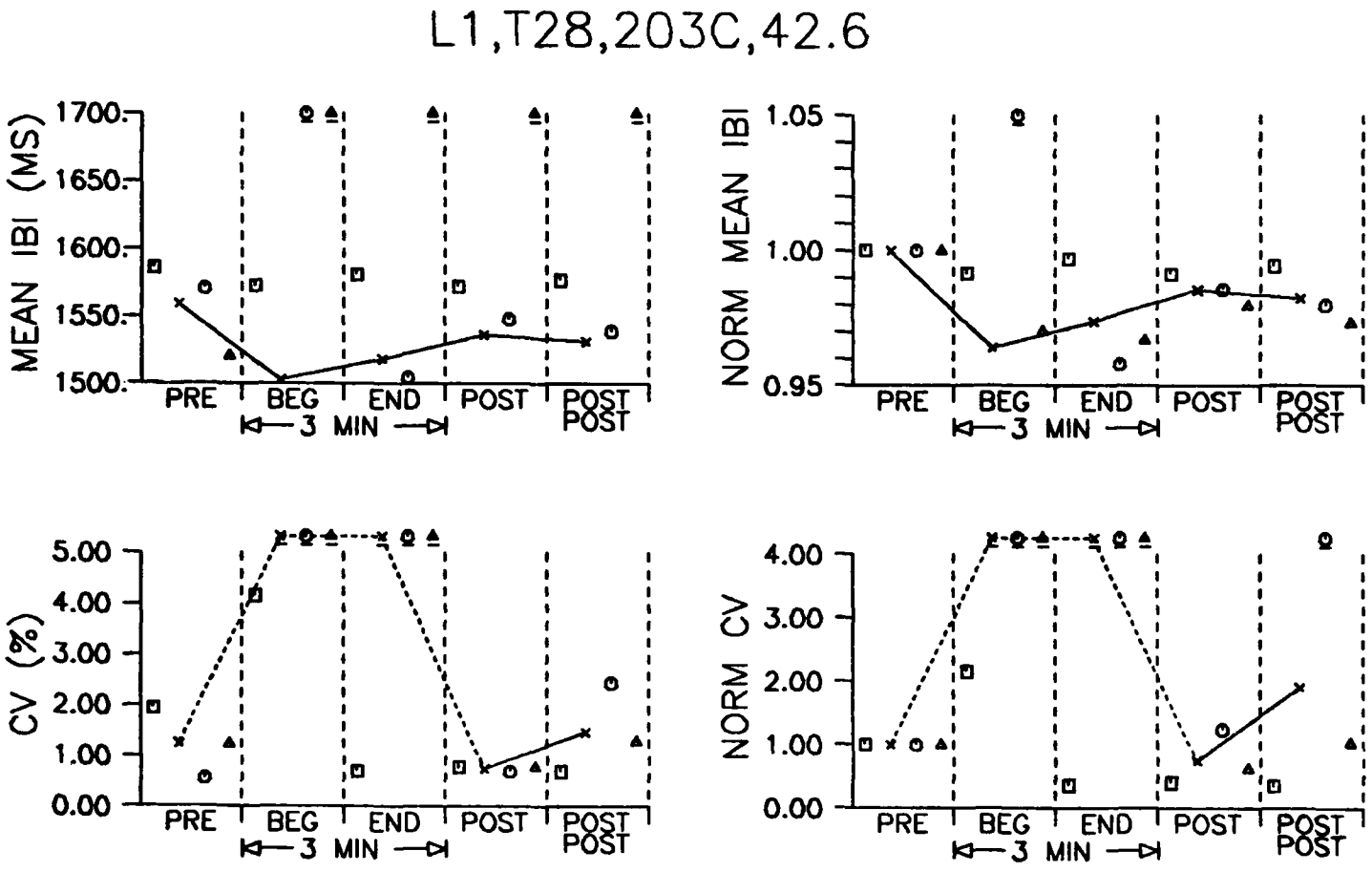

Figure 36. Results from experiment L at 28°C, exposures to 42.6 mW/g CW. Actual values of average CV for BEG and END are 9.42 and 5.64, respectively; of average normalized CV, 12.26 and 7.52.

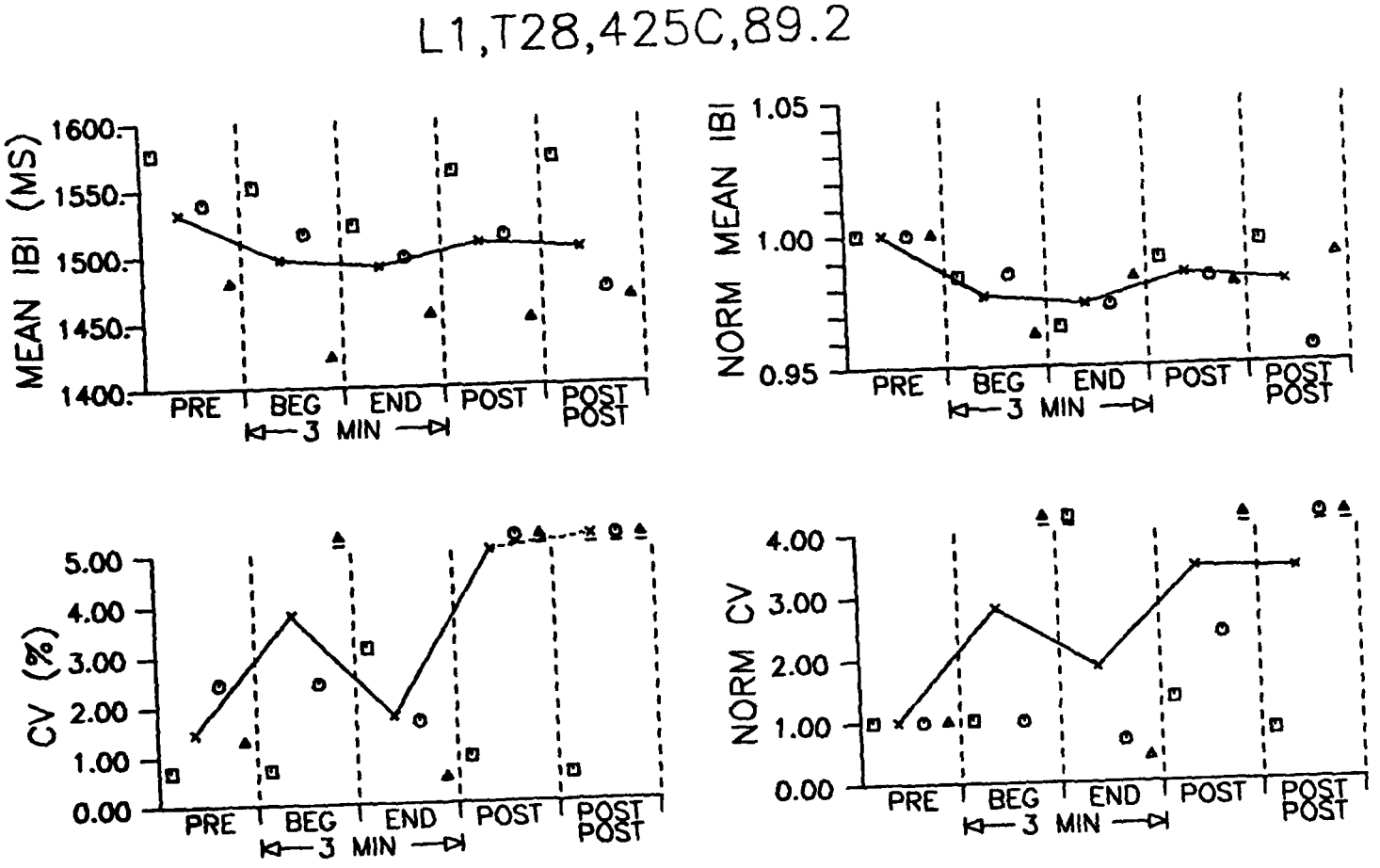

Figure 37. Results from experiment L at 28°C, exposures to 89.2 mW/g CW. Actual value of POSTPOST average CV is 5.98.

value for BEG through POSTPOST. Normalized CV was higher (3.44 and 3.40) after exposure with intermediate values of 2.82 and 1.87 during exposure. The changes in normalized mean IBI during exposure at 28°C (Figures 36 and 37) were comparable to those seen with similar SARs for spring experiments at 37°C (Figures 30 and 33) with a slightly larger decrease during exposure at 28°C and all POST-exposure decreases larger at 28°C. The changes in normalized CV at 28°C were larger than for similar SARs at 37°C while retaining the same general shape, except for the prolonged high values with the higher SAR at 28°C.

A comprehensive presentation of results from RFR experiments on cardiac-cell aggregate IBI has been given above. These results are discussed further below.

B. Temperature Effects on Aggregate Interbeat Interval

Temperature effects on the interbeat interval of cardiac-cell aggregates, which had been previously studied, were also investigated in this program. This was done so that RFR effects could be interpreted in terms of the RF heating which occurred during exposure. Figure 38, also included in Annual Technical Report No. 1, shows IBI which was measured in another experimental setup in which temperature was adjusted over a wide range. Interbeat interval decreased with higher temperature; however, when computed on a percentage basis, the change at 28°C was -7.3%/°C and the change at 37°C was -8.0%/°C. These similar rates of change were not unexpected since the IBI-temperature curve had the shape of a decreasing exponential. From data presented in Figure 17 of Annual Technical Report No. 1, rate of change was calculated from the slope of a regression line as -9.8%/°C after conversion of beat rate to IBI for 37°C to 38.5°C. These rates agreed with the 11%/°C decrease calculated in the first year for 36.5 to 37.5°C, but they were about one-half the value of 20% calculated for much lower temperatures of 20 to 21°C.

From IBI data during sham exposures at 36°C and 37°C in fall experiments B and E, rates of change were calculated as -9.1%/°C and -3.5%/°C. From 37°C to 38°C, the rate was calculated to be -5.8%/°C for fall experiment B. From sham exposures at 28°C and 37°C in spring experiment L, a rate of -6.3%/°C was calculated. These rates of decrease ranged between

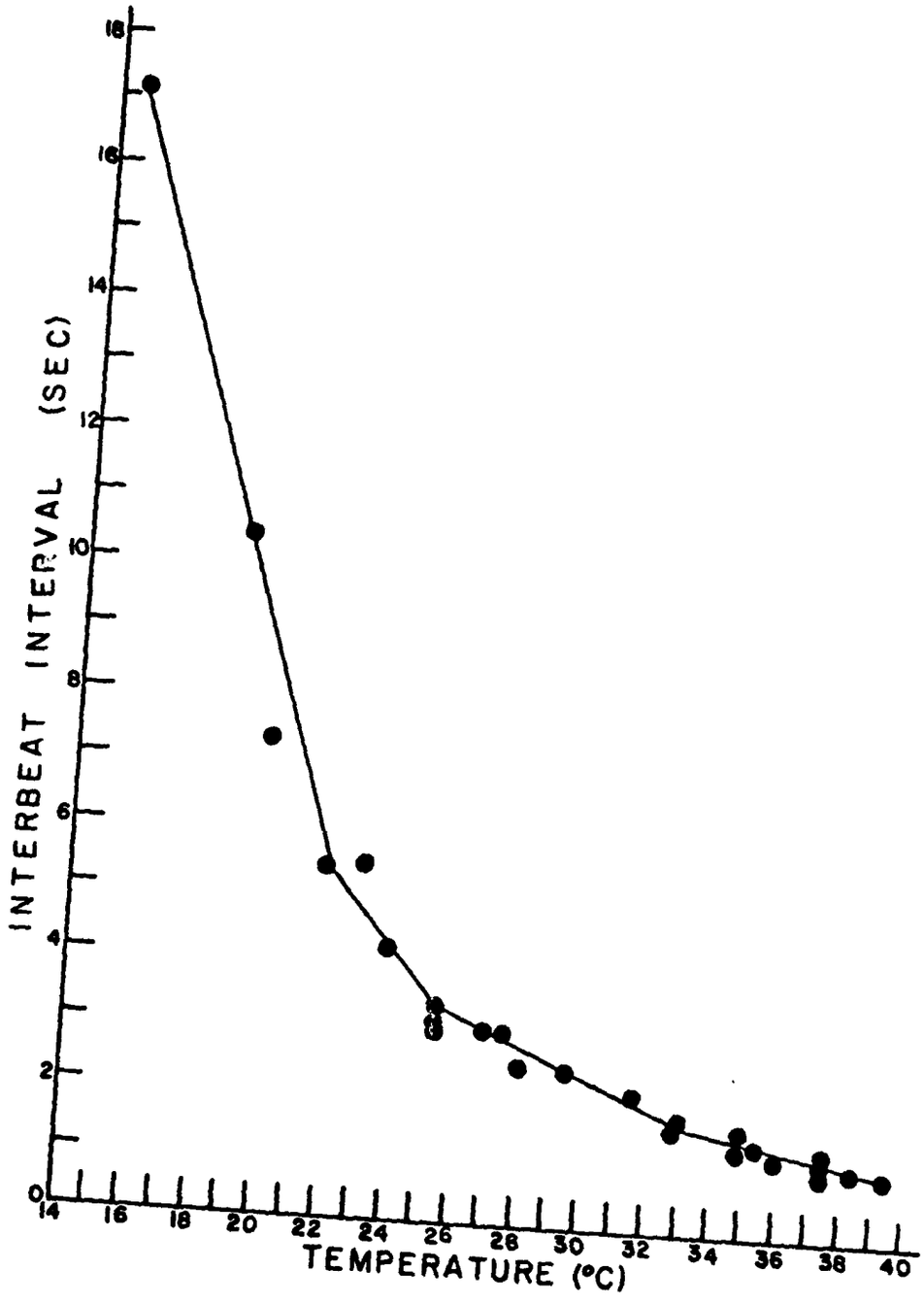

Figure 38. Effects of ambient temperature on mean IBI. Data from 150-μm ventricular aggregates prepared from 7-day heart culture.

3.5 and 9.1%/°C and probably depended on individual aggregate properties as well as temperature conditions. Temperature effects on CV could also be assessed in these same experiments. Averaged over the five intervals' average CV for sham exposures, CV (± S.D.) can be summarized as follows:

	28°C	36°C	37°C	38°C
Experiment B	--	3.48	4.82	4.72
	--	±1.22	±2.03	±1.21
Experiment E	--	7.51	3.35	--
	--	±1.94	±1.54	--
Experiment L	5.10	--	0.90	--
	±3.38	--	±0.24	--

The CV for experiment B remained constant from 36°C to 38°C while for experiment E, it decreased slightly from 36°C to 37°C. Over the wider range of temperature of 28°C to 37°C, CV in Experiment L decreased providing some of the most regular beating seen in any experiment.

C. Discussion of Experimental Results

During the course of this program, the first two research objectives listed in Section IB were met. The remaining research objectives were not pursued in depth because of the efforts necessary to develop an appropriate exposure system and to investigate alterations in aggregate IBI. As described in the next paragraph, some initial work was done on the remaining objectives. As described in Section III, an exposure system using an open-ended coaxial exposure device was developed. This system was used to deliver well-characterized RFR to individual aggregates whose activity was being monitored continuously during exposure. Limited information on action potential parameters was obtained because of the sensitivity of the intracellular-electrode recording to aggregate movement. Successful intracellular recordings suggested that aggregate beat rate and action potential maximum upstroke velocity became more variable for CW and PW RFR in the SAR range of 10-40 mW/g. These results led to implementation of recording techniques for long-term monitoring of interbeat intervals (IBIs) to be statistically analyzed. Video techniques were used successfully for this purpose in two experiments but technical difficulties prevented them from being used extensively.

Extracellular-electrode recording techniques proved to be well-suited to the long-term monitoring of IBI. Results from the several

successful experiments using extracellular electrodes to record IBI of RFR-exposed aggregates in normal bathing media are given above. Highest priority was given to determining the RFR effects on IBI of single cardiac-cell aggregates under normal bathing medium conditions. It was felt that knowledge of these effects would provide a data base against which effects on aggregate chains and on single aggregates in other media could be assessed. Therefore, all results reported here were obtained for single aggregates in normal culture medium or balanced salt solution containing 1.3 mM potassium. Also, no experiments were conducted with neurotransmitter agents present in the medium. Two attempts were made to record extracellular potentials in the presence of tetrodotoxin, a neurotoxin which acts on membrane sodium channels and consequently slows the action potential upstroke velocity. However, the reduced amplitude of extracellular currents caused by slowing of the action potential made long-term recording difficult under these conditions. Although some indirect information was obtained on sodium currents in early data on maximum upstroke velocity, no study was made of specific ion currents through the aggregate membrane. Investigation of RFR effects on specific ion currents and their membrane channels is a natural extension of the work done on this program.

Mean IBI and IBI coefficient of variation (CV) changed for some of the RFR conditions imposed on aggregates in this program. The results on IBI are given in the plots of Figures 14 through 37. In general, mean IBI during exposure decreased and the decrease was greater for larger SAR, independent of modulation. This trend can be seen in Figure 39 in which mean IBI change and normalized CV during exposure (both average of BEG and END values) for all modulations were plotted against SAR. The data in Figure 39 were averaged across experiments for each SAR except for 2.1 mW/g (from experiment H) and for 72.0 mW/g (from experiment A). Mean IBI did not appreciably decrease during PW RFR at 12.1 mW/g but did decrease sharply after exposure (see Figure 27). Mean IBI increased by small amounts for CW and PW RFR at 1.2 mW/g, the smallest SAR studied (see Figures 21 and 22). Values of average changes during

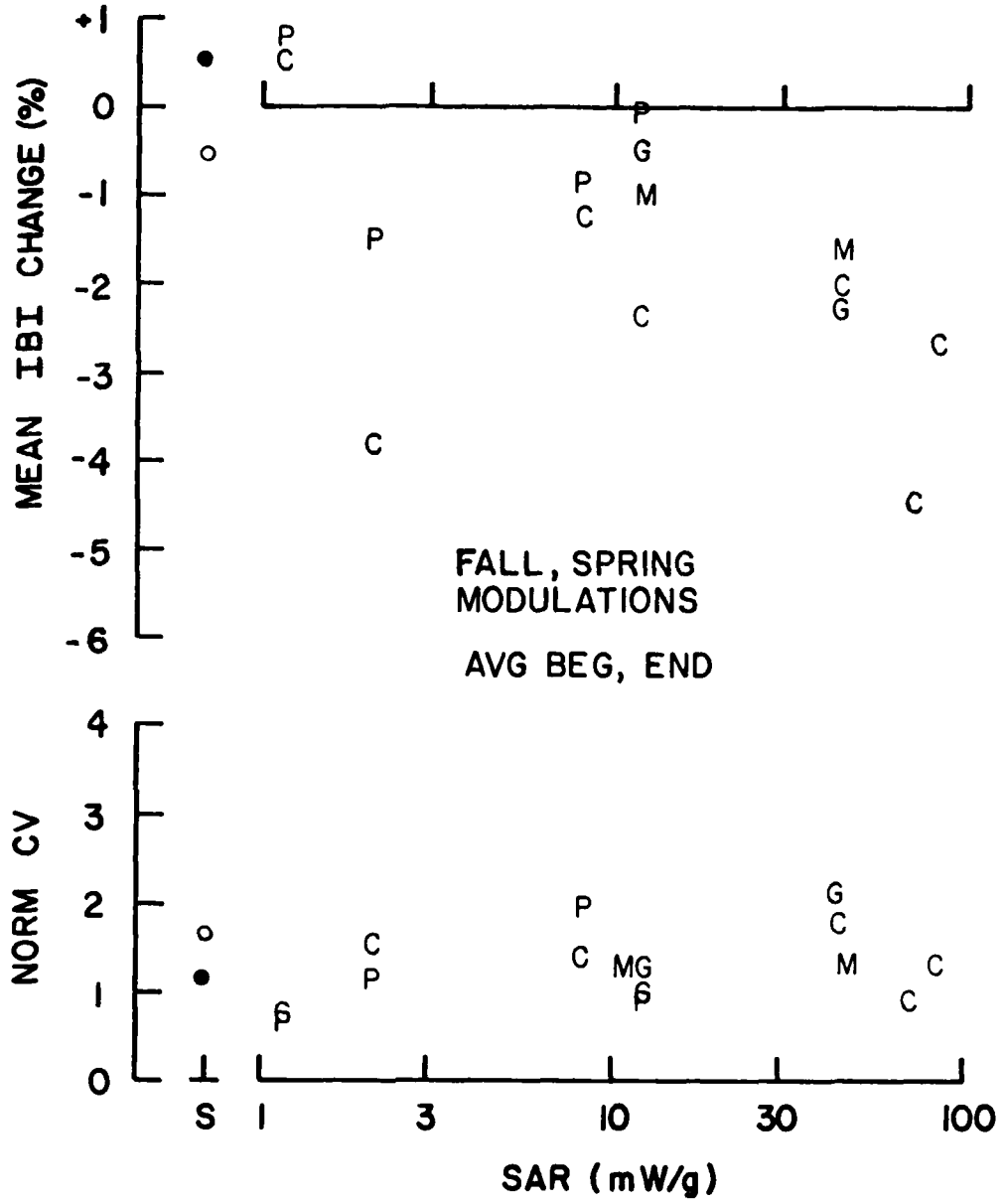

Figure 39. Mean IBI changes and normalized CV during RFR exposures versus SAR. Average of BEG and END values for each SAR and modulation. S = sham, C = CW, P = PW, M = 16 Hz square-wave modulated, G = 1.6 Hz square-wave modulated.

CW exposures, for which data were available over the SAR range studied, were plotted separately, as shown in Figure 40. After excluding the value for 2.1 mW/g for reasons explained below, a regression line based on a linear relation between IBI change and log SAR was determined for the 6 remaining changes. This straight line and the increase in mean IBI at 1.2 mW/g indicated that increases may occur with RFR at SARs less than about 2 mW/g. This conclusion was qualified by the fact that a regression line through the values for the 5 largest SARs intercepted the SAR axis at a lower value of 1.1 mW/g. Also, changes on the order of 0.5% were of the same magnitude as the resolution of our analysis method, as well as being similar to values for sham exposures.

The trend for IBI decreases at higher SAR and for small increases at small SAR was similar to those reported (in terms of BR) for intact turtle and rat hearts for 1 to 10 mW/g at 960 MHz CW RFR [9-12]. Further work will be required in the 1 to 10 mW/g range to determine more accurately aggregate mean IBI changes for small SAR. However, if the change at small SAR is indeed an increase in mean IBI (slowing of BR) for aggregates, then slowing of turtle and rat hearts may warrant re-examination since the neural components to which those effects were attributed were not present in the aggregate preparation.

Normalized CV was also plotted for all modulations (Figure 39) and for CW alone (Figure 40). In general, normalized CV, averaged for BEG and END values, did not change by large degrees, with most values falling between 1 and 2, or 1 and 2 times PRE-exposure values. The largest value was 2.1 for RFR square-wave modulated (gated) at 1.6 Hz and 42.5 mW/g. The smallest values were 0.78 and 0.74 for CW and PW RFR at 1.2 mW/g. For CW values in Figure 40, there was a gradual increase in normalized CV as seen from the slope of the regression line from which the value at 2.1 mW/g was excluded. The small values at 1.2 mW/g corresponded to intervals during which mean IBI increased. They were also consistent with some observations of rat hearts exposed to 960-MHz CW RFR at 2.1 mW/g in which variability was smaller [11, Figure 5].

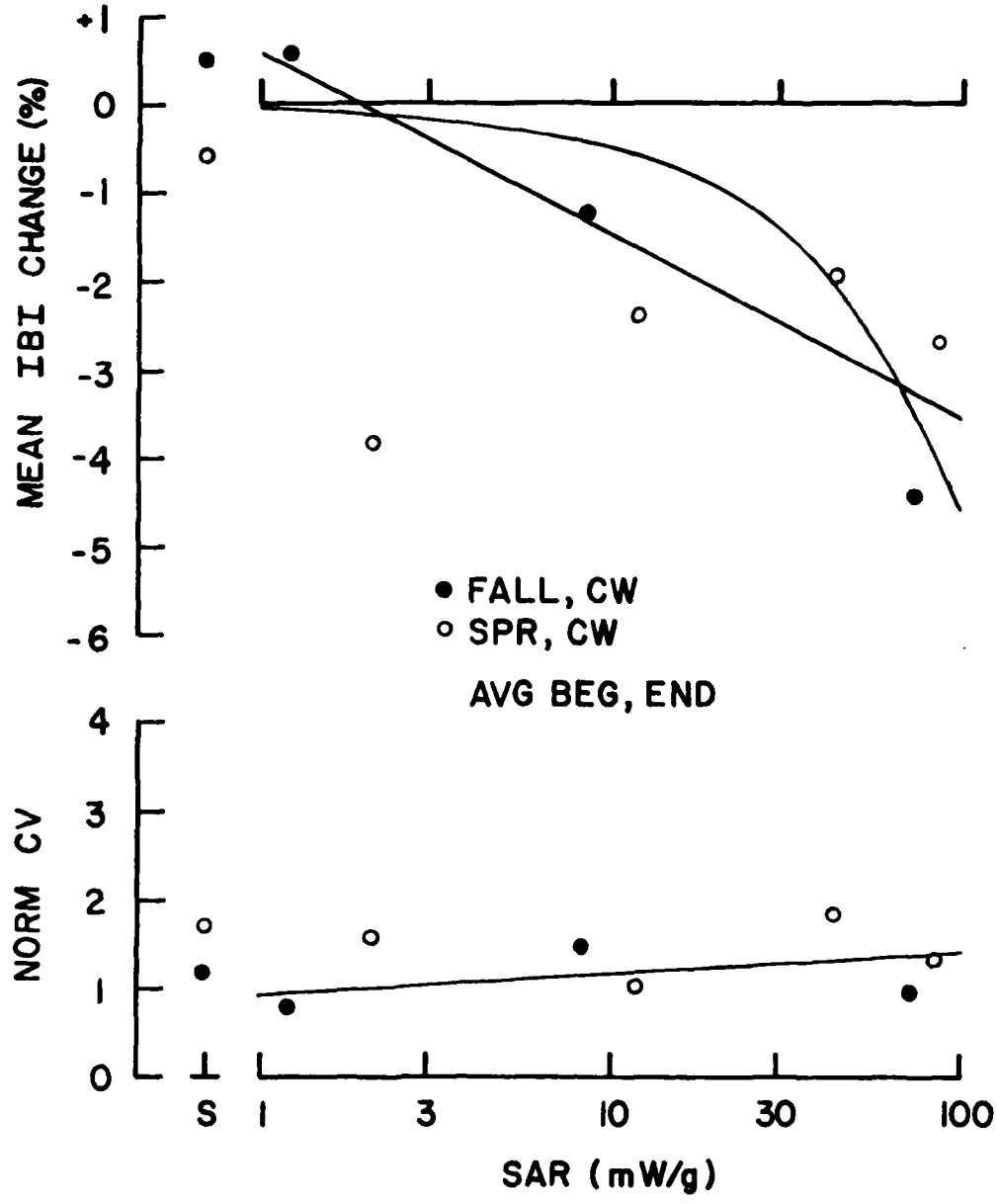

Figure 40. Mean IBI changes and normalized CV during CW RFR exposures versus SAR. Straight lines are regression lines through respective data, with exclusion of values for 2.1 mW/g. Curve is estimate of mean IBI change based on thermal changes.

Changes in IBI parameters after RFR exposure were sometimes larger than those occurring during exposure. Figure 41 shows the changes in mean IBI and normalized CV for all modulations for POST intervals. If an RFR effect on these parameters were reversible over a period of a minute or so, POST mean IBI change would approach zero and POST normalized CV would approach unity, returning to PRE-exposure values. For mean IBI, several POST values were near zero and the nonzero changes of -0.9 to -1.6% for SAR above 30 mW/g may be explained by a recovery from a temperature increase during exposure. The nonzero changes seen for SAR smaller than 30 mW/g were not as easily explained. The only POST increase, +1.6%, occurred after exposure to PW RFR at 1.2 mW/g and reflected the progressive slowing seen for this type exposure (see Figure 22). A decrease of 1.8% occurred after exposure to PW RFR at 8.4 mW/g. These changes for PW were much larger than the changes for the same aggregates with CW RFR at the same SAR. A difference between CW and PW POST values of mean IBI change also occurred at 2.1 and 12.1 mW/g both of which included results from experiment H. Values for the CW case were -3.1 and -3.4%, respectively, while for the PW case they were -5.7 and -5.5%, respectively. The IBI for experiment H showed a variability larger than in most spring experiments which may be responsible for the larger changes seen during and after exposure (Figures 39 and 41) for this aggregate.

Normalized CV values for POST were mostly in the 0.8 to 2.0 range as shown in Figure 41. However, there were five exceptions: smaller than usual values for 1.2 mW/g PW and 72.0 mW/g CW and larger than usual values for 8.4 mW/g PW, 12.1 mW/g PW, and 42.6 mW/g square-wave modulated (M) at 16 Hz. The small value at 1.2 mW/g PW reflected a progressive trend for this type exposure (Figure 22) and occured with a larger mean IBI. The small value at 72.0 mW/g PW reflected a reduced CV during 3 exposures in experiment A (Figure 16). The increase in CV for 8.4 mW/g PW was part of the M-like response seen in Figure 24 while the increase for 12.1 mW/g PW followed normal values during exposure as seen in Figure 27. The increase for 42.6 mW/g M also followed normal values and was caused mainly by a very large value in 1 of 3 experiments (Figure 31).

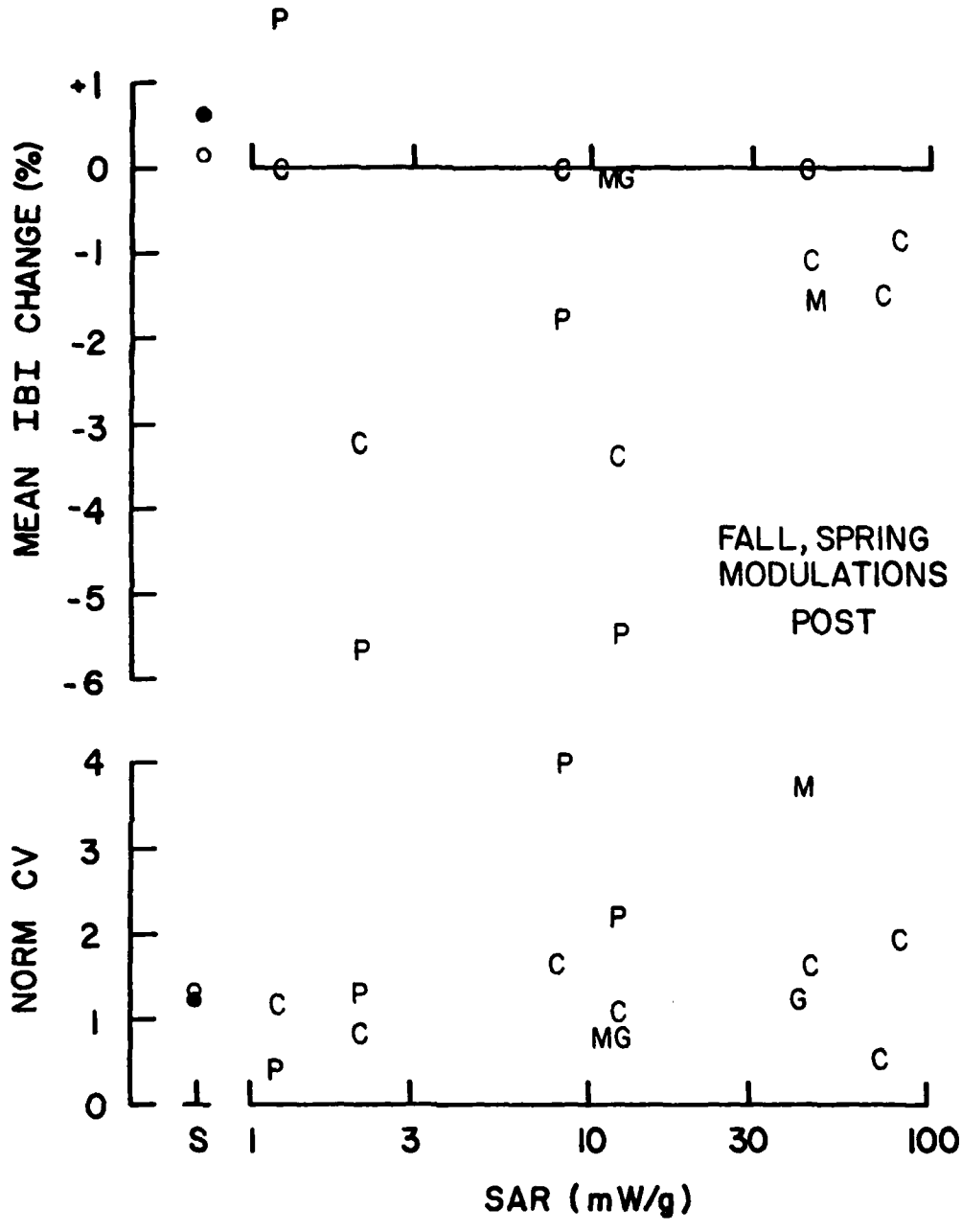

Figure 41. Mean IBI changes and normalized CV after RFR exposures versus SAR. Values for POST intervals. Symbols same as for Figure 39.

There is no immediately available explanation for the changes seen in POST IBI parameters for SAR less than 30 mW/g. They occurred for PW modulation (10.9-microsecond pulses at 10,000 pps) most often and were always greater for PW RFR than for CW RFR, indicating a possible difference in interaction with aggregate membrane components. These "after effects" with PW RFR certainly should be further investigated. Mechanisms responsible for flurries in beating may have been involved in the observed changes with PW RFR since flurries were most often the cause of large CVs.

Beat rates in two spring experiments were more irregular than normal and had an apparent greater sensitivity to RFR. Experiment H was conducted before the streptococcal contamination was checked by the new antibiotic. The variability in that experiment was probably due to a contamination not visible under the microscope or to residual effects of contamination during culture since the aggregate studied was from the only apparently uncontaminated culture flask available that day. Results from experiment H are represented in Figures 39, 40, and 41 in data at 2.1 and 12.1 mW/g for CW and PW RFR (see Table III). At 12.1 mW/g, these results are also represented by the first data points in Figures 26 and 27; at 2.1 mW/g, by the last data points in Figures 34 and 35. In each of these four figures, it is seen that results from experiment H usually contributed the largest changes in mean IBI and CV. In experiment L, the aggregate was exposed to similar SARs of CW RFR at bulk temperatures of 28°C and 37°C, with larger CVs at 28°C. Changes in mean IBI for 42.6 mW/g at 28°C (Figure 36) were about 2.5 times larger than at 37°C for this aggregate (last data points in Figure 30) and for the change averaged over three experiments (Figure 30). Changes in averaged CV for 42.6 mW/g at 28°C were much larger than that at 37°C for this aggregate and for results averaged over three experiments. Changes in mean IBI during exposure for 89.2 mW/g at 28°C (Figure 37) were comparable to those for 85.5 mW/g at 37°C (Figure 33), but changes after exposure were larger for 28°C. Changes in averaged CV showing a progressive increase at 28°C were larger than those showing an M-like pattern at 37°C.

To summarize results from experiments H and L, there seemed to be an increased sensitivity to RFR in relation to results from other experiments. The common factor in these two experiments was the less regular beating which was reflected in higher-than-normal CV values for IBI. Thus, pacemaking cardiac tissue which is beating irregularly may be more sensitive to RFR through thermal or other interaction mechanisms. Further experimentation will be necessary to study this possibility.

A thermal mechanism could be proposed for the changes in mean IBI and CV reported here to occur with RFR exposure. To estimate temperature changes during exposure, temperature measurements made for calculation of SAR were re-examined to determine steady-state temperature elevations. It was found that, for the position of aggregates during extracellular recording, the steady-state temperature was elevated above ambient temperature by 0.3°C per watt of net input power to the exposure device. Since SAR at this location was 83.5 mW/g per watt of net input power, the temperature rise was 0.0036 °C per mW/g. For example, at 100 mW/g, the steady-state temperature rise was 0.36°C, a small change. For the three highest CW SARs in Figure 40, the mean IBI changes were -2.0, -4.45, and -2.7% and temperature changes were calculated as 0.16, 0.26, and 0.31°C. These represented rates of IBI change with temperature of -12.5, -17.1, and -8.7%/°C which were similar to, but larger than, the range of 3 to 10%/°C derived from temperature data. Using the average of -12.8%/°C for the 3 RFR values and a temperature change of 0.0036°C/mW/g, IBI change caused by temperature elevation was given by $\Delta IBI = -0.046 \times SAR$. This linear relation was plotted to give the curve in Figure 40. This curve matched well the data points for high SAR as it should but approached zero too fast to come near the data points at 8.4 and 12.1 mW/g. The curve, of course, remained below the zero axis and could not come near the positive data point at 1.2 mW/g. Similar curves closer to the zero axis would result from using smaller rates of change so that the straight regression line for CW data in Figure 40 could not be approximated. Thus, it was difficult to explain the mean IBI changes with SAR in purely thermal terms.

A temperature basis for the changes in normalized CV was even more difficult to assign since there was no clear trend established in temperature data. If CV was relatively constant as suggested by data obtained here and previously [41], then the small changes in Figures 39 and 40 can be expected. However, the large increases in CV seen with onset of RFR exposure at 8.4 mW/g PW (Figure 24) and after RFR exposures at 8.4 mW/g PW, 12.1 mW/g PW, and 42.6 mW/g M (Figures 24, 27, 31 and summarized in Figure 41) could not be explained as a temperature effect since they did not occur for all modulations at a given SAR. Also, the RF-induced temperature changes were all less than 1°C which would not be expected to cause such large changes. The CV changes were most prevalent for PW modulation which had the highest peak to average power ratio of 9.17.

V. CONCLUSIONS AND RECOMMENDATIONS

During this program, cardiac-cell aggregates provided many useful data on RFR effects on beat rate of living cardiac tissue. The exposure system using an open-ended coaxial exposure device worked very well for the 2450-MHz RFR exposure of aggregates. This system was used to obtain the experimental results on aggregate beat rate described and discussed in Section IV in terms of interbeat interval (IBI). This information is not only applicable to cardiac cells but also to other excitable cells since the well-studied aggregate membrane has representative excitable properties. In this section, conclusions based on the results are given and recommendations for further research are made.

Several conclusions can be drawn from the experimental results. Changes seen during RFR at SARs greater than 30 mW/g were most likely caused by elevated temperature since decreases in mean IBI closely matched those expected from RF-induced temperature rise. Decreases at lower SAR did not match those expected from induced temperature rise. This was also true for the increase in IBI at 1.2 mW/g. Decreases in mean IBI after exposure for SAR greater than 30 mW/g was probably a delayed return to PRE-exposure values similar to those seen in other temperature studies in the laboratory. Irregular beat rates were more sensitive to RFR than regular beat rates. Exposure to RFR modulated as 10.9-microsecond pulses at 10,000 pps (PW) produced results similar to those for other modulations during exposure but was more effective in producing changes after exposure. Therefore, pulsed RFR may have interacted with the aggregate differently.

Personnel exposure levels which correspond to the SARs used in this program can be derived by using the Radiofrequency Radiation Dosimetry Handbook [46]. The average SAR at 2450 MHz in prolate spheroidal models of adult humans can be as high as 0.05 mW/g per mW/cm^2 of incident plane-wave power density as seen in Figures 17 through 22 of the Handbook. This conversion factor was used to calculate incident power densities of 24 mW/cm^2 for 1.2 mW/g, 850 mW/cm^2 for 42.5 mW/g, and 1710 mW/cm^2 for 85.5 mW/g. These estimates were on the low side since the maximum value of induced SAR for the prolate spheroidal models was used.

The following recommendations for further research are based on the experiences with RFR exposure of cardiac-cell aggregates in this program and on the conclusions reached from the results of several experiments:

- investigate changes in aggregate membrane electrical properties in the SAR range of 1 to 10 mW/g in which beat rate changes were not fully explained by temperature rises and, in some cases, were opposite to those expected with elevated temperature,
- investigate differences in the effects of pulse-modulated and CW RFR in order to delineate the role of peak power in causing beat rate changes, especially those seen after exposure,
- investigate the role of PRE-exposure variability in beat rate on sensitivity to RFR which was suggested in this program,
- study membrane electrical properties in nonbeating aggregates to obtain information on RFR effects on individual ion conductances,
- develop an improved system for monitoring and analyzing IBI data in the areas of (1) video recording of beating and (2) on-line statistical analysis, and
- develop the capability to expose aggregates to higher peak and average powers during pulse-modulated RFR.

VI. LIST OF SYMBOLS AND ABBREVIATIONS

BEG	95-second interval at beginning of exposure
BR	beat rate in beats per minute or per second
CV	coefficient of variation in percent
CW	continuous wave
END	95-second interval at end of exposure
G	"gated" square-wave modulation usually at 1.6 Hz
IBI	interbeat interval in milliseconds
M	square-wave modulation at 16 Hz
P, PW	pulsed (wave) modulation
POST	95-second interval after exposure
POSTPOST	second 95-second interval after exposure
PRE	95-second interval prior to exposure
RFR	radiofrequency radiation
SAR	Specific Absorption Rate in mW/g
μm	micrometer = 10^{-6} meter

VII. REFERENCES

1. A. S. Presman, Electromagnetic Fields and Life, Plenum Press, New York, 1970, 336 pp.

2. S. Baranski and P. Czerski, Biological Effects of Microwaves, Dowden, Hutchinson and Ross, Stroudsburg, PA, 1976, 234 pp.

3. I. T. Kaplan, W. Metlay, M. M. Zaret, L. Birenbaum, and S. W. Rosenthal, "Absence of Heart-Rate Effects in Rabbits During Low-Level Microwave Irradiation," IEEE Trans. Microwave Theory Techs. MTT-19: 168-173, 1971.

4. L. Birenbaum, I. T. Kaplan, W. Metlay, S. W. Rosenthal, and M. M. Zaret, "Microwave and Infra-red Effects on Heart Rate, Respiration Rate and Subcutaneous Temperature of the Rabbit," J. Microwave Power 10:3-18, 1975.

5. C. K. Chou, L. F. Han, and A. W. Guy, "Microwave Radiation and Heart-Beat Rate of Rabbits," J. Microwave Power 15:87-93, 1980.

6. A. H. Frey and E. Seifert, "Pulse Modulated UHF Energy Illumination of the Heart Associated with Change in Heart Rate," Life Sciences, Part II, 7:505-512, 1968.

7. R. M. Clapman and C. A. Cain, "Absence of Heart-Rate Effects in Isolated Frog Heart Irradiated with Pulse Modulated Microwave Energy," J. Microwave Power 10 (4): 411-419, 1975.

8. L. M. Liu, F. J. Rosenbaum, and W. F. Pickard, "The Insensitivity of Frog Heart Rate to Pulse Modulated Microwave Energy," J. Microwave Power 11(3):225-232, 1976.

9. J. L. Lords, C. H. Durney, A. M. Borg, and C. E. Tinney, "Rate Effects in Isolated Hearts Induced by Microwave Irradiation," IEEE Trans. Microwave Theory Techs. MTT-21:834-836, 1973.

10. C. E. Tinney, J. L. Lords and C. H. Durney, "Rate Effects in Isolated Turtle Hearts Induced by Microwave Radiation," IEEE Trans. Microwave Theory and Techs. MTT-24:1-18, January 1976.

11. R. G. Olsen, J. L. Lords and C. H. Durney, "Microwave-Induced Chronotropic Effects in the Isolated Rat Heart," Arn. Biomed. Eng. 5:395-409, 1977.

12. J. R. Reed, J. L. Lords, and C. H. Durney, "Microwave Irradiation of the Isolated Rat Heart After Treatment with ANS Blocking Agents," Radio Science 12(6S):161-165, 1977.

AD-A109 813 GEORGIA INST OF TECH ATLANTA ENGINEERING EXPERIMENT --ETC F/G 6/18
INVESTIGATION OF RADIOFREQUENCY RADIATION EFFECTS ON EXCITABLE --ETC(U)
JUL 81 R L SEAMAN, E C BURDETTE, R L DEHAAN F49620-79-C-0055
UNCLASSIFIED AFOSR-TR-82-0020 NL

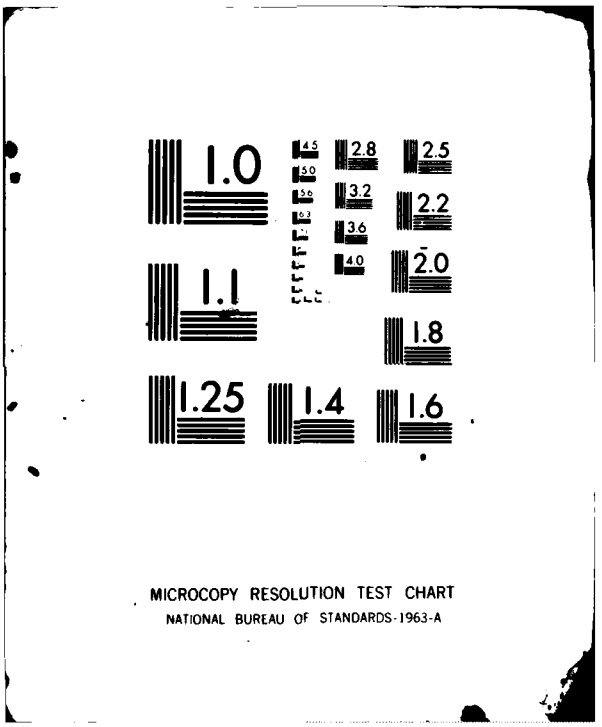
1.0
1.1
1.25
1.4
1.6
1.8
2.0
2.2
2.5
2.8
3.2
3.6
4.0
4.5
5.0
5.6
6.3
MICROCOPY RESOLUTION TEST CHART
NATIONAL BUREAU OF STANDARDS-1963-A

13. Yu. I. Kamenskii, "Effect of Microwaves on the Functional State of the Nerve," Biophysics 9:758-764, 1964.

14. D. I. McRee and H. Wachtel, "The Effects of Microwave Radiation on the Vitality of Isolated Frog Sciatic Nerves," Radiation Res. 82:536-546, 1980.

15. C. K. Chou and A. W. Guy, "Effects of Electromagnetic Fields on Isolated Nerve and Muscle Preparations," IEEE Trans. Microwave Theory Techs. MTT-26:141-147, 1978.

16. K. R. Courtney, J. C. Lin, A. W. Guy, and C.-K. Chou, "Microwave Effect on Rabbit Superior Cervical Ganglion," IEEE Trans. Microwave Theory Techs. MTT-23:809-813, 1975.

17. D. I. McRee and H. Wachtel, "Elimination of Microwave Effects on the Vitality of Nerves after Active Transport Has Been Blocked," Bioelectromagnetics Society First Annual Meeting, Seattle, Washington, 1979.

18. H. Wachtel, R. Seaman, and W. Joines, "Effects of Low-Intensity Microwaves on Isolated Neurons," Ann. of the New York Acad. Sci. 247:46-61, 1975.

19. R. L. Seaman and H. Wachtel, "Slow and Rapid Responses to CW and Pulsed Microwave Radiation by Individual Aplysia Pacemakers," J. Microwave Power 13(1):77-86, 1978.

20. P.V.K. Brown and L. E. Larsen, "Differing Effects of Pulsed and CW Microwave Energy upon Nerve Function as Detected by Birefringence Measurement," IEEE Trans. Microwave Theory Techs. MTT-28: 1126-1133, 1980.

21. R. J. MacGregor, "A Possible Mechanism for the Influence of Electromagnetic Radiation on Neuroelectric Potentials," IEEE Trans. Microwave Theory Techs. MTT-27:914-921, 1979.

22. F. S. Barnes and C. L. Hu, "Model for Some Nonthermal Effects of Radio and Microwave Fields on Biological Membranes," IEEE Trans. Microwave Theory Techs. MTT-25:742-746, 1977.

23. G. C. Berkowitz and F. S. Barnes, "The Effects of Nonlinear Membrane Capacity on the Interaction of Microwave and Radio Frequencies with Biological Materials," IEEE Trans. Microwave Theory Techs. MTT-27: 204-207, 1979.

24. H. Wachtel, J. D. Forster, and F. S. Barnes, "Microwave Effects on Isolated Neurons Vary with Field Orientation," (abstract) Bioelectromagnetics 1:205, 1980.

25. W. F. Pickard, Y. H. Barsoum, and F. J. Rosenbaum, "Is the Characean Plasmalemma a Radio-Frequency Rectifier?" (abstract), Bioelectromagnetics 1:216, 1980.

26. W. F. Pickard and R. J. Rosenbaum, "Biological Effects of Microwaves at the Membrane Level: Two Possible Athermal Electrophysiological Mechanisms and a Proposed Experimental Test," Math. Biosci. 39: 235-253, 1978.

27. C. A. Cain, "A Theoretical Basis for Microwave and RF Field Effects on Excitable Cellular Membranes," IEEE Trans. Microwave Theory Techs. MTT-28:142-147, 1980.

28. R. J. Spiegel and W. T. Joines, "A Semiclassical Theory for Nerve Excitation by a Low Intensity Electromagnetic Field," Bull. Math. Biol. 35:591-605, 1973.

29. R. L. DeHaan and H. G. Sachs, "Cell Coupling in Developing Systems: The Heart-Cell Paradigm," Chapter 5 in Current Topics in Developmental Biology, Vol. 7, Academic Press, New York, 1972, pp. 193-228.

30. R. L. DeHaan and L. J. DeFelice, "Oscillatory Properties and Excitability of the Heart Cell Membrane," Theoretical Chemistry, Vol. 4, Academic Press, New York, 1978, pp. 181-233.

31. T. F. McDonald, H. G. Sachs, and R. L. DeHaan, "Development of Sensitivity to Tetrodotoxin in Beating Chick Embryo Hearts, Single Cells, and Aggregates," Science 176:1248-1250, 1972.

32. H. G. Sachs and R. L. DeHaan, "Embryonic Myocardial Cell Aggregates: Volume and Pulsation Rate," Dev. Biol. 30:233-240, 1973.

33. J. R. Clay, L. J. DeFelice, and R. L. DeHaan, "Current Noise Parameters Derived from Voltage Noise and Impedance in Embryonic Heart Cell Aggregates," Biophys. J. 28:169-184, 1979.

34. R. L. DeHaan and H. A. Fozzard, "Membrane Response to Current Pulses in Spheroidal Aggregates of Embryonic Heart Cells," J. Gen. Physiol. 65:207-222, 1975.

35. L. J. DeFelice and R. L. DeHaan, "Membrane Noise and Intercellular Communication," Proceedings of the IEEE 65:796-799, 1977.

36. R. D. Nathan and R. L. DeHaan, "Voltage Clamp Analysis of Embryonic Heart Cell Aggregates," J. Gen. Physiol. 73:175-198, 1979.

37. L. J. Elsas, F. B. Wheeler, D. J. Danner, and R. L. DeHaan, "Amino Acid Transport by Aggregates of Cultured Chicken Heart Cells. Effect of Insulin," J. Biol. Chem. 250:9381-9390, 1975.

38. D. L. Ypey, D. E. Clapham, and R. L. DeHaan, "Development of Electrical Coupling and Action Potential Synchrony Between Paired Aggregates of Embryonic Heart Cells," Membrane Biol. 51:75-96, 1979.

39. D. E. Clapham, A. Shrier, and R. L. DeHaan, "Junctional Resistance and Action Potential Delay Between Embryonic Heart Cell Aggregates," J. Gen. Physiol. 75:633-654, 1980.

40. R. D. Nathan and R. L. DeHaan, "In-Vitro Differentiation of a Fast Na^+ Conductance in Embryonic Heart Cell Aggregates," Proc. Natl. Acad. Sci. 75:2776-2780, 1978.

41. J. R. Clay and R. L. DeHaan, "Fluctuations in Interbeat Interval in Rhythmic Heart-Cell Clusters," Biophys. J. 28:377-389, 1979.

42. R. D. Nathan, J. P. Pooler, and R. L. DeHaan, "Ultraviolet-Induced Alterations of Beat Rate and Electrical Properties of Embryonic Chick Heart Cell Aggregates," J. Gen. Physiol. 67:27-44, 1976.

43. R. L. DeHaan and S. H. Gottlieb, "The Electrical Activity of Embryonic Chick Heart Cells Isolated in Tissue Culture Singly or in Interconnected Cell Sheets," J. Gen. Physiol. 52:643-665, 1968.

44. R. R. Bowman, "A Probe for Measuring Temperature in Radio-Frequency-Heated Material," IEEE Trans. Microwave Theory Techs. MTT-24:43-45, 1976.

45. E. C. Burdette, F. L. Cain, and J. Seals, "In-Vivo Probe Measurement Technique for Determining Dielectric Properties at VHF Through Microwave Frequencies," IEEE Trans. Microwave Theory Techs. MTT-28:414-427,1980.

46. C. H. Durney, et al., "Radiofrequency Radiation Dosimetry Handbook (Second Edition), Report SAM-TR-78-22, USAF School of Aerospace Medicine, Brooks AFB, Texas, 1978.

VIII. PROFESSIONAL STAFFING, PUBLICATIONS, INTERACTIONS, AND PATENT

A. Project Professional Personnel

Ronald L. Seaman, Ph.D., Current Principal Investigator
Everette C. Burdette, M.S., Prior Principal Investigator
James C. Toler, M.S., Manager, Biomedical Research Division
Allan R. Moser, Ph.D.
Paul G. Friederich, B.S.
D. Jay Freedman, M.S.
Biomedical Research Division
Engineering Experiment Station
Georgia Institute of Technology

Robert L. DeHaan, Ph.D., Co-Investigator
Louis J. DeFelice, Ph.D.
R. Clark Lantz, Ph.D.
Department of Anatomy
School of Medicine
Emory University

No advanced degrees were awarded during this program.

B. Publications in Technical Journals

No papers were published in technical journals and no manuscripts were submitted for publication during the 1 March 1979 through 30 April 1981 performance period. However, two manuscripts based upon this Final Technical Report are being planned. One will describe the open-ended coaxial exposure device and the other will present the experimental results. Preprints will be sent to the appropriate program monitor before submission.

C. Interactions and Paper Presentations

1. E. C. Burdette, R. L. Seaman, and R. L. DeHaan, "Investigation of Radiofrequency Radiation Effects on Excitable Tissues," Review of Air Force Sponsored Basic Research in Environmental Protection, Toxicology, and Electromagnetic Radiation Bioeffects, 15-17 January 1980, San Antonio, Texas.

2. R. L. Seaman, E. C. Burdette, and R. L. DeHaan, "Alteration of Action Potential Parameters in Embryonic Heart Cell Aggregates by Radiofrequency Radiation," Review of Air Force Sponsored Basic Research in Environmental Protection, Toxicology, and Electromagnetic Radiation Bioeffects, 15-17 January 1980, San Antonio, Texas, (presented by R. L. DeHaan).

3. E. C. Burdette, R. L. Seaman, and R. L. DeHaan, "Investigation of Radiofrequency Radiation Effects on Excitable Tissues," Annual Technical Report No. 1, Contract F49620-79-C-0055, Project A-2335, April 1980.

4. E. C. Burdette, R. L. Seaman, and R. L. DeHaan, "Open-Ended Coaxial Exposure System for Small Biological Preparations," Bioelectromagnetics Society Second Annual Meeting, 14-18 September 1980, San Antonio, Texas.

5. R. L. Seaman, E. C. Burdette, and R. L. DeHaan, "RF Radiation Alteration of Cardiac-Cell Aggregate Electrical Parameters," Bioelectromagnetics Society Second Annual Meeting, 14-18 September 1980, San Antonio, Texas

6. R. L. Seaman, E. C. Burdette, and R. L. DeHaan, "RF Radiation Effects on Cardiac-Cell Aggregate Beat Rate," Bioelectromagnetics Society Third Annual Meeting, 10-12 August 1981, Washington, D.C. (abstract accepted).

7. R. L. Seaman, "Radiofrequency Radiation Effects on Excitable Tissues," U.S. Air Force Radiation Bioeffects Research Program Review, 22-24 June 1981, Brooks AFB, Texas.

D. Patent of Exposure Device

The open-ended coaxial exposure device developed during this program has been determined to have patentable features. Application for U.S. Letters Patent is being handled by the Hanscom Patent Prosecution Office, Office of the Judge Advocate General, U.S. Air Force, as AF Invention No. 14,382. The invention is entitled OPEN-ENDED COAXIAL EXPOSURE DEVICE with Everette Clifton Burdette II and Ronald Leon Seaman as inventors.

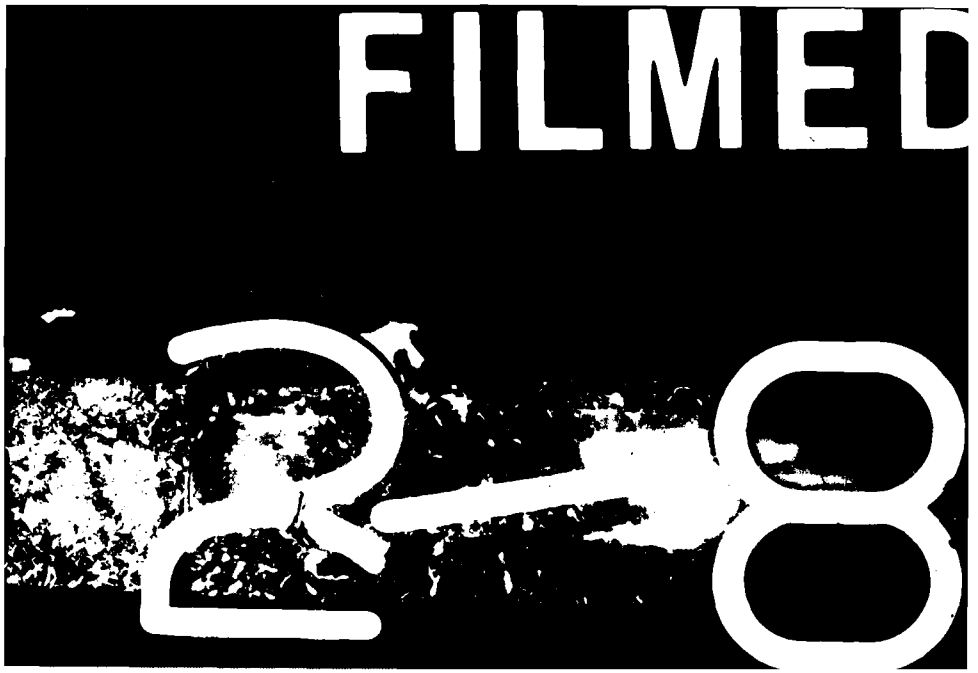
FILMED
R 8